Performance Optimization for 5G Wireless Communication Systems

A Thesis Submitted for obtaining
the Scientific Title of PhD in Engineering
from
Politehnica University Timișoara
in the Field of Electronic Engineering and Telecommunications
by

Eng. Gordana-Raluca Barb

PhD Committee Chair:
PhD Supervisor: Prof.univ.dr.ing. Marius OTESTEANU
Scientific Reviewers:

Date of the PhD Thesis Defense:

The PhD thesis series of UPT are:

1.Automation
2.Chemistry
3.Energetics
4.Chemical Engineering
5.Civil Engineering
6.Electrical Engineering
7.Electronic Engineering and Telecommunications
8.Industrial Engineering
9.Mechanical Engineering
10.Computer Science and Information Technology
11.Science and Material Engineering
12.Systems Engineering
13.Energy Engineering
14.Computers and Information Technology
15.Materials Engineering
16.Engineering and Management
17.Architecture
18.Civil Engineering and Installations
19.Electronics, Telecommunications and Information Technologies

Politehnica University Timișoara, Romania, initiated the above series to disseminate the expertise, knowledge and results of the research carried out within the doctoral school of the university. According to the Decision of the Executive Office of the University Senate No. 14/14.07.2006, the series includes the doctoral theses defended in the university since October 1, 2006.

Romania, 300223 Timișoara, Bd. Vasile Pârvan no. 2B
Tel./fax +40-(0)256 404677
e-mail: editura@upt.ro

Foreword

This PhD thesis has been elaborated during my activity at the faculty of Electronics, Telecommunications and Information Technologies, Department of Communications, of the Politehnica University Timisoara and at the R&D laboratory of Nokia Networks Timisoara.

I want to start by expressing my profound gratitude to my PhD supervisor, Prof.univ.dr.ing Marius Otesteanu, who guided and supported me with the experience and tenacity necessary so I could be able to elaborate the complex work of research and to achieve the objectives of the thesis.

My sincere appreciation goes to the professors and colleagues from the Department of Communications, especially to Prof.univ.dr.ing Florin Alexa and Sl.dr.ing. Cornel Balint, who generously offered me their time, knowledge and encouraged me to innovate.

I would also like to thank my colleagues from Nokia Networks Timisoara with whom I collaborated for the research for the trust, support and couching I received.

A special thank you goes to my family, particularly to my mother and my father, which are the two most important persons of my life, for the unconditional love, attention, advice, effort and support.

Last but not least, I want to thank me personally, for all the moments when giving up was an easy way out and yet, here I am writing these lines at the almost end of a wonderful journey that taught me perseverance and endurance and from which I grew richer spiritually, emotionally and mentally.

To everyone who has been part of this journey with me, thank you.

Timişoara, May 2021 Gordana Barb

To my parents.

FAMILY NAME, First Name

Thesis title

PhD theses of UPT, Series X, No. YY, Editura Politehnica, 200Z,
168 pages, 39 figures, 27 tables.

ISSN:
ISBN:

Keywords
.....
.....

Abstract
.....
.....
.....
.....
.....
.....
.....
.....
.....
.....

Contents

List of Figures

List of Tables

Acronyms

1G	1st Generation
2G	2nd Generation
3G	3rd Generation
3GPP	3rd Generation Partnership Project
4G	4th Generation
5G	5th Generation
ADC	Analog-to-Digital Conversion
AMPS	Advanced Mobile Phone System
AoA	Angle of Arrival
AoD	Angle of Departure
AuC	Authentication Centre
BCH	Broadcast Channels
BER	Bit Error Rate
BS	Base Station
BSC	Base Station Controller
BSS	Base Station Subsystem
BTS	Base Transceiver Station
CCCH	Common Control Channels
CCH	Control Channels
CDL	Clustered Delay Line
CDMA	Code Division Multiple Access
CN	Core Network
CP	Cyclic Prefix
CR	Cognitive Radio
CRM	Common Resource Manager
CSI-RS	Channel-State Information Reference Signal
D-AMPS	Digital Advanced Mobile Phone System
DAC	Digital-to-Analog Conversion
DCCH	Dedicated Control Channels
DCS	Digital Cellular System
DL	Downlink
DMRS	Demodulation Reference Signals
DS	Delay Spread
DSS	Dynamic Spectrum Sharing
E-UTRAN	Evolved Universal Mobile Telecommunication System Terrestrial Radio Access Network
EBB	Eigen Based Beamforming
EIR	Equipment Identity Register
eMBB	Enhanced Mobile Broadband
eNodeB	Evolved Base Station
EPC	Evolved Packet Core

ETSI	European Telecommunications Standards Institute
FBMC	Filter Bank Multicarrier
FDD	Frequency Division Duplex
FDM	Frequency Division Multiplexing
FDMA	Frequency Division Multiple Access
FFT	Fast Fourier Transformation
FR	Frequency Range
FTN	Faster-than-Nyquist
GFDM	Generalized Frequency Division Multiplexing
GGSN	Gateway GPRS Support Node
GMSC	Gateway MSC
GoB	Grid of Beams
GPRS	General Packet Radio Service
GPS	Global Positioning System
GSM	Global System for Mobile Communications
GSN	GPRS Support Nodes
HLR	Home Location Register
HSDPA	High Speed Downlink Packed data Access
HSPA	High Speed Packet Data Access
HSS	Home Subscriber Server
HSUPA	High Speed Uplink Packet Data Access
IFFT	Inverse Fast Fourier Transformation
IP	Internet Protocol
ISI	Inter-Symbol Interference
JDC	Japanese Digital Cellular
LOS	Line-of-Sight
LTE	Long Term Evolution
LTE-A	Long Term Evolution – Advanced
MBSFN	Multicast-Broadcast Single Frequency Network
MCS	Modulation and Coding Scheme
ME	Mobile Equipment
MME	Mobility Management Entity
MMSE	Minimum Mean Square Error
mMTC	Massive Machine Type Communication
mmW	Millimeter Waves
MS	Mobile Station
MSC	Mobile Switching Centre
NG	Next Generation
NGC	Next Generation Core
NLOS	Non-Line-of-Sight
NMT	Nordic Mobile Telephone
NOMA	Non-Orthogonal Multiple Access
NR	New Radio
NSA	Non-Standalone

NSS	Network Switching Subsystem
NTT	Nippon Telephone & Telegraph
OFDM	Orthogonal Frequency Division Multiplexing
OFDMA	Orthogonal Frequency Division Multiple Access
OSS	Operational Support Subsystem
PAPR	Peak to Average Power Ratio
PBCH	Physical Broadcast Channel
PCS	Personal Communications Service
PCRF	Policy and Charging Rules Function
PDCCH	Physical Downlink Control Channel
PDSCH	Physical Downlink Shared Channel
PGW	Packet Data Network Gateway
PMI	Precoding Matrix Index
PRACH	Physical Random Access Channel
PRB	Physical Resource Block
PSS	Primary Synchronization Signal
PTRS	Phase-Tracking Reference Signals
PUCCH	Physical Uplink Control Channel
PUSCH	Physical Uplink Shared Channel
QAM	Quadrature Amplitude Modulation
QoS	Quality of Service
QPSK	Quadrature Phase Shift Keying
RAN	Radio Access Network
RNC	Radio Network Controller
RSRP	Reference Signal Receive Power
SA	Standalone
SC-FDMA	Single Carrier Frequency Division Multiple Access
SCS	Subcarrier Spacing
SDL	Supplementary Downlink
SGSN	Serving GPRS Support Node
SGW	Serving Gateway
SIB	System Information Block
SISO	Single-Input-Single-Output
SMS	Short Messages Services
SNIR	Signal-to-Noise-Plus-Interference Ratio
SON	Self Organizing Network
SRS	Sounding Reference Signal
SSS	Secondary Synchronization Signal
SUL	Supplementary Uplink
TACS	Total Access Communications Systems
TCH	Traffic Channels
TDD	Time Division Duplex
TDL	Tapped Delay Line
TDM	Time Division Multiplexing

TDMA	Time Division Multiple Access
TRAU	Transcoding Rate & Adaptation Unit
TS	Time Slot
UE	User Equipment
UL	Uplink
UMTS	Universal Mobile Telecommunications System
URLLC	Ultra Reliable Low Latency Communications
USIM	UMTS Subscriber Identity Module
UTRAN	UMTS Terrestrial Radio Access Network
VLR	Visitor Location Register
WCDMA	Wideband Code Division Multiple Access
XPR	Cross Polarization Power Ratio
ZoA	Zenith Angle of Arrival
ZoD	Zenith Angle of Departure

1. Introduction

This chapter starts with the presentation of the background and the evolution of mobile communication systems, providing an overview on all previous and current mobile generations. This allows a better understanding of the history and growth observed in the mobile communication's field. Following, the objectives and motivations of this work are presented. An outline of the thesis is identified and lastly, research contributions are described.

1.1 Background and Evolution of Mobile Communication Systems

It is typical to think of generations when dealing with cellular networks. 1st Generation (1G) systems appeared in the 1980s, being characterized by an analog telephony transmission, offering a very low-quality voice service with no security and with low spectrum efficiency. It was first introduced by Advanced Mobile Phone System (AMPS) in the United States, Total Access Communications Systems (TACS) in the UK, Nippon Telephone & Telegraph (NTT) in Japan and Nordic Mobile Telephone (NMT) System in Scandinavian countries [1]. Moreover, since each country had its own standards regarding the cellular network, there was an incompatibly amongst them. 2nd Generation (2G) systems were implemented in the 1990s, with the major difference compared to 1G systems being the transmission mode that was upgraded from analog to digital. 3rd Generation (3G) is defined as high speed digital telephony and data transfer and the 4th Generation (4G) came with an increase on capacity and data rates compared to 3G [2]. Each mobile generation is detailed below individually.

1.1.1 2nd Mobile Generation

2G systems were deployed based on three standards developed around the globe: Global System for Mobile Communications (GSM) standard in Europe, Japanese Digital Cellular (JDC) in Japan and Digital Advanced Mobile Phone System (D-AMPS) IS-54 in the United States [3]. The GSM standard ended being the standard that achieved the more popularity, with a market share over 90% and being widely used in more than 200 countries [4] [5]. With GSM, the transmission upgraded from analog to digital, voice signal quality improved slightly compared to 1G and Short Messages Services (SMS) were introduced, allowing short messages with a maximum of 160 characters to be sent and received among Mobile Stations (MS). The multiple access schemes used by GSM are Time Division Multiple Access (TDMA) and Frequency Division Multiple Access (FDMA) [6]. In TDMA, there are several Time Slots (TS), and one MS transmits only during the duration of a certain slot. In FDMA, the spectrum is

divided into several frequencies and each MS uses one carrier frequency for the duration of the transmission. In order to avoid interference among adjacent frequency channels and time slots, a guard band is added. Generally, MSs have different frequency bands for Uplink (UL) and Downlink (DL) [7]. Figure 1 depicts the TDMA and FDMA schemes.

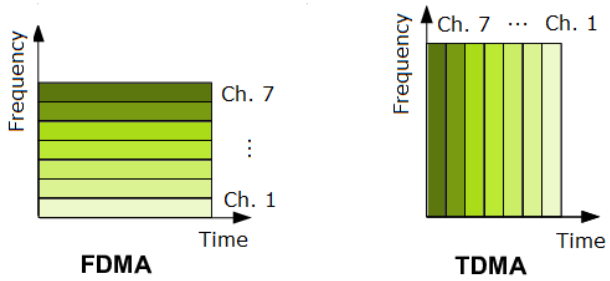

Figure 1: TDMA and FDMA user separation schemes.

There are two types of channels used to transmit and receive data in GSM systems: physical channels and logical channels. A physical channel is assigned to each user during the call and represents one time slot on a carrier. The logical channels carry the information to be transmitted over the physical channel, between the Base Station (BS) and MS. Furthermore, there are two types of logical channels: Traffic Channels (TCH), that contain the data or user speech, and Control Channels (CCH), that transmit signaling messages. There are three categories for the control channels, as it can be seen in figure 2:

- Broadcast Channels (BCH): transmitted only by the BS, downlink only, contain information such as cell identity, access and power control, available features, configuration and the list of Absolute Radio Frequency Channel Number (ARFCN) used in neighboring cells. The information carried in the BCH is used by the MS to access the GSM network;
- Common Control Channels (CCCH): transmitted between the BS and MS, uplink and downlink, contain signaling messages that are used by the MS during paging and to request access to the GSM network;
- Dedicated Control Channels (DCCH): transmitted between the BS and MS, uplink and downlink, contain dedicated control information for the call setup, authentication and SMS [8].

The configuration of a GSM architecture network is divided into three main structures: Base Station Subsystem (BSS), Network Switching Subsystem (NSS) and Operational Support Subsystem (OSS), see figure 3. The BSS is also known as the Radio Access Network (RAN) system, it controls the radio transmission, traffic, signaling and interfaces between the MS and NSS. It is composed by the Base Transceiver Station (BTS), Base Station Controller (BSC) and Transcoding Rate & Adaptation Unit (TRAU). The BTS is the physical equipment that transmits and receives the radio information for a specific coverage area, denominated cell. The frequency band adopted plays an important role, since the lower the frequency band, the higher the range of the coverage area. The BSC is the component that makes the connection between the BTS and the Mobile Switching Centre (MSC). It handles the resource allocation of the BTS, such as frequency and radio channels allocation and

establishes, maintains and releases all the connections. The TRAU is the last element of the BSS. It is used to compress and decompress the speech signal but also to adapt the data rates in conformity with the transmission types in the GSM network. The second main structure of the GSM architecture is the NSS, composed by the MSC, Home Location Register (HLR), Visitor Location Register (VLR), Equipment Identity Register (EIR) and Authentication Centre (AuC) [9]. The MSC is main component of the network, it controls the communication between the GSM network and other external networks, it is responsible for call setup, routing, switching functions and all the user management in a voice call. The HLR is a permanent database that stores information regarding the users and other additional information. The VLR is, contrary to the HLR, a temporary database that stores and updates the information regarding the users that enter the coverage area [10]. The EIR is also a database that stores information regarding the users in the network. Each mobile equipment has its own identity number, stored in the EIR. The last component of the NSS is the AuC, which performs the authentication of the users/subscribers [11] [12]. The OSS is connected to both BSS and NSS elements and it is responsible for the monitorization and control of the entire GSM network.

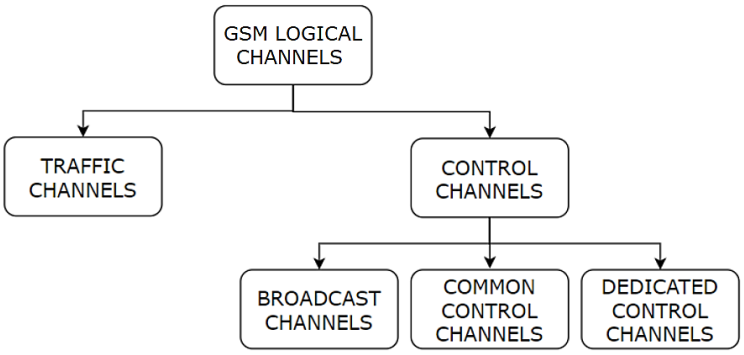

Figure 2: GSM logical channels diagram.

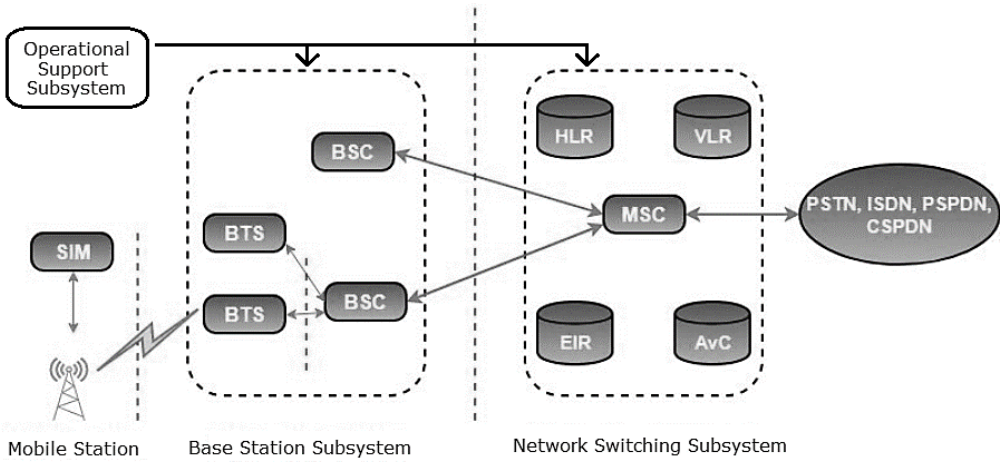

Figure 3: GSM network architecture [13].

The MS sends measurement reports periodically that are used to provide information regarding channel quality and assisting the GSM network with power control decisions and when to perform handover. Handover is the process in which an on-going call is transferred, as the user moves, from one cell to another, without interrupting the connection [14] [15]. It is implemented in the MS, BSS and MSC. There are four different types of handover in GSM systems, that are depicted in figure 4 [16]:

- Intra-cell handover: this type of handover is performed only when the root cause is interference or to improve the quality of the connection. It is triggered in the same cell, and the call is handled from one time slot to another or from one carrier frequency to another. The MS is attached to the same BTS the entire procedure;
- Intra-BSC handover: this type of handover is performed between different BTSs that are controlled by the same BSC, when the MS moves from a cell to another one;
- Inter-BSC handover: contrary to the intra-BSC handover, this type is performed between different BTSs that are controlled by different BSCs. This handover is managed by the MSC;
- Inter-MSC handover: this type of handover is performed between different BTSs that are controlled by different BSCs, which are also controlled by different MSCs.

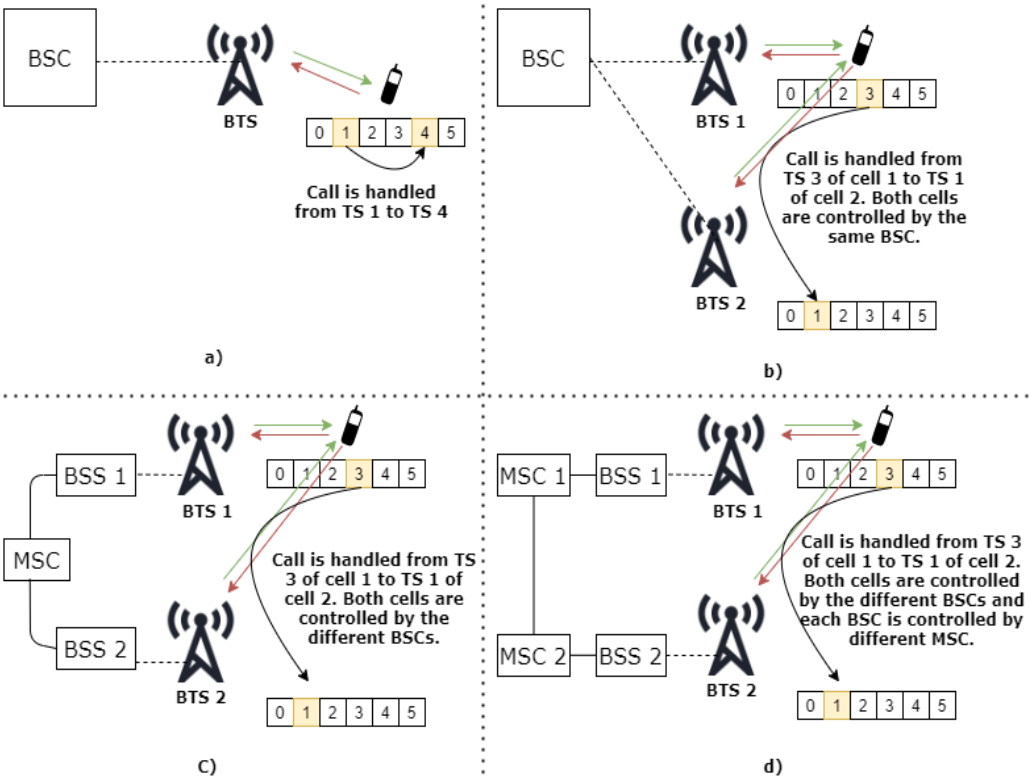

Figure 4: Handover types: a) Intra-cell handover b) Intra-BSC handover c) Inter-BSC handover d) Inter-MSC handover [17].

GSM was primarily intended to be used with frequencies in the 900 MHz frequency band, but later it was extended to the 800 MHz, 1800 MHz and 1900 MHz frequency bands. As it can be observed in figure 5, there are separate frequencies for uplink and downlink. The carrier separation is 200 kHz for all cases. The 900 MHz and 1800 MHz bands are the most common ones and used widely in regions of the world such as Europe, Africa, Middle East and some countries in Asia. In some parts of the world, the 1800 MHz GSM band is also referred to as Digital Cellular System (DCS). The 1900 MHz band is most commonly used in Central, North and South America, being also labelled as Personal Communications Service (PCS).

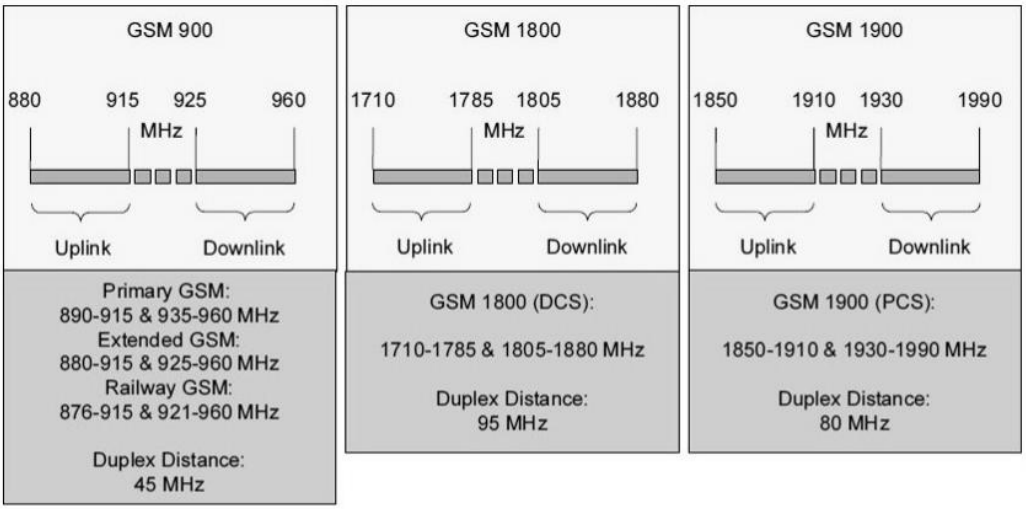

Figure 5: GSM frequency bands [18].

The GSM concept is focused on voice services only. With the increasing demand for non-voice services and higher data rates, and due to the fact that the GSM architecture is not efficient to provide these services, a new standard emerged to fulfil the needs: General Packet Radio Service (GPRS). GPRS was initially standardized by the European Telecommunications Standards Institute (ETSI), in Release 97, and presently is sustained by the Third Generation Partnership Project (3GPP). Among the main features of GPRS, there is the transmission of packet switch data besides the circuit switched voice from GSM, higher data transfer speeds, access to internet, enhanced applications and increased flexibility [19]. Thus, voice services are circuit switched, which means that each user has a different dedicated physical circuit for the entire duration of the voice call, while with packed switching the data is segmented and transported in small packets in the network, not needing a reserved physical circuit for the duration of the connection [20].

There are two main novel network elements in the GPRS architecture in the NSS component: Serving GPRS Support Node (SGSN) and Gateway GPRS Support Node (GGSN). The SGSN is responsible for authentication of users, mobility management of data traffic and encryption of the data connection towards the MS. On the other hand, the GGSN delivers the interface between the GPRS network and the external

packet switched data networks. Jointly, the SGSN and GPRS and commonly referred to as GPRS Support Nodes (GSN) [21] [22].

In conclusion, GSM is the main standard that is used worldwide, even nowadays, for 2G communication systems. Moreover, the GSM Association presented at the Mobile World Congress 2019 that, in 2017, 2G was the technology with the highest number of mobile connections among 2G, 3G and 4G technologies. The main goal of GSM was focused solely on voice communication, through circuit switching. However, with the growth of internet and the need for data services, packet switching was introduced with the GPRS concept. Data transfer rates were on average 14 kbps for uplink and 40 kbps for downlink. Besides the increase on transfer speeds, other advantages brought by GPRS consisted on more flexibility and efficiency, access to internet and enhanced applications and services overall.

1.1.2 3rd Mobile Generation

The 3rd mobile generation was released as the successor of 2G, being commercially available by 2000, with the major difference compared to 2G systems being the support for data services besides the voice services. Universal Mobile Telecommunications System (UMTS) is the standard adopted for 3G. Some of the features and improvements brought by UMTS in comparison to GSM are: higher capacity; enhanced spectrum efficiency; increased data rates reaching a maximum of 144 kbps and a mobility of 500 km/h for vehicular/macro-cell environments, 384 kbps and a mobility of 120 km/h for pedestrian/micro-cell environments and up to 2 Mbps and a mobility less than 10 km/h for indoor/pico-cell scenarios [23]. Additionally, UMTS supports both duplex schemes Frequency Division Duplex (FDD) and Time Division Duplex (TDD), albeit FDD frequency bands are used mostly by UMTS [24].

The duplex scheme FDD uses two different channels for uplink and downlink, thus there are two different frequency bands, one for transmission, and one for reception. Contrary to FDD, TDD uses merely one frequency band for transmission and reception, however there is a separation in time, meaning that uplink and downlink signals are transmitted in different periods of time [25]. The figure below depicts the difference between both duplex schemes.

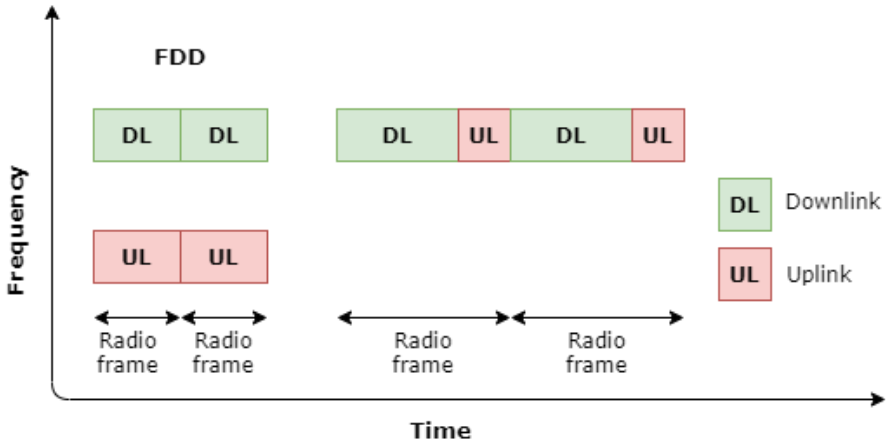

Figure 6: FDD and TDD duplex schemes [26].

The requirements and features implemented by UMTS were achieved due to the implementation of two concepts: Code Division Multiple Access (CDMA) and Wideband Code Division Multiple Access (WCDMA). CDMA is a multiple access scheme, similar to TDMA and FDMA that were previously described, that allows multiple and independent transmissions using the same frequency for all cells, which leads to the entire bandwidth being used in each cell, and also by each user simultaneously [27] [28]. In order to avoid inter-cell and intra-cell interference, cell orthogonality and user orthogonality are achieved by assigning an individual code to each user. The code is added to the information signal, and solely the intended receiver has a copy of the same code, which allows it to decode and extract the information from the received signal. The other users are not able to decode the respective signal, since for them it appears as a noise signal only. This way, interference is minimized while sharing the same frequency [29].

WCDMA is a derivation of CDMA, the main difference being the spreading bandwidth: for WCDMA, the spreading bandwidth is 5 MHz wide while for CDMA is 1.25 MHz wide. Additionally, this leads to faster data rates.

The UMTS architecture is composed by three main components, as seen in figure 7:

- User Equipment (UE);
- UMTS Terrestrial Radio Access Network (UTRAN);
- Core Network (CN).

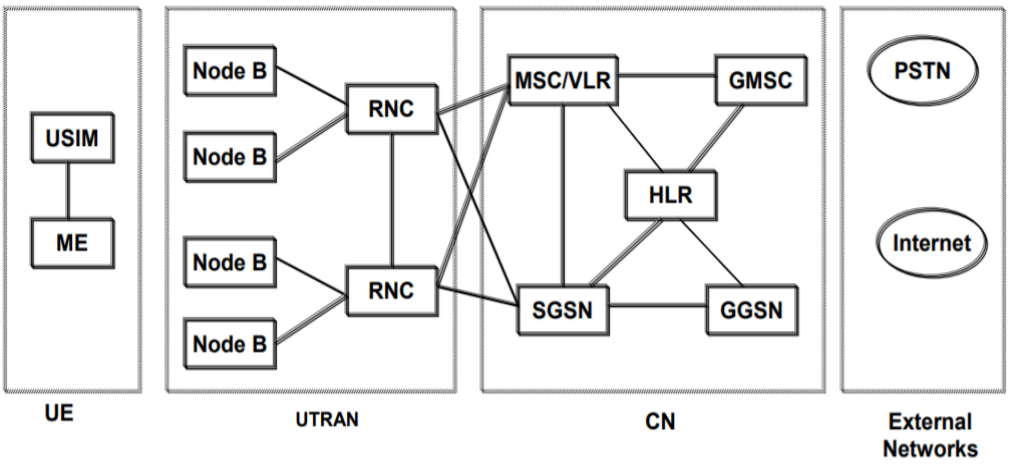

Figure 7: UMTS architecture [30].

The UE is equivalent to the MS of the GSM network architecture, meaning that is the interface with the user. It comprises the Mobile Equipment (ME) and the UMTS Subscriber Identity Module (USIM), that contains specific information of the user.

The UTRAN is composed by one or more node B and Radio Network Controller (RNC). The node B is the base station (BTS in GSM architecture), operates the air interface for the transmit and receive antennas and performs modulation and demodulation. The RNC is the control component of the node B. Its functions consist

on radio resource control and management, power and handover control, channel allocation, etc [31].

The CN is responsible for transport, mobility and subscriber data management. It has five main elements: the MSC, SGSN, GGSN, HLR (similar to the GSM architecture) and the Gateway MSC (GMSC), which has the function of switching at the moment when the UMTS network connects to other external networks.

The most common frequency bands used by UMTS are depicted in figure 8, consist on 1900-2025 MHz for uplink and 2110-2200 MHz for downlink. The difference between paired and unpaired spectrum is that paired spectrum allows two different frequency bands for uplink and downlink, while unpaired spectrum allocates a single frequency band for both uplink and downlink [32].

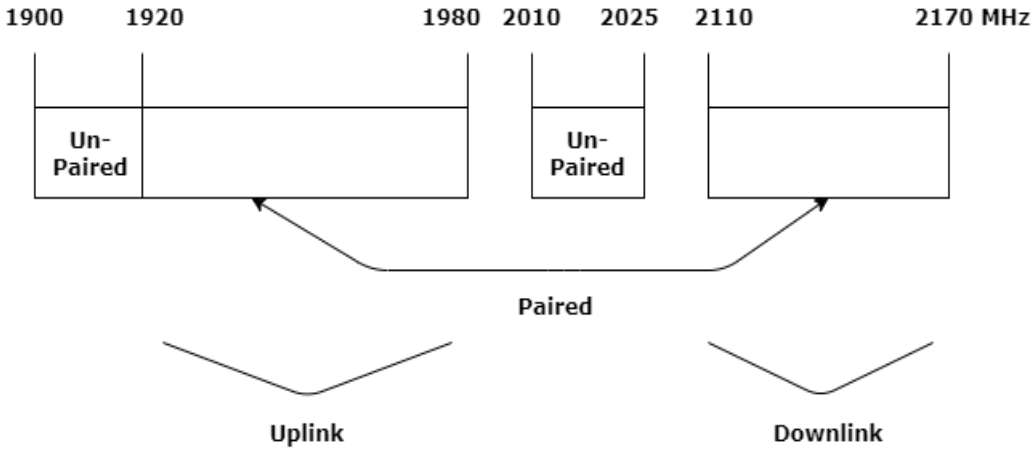

Figure 8: UMTS frequency spectrum [33].

The need for increased data transfer rates kept raising and its demand led to the appearance of High Speed Packet data Access (HSPA), defined as an enhancement to WCDMA radio networks, working with both FDD and TDD duplex modes. Firstly, the High Speed Downlink Packed data Access (HSDPA) was introduced in in 3GPP Release 5 [34], and later on, in 3GPP Release 6 [35], was introduced the High Speed Uplink Packet data Access (HSUPA). Further improvements led to the appearance of HSPA+ or also known as evolved HSPA, that were introduced in 3GPP Release 7 [36] and following Releases [37] [38].

Figure 9 shows the roadmap and evolution of the 3GPP technologies. HSPA reached data rates up to 14.4 Mbps for DL and 5.7 Mbps for UL, while HSPA+ increased these values up to a maximum of 84 Mbps for DL and 23 Mbps for UL, with 3GPP Release 9 and further Releases. Moreover, characteristics such as Quality of Service (QoS), that is defined as a set of parameters that measures the performance of the network, also increased, leading to a more robust and stable connection for diverse applications and services.

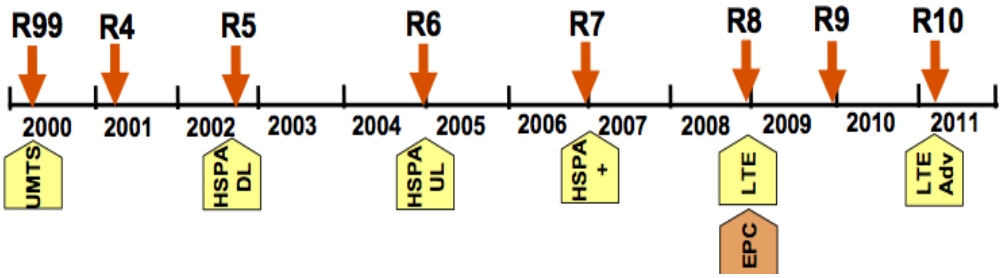

Figure 9: Roadmap of 3GPP technologies [39].

1.1.3 4th Mobile Generation

The number of mobile users is continuously evolving, hence the constant need for higher data rates, lower latency, increased spectrum effiency, energy efficiency and enhanced robustness. Long Term Evolution (LTE) is the standard that defines the 4th mobile generation, 4G. It became commercially available by 2009, and since then has been used massively worldwide by the majority of network operators [40].

LTE was standardized in 3GPP Release 8 and 9, having the following requirements for its implementation:

- Increase of spectrum efficiency by 3/4 times of the values in Release 6 HSDPA for DL and by 2/3 times of the values in Release 6 HSUPA for UL;
- Scalable bandwidth with values of 1.4, 3, 5, 10, 15 and 20 MHz;
- Peak data rates higher than 100 Mbps for DL and 50 Mbps for UL when considering a bandwidth of 20 MHz;
- Minimize the interruption time when performing the handover procedure;
- Increase coverage with cell ranges up to 5 km considering the highest values for throughput and mobility, minimize cost and power consumption [41].

The LTE network architecture was designed with the main goal of supporting high data transfer rates, low latency, an all Internet Protocol (IP) network and to provide a robust connection. It is composed by three main components: the UE, the Evolved Universal Mobile Telecommunication System Terrestrial Radio Access Network (E-UTRAN) and the Evolved Packet Core (EPC), similar to the UMTS network architecture, see figure 10. The LTE UE communicates with the BS, denominated Evolved Base Station (eNodeB), through the E-UTRAN. The connection between two eNodeB is established via the X2 interface, and each one of them connects to the LTE EPC core network via the S1 interface. Additionally, the EPC is composed by five main parts: the Mobility Management Entity (MME), which deals with signaling between the LTE UE and the EPC; the Serving Gateway (SGW), that is responsible for the transmission of the data packets from the eNodeB to the Packet Data Network Gateway (PGW), which communicates with external networks; the Policy and Charging Rules Function (PCRF) and the Home Subscriber Server (HSS), defined as a data base filled with information of all the subscribers from the respective network operator [42] [43].

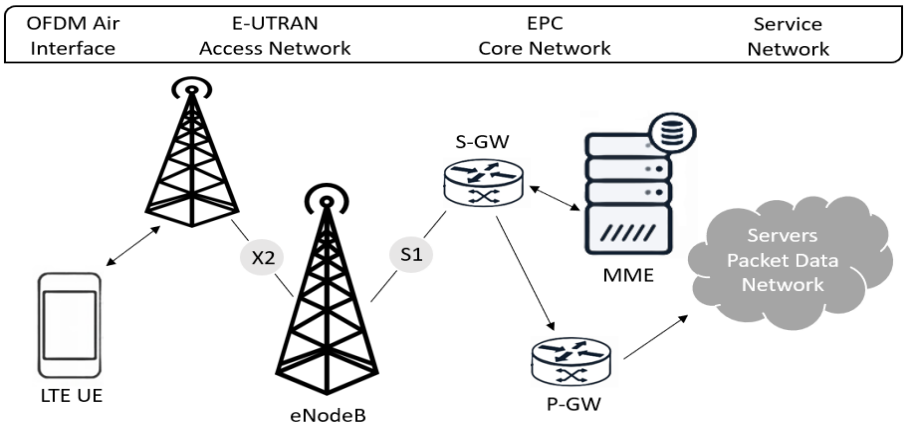

Figure 10: LTE network architecture [44].

LTE uses both TDD and FDD duplex schemes. According to 3GPP Technical Specification 36.104 V14.3.0 from 04.2017, table 1 and 2 summarize the frequency spectrum bands where LTE operates, for both UL and DL, and the associated duplex mode.

Note 1: Band 6, 23 are not applicable.

Note 2: Restricted to E-UTRA operation when carrier aggregation is configured. The downlink operating band is paired with the uplink operating band (external) of the carrier aggregation configuration that is supporting the configured cell.

Note 3: The range 2180 – 2200 MHz of the DL operating band is restricted to E-UTRA operation when carrier aggregation is configured.

E-UTRA Operating Band	UL Operating Band (MHz)	DL Operating Band (MHz)	Duplex Mode
34	2010 – 2025	2010 – 2025	TDD
35	1850 – 1910	1850 – 1910	TDD
36	1930 – 1990	1930 – 1990	TDD
37	1910 – 1930	1910 – 1930	TDD
38	2570 – 2620	2570 – 2620	TDD
39	1880 – 1920	1880 – 1920	TDD
40	2300 – 2400	2300 – 2400	TDD
41	2496 – 2690	2496 – 2690	TDD
42	3400 – 3600	3400 – 3600	TDD
43	3600 – 3800	3600 - 3800	TDD
44	703 – 803	703 – 803	TDD
45	1447 – 1467	1447 – 1467	TDD
46	5150 – 5925	5150 – 5925	TDD
47	5855 – 5925	5855 – 5925	TDD

Table 1: LTE frequency bands for TDD.

E-UTRA Operating Band	UL Operating Band (MHz)	DL Operating Band (MHz)	Duplex Mode
1	1920 – 1980	2110 – 2170	FDD
2	1850 – 1910	1930 – 1990	FDD
3	1710 – 1785	1805 – 1880	FDD
4	1710 – 1755	2110 – 2155	FDD
5	824 – 849	869 – 894	FDD
6 (Note 1)	830 – 840	875 – 885	FDD
7	2500 – 2570	2620 – 2692	FDD
8	880 – 915	925 – 960	FDD
9	1749.9 – 1784.9	1844.9 – 1879.9	FDD
10	1710 – 1770	2110 – 2170	FDD
11	1427.9 – 1447.9	1475.9 – 1495.9	FDD
12	699 – 716	729 – 746	FDD
13	777 – 787	746 – 756	FDD
14	788 – 798	758 – 768	FDD
15	Reserved	Reserved	FDD
16	Reserved	Reserved	FDD
17	704 – 716	734 – 746	FDD
18	815 – 830	860 – 875	FDD
19	830 – 845	875 – 890	FDD
20	832 – 862	791 – 821	FDD
21	1447.9 – 1462.9	1495.9 – 1510.9	FDD
22	3410 – 3490	3510 – 3590	FDD
23 (Note 1)	2000 – 2020	2180 – 2200	FDD
24	1626.5 – 1660.5	1525 – 1559	FDD
25	1850 – 1915	1930 – 1995	FDD
26	814 – 849	859 – 894	FDD
27	807 – 824	852 – 869	FDD
28	703 – 748	758 – 803	FDD
29	N/A	717 – 728	FDD (Note 2)
30	2305 – 2315	2350 – 2360	FDD
31	452.5 – 457.5	462.5 – 467.5	FDD
32	N/A	1452 – 1496	FDD (Note 2)
65	1920 – 2010	2110 – 2200	FDD
66	1710 – 1780	2110 – 2200	FDD (Note 3)
67	N/A	738 – 758	FDD (Note 2)
68	698 – 728	753 – 783	FDD
69	N/A	2570 – 2620	FDD (Note 2)
70	1695 – 1710	1995 – 2020	FDD

Table 2: LTE frequency bands for FDD.

There are different possibilities to send the information over a specific frequency band and to share the radio resources available. 2G uses TDMA and FDMA, 3G uses CDMA and WCDMA, while 4G uses Orthogonal Frequency Division Multiple Access (OFDMA) for DL and Single Carrier Frequency Division Multiple Access (SC-FDMA) for

UL. Additionally, OFDMA is also used in different standards such as IEEE 802.11a/b/g, 802.16, DAB and DVB [45].

OFDMA is a multiple access scheme based on the Orthogonal Frequency Division Multiplexing (OFDM) modulation technique, where the main stream of data is divided into multiple smaller streams that are sent over a specific number of subcarriers simultaneously. In OFDMA, the available subcarriers are allocated to the multiple users dynamically, which portrays the flexibility of the OFDMA systems [46]. The allocation of the subcarriers can be either localized or distributed. For the first case, the allocation of the subcarriers is made in an adjacent way, meaning that the subcarriers mapped for each user are continuous and there is no space between them. For the latter case, the subcarrier mapping is made arbitrarily, meaning that the subcarriers allocated are not necessarily adjacent. Figure 11 depicts graphically the two types of subcarrier mapping/allocation.

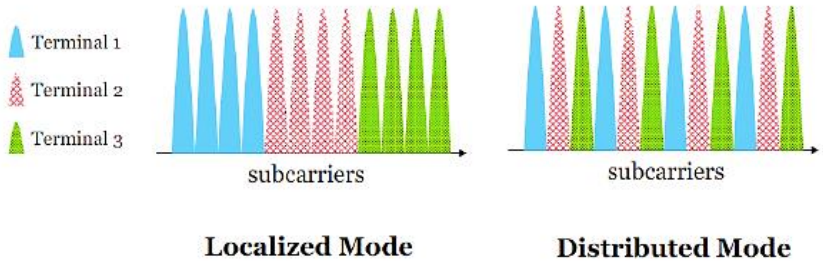

Figure 11: OFDMA subcarrier allocation types [47].

One of the main characteristics of the OFDM multiplexing scheme is the notion of orthogonality. The basic idea is that the channel bandwidth allocated is divided into multiple sub channels, in order to reduce Inter-Symbol Interference (ISI). Therefore, a single wideband signal is divided into several narrow band signals that are transmitted simultaneously over orthogonal subcarriers. This means that when one subcarrier reaches its maximum peak value, the others cross their zero point values and consequently avoiding interference between them [48] [49].

When transmitting a signal through air, it is affected by different phenomena such as reflection or diffraction, which can cause the receiver to receive different and delayed versions of the same signal, which leads to ISI, and hence the receiver is not able to decode properly the received symbols. To solve this issue, a guard time interval is added between each symbol, denominated Cyclic Prefix (CP). The CP consists on a copy from the last part of the symbol that is added to the beginning of the OFDM symbol itself, increasing its length. The duration of the extended OFDM symbol is:

$$T_{\text{extendedOFDM}} = T_{CP} + T_{OFDM} \tag{1.1}$$

The OFDMA transmitter and receiver diagram is depicted in figure 12. At the transmitter side, the bit stream is modulated into symbols with either Quadrature Phase Shift Keying (QPSK) or Quadrature Amplitude Modulation (QAM) modulation. If QPSK is used, the result is 2 bits/symbol. With QAM, there are 4 bits/symbol if 16-QAM is used and 6 bits/symbol if 64QAM is used. Inverse Fast Fourier Transformation

(IFFT) is applied to transform a discrete sequence of sinusoids from the frequency domain to time domain. Lastly, CP is added to ensure that ISI is removed.

At the receiver side, firstly the CP is removed. Then, Fast Fourier Transformation (FFT) is applied to transform the function from time domain to frequency domain, into a sequence of sinusoids. An equalizer may be used to eliminate channel effects. Finally, the symbols are demodulated, and the initial bit stream is obtained.

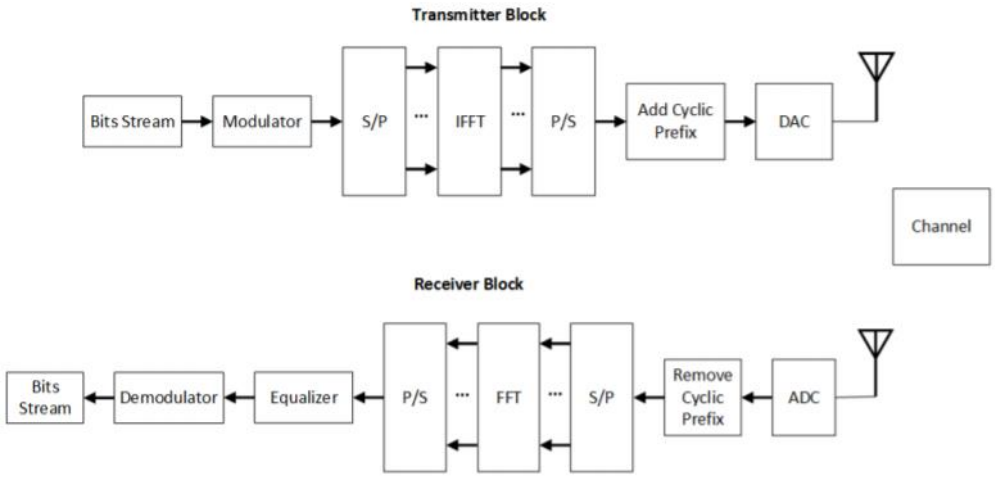

Figure 12: OFDMA transmitter and receiver diagram [50].

The main advantages of using OFDMA are robustness against ISI and fading, high spectrum efficiency and an effective implementation due to the use of FFT. However, there is one main disadvantage associated to OFDMA: high Peak to Average Power Ratio (PAPR). This led 3GPP to choose another modulation scheme for uplink. Thus, the multiple access scheme selected for uplink in LTE systems is SC-FDMA [51].

SC-FDMA is a modified form of OFDMA, that improves dramatically the PAPR in comparison to OFDM. This leads to a reduction on the power amplifiers for the mobile and also to an increased coverage. The main difference between OFDMA and SC-FDMA is the way symbols are transmitted. In OFDM, the symbols are transmitted in parallel, while in SC-FDMA, these are sent in series [52] [53].

The evolution of mobile communication systems does not stop at LTE. In 2011, 3GPP Release 10 brought LTE-Advanced (LTE-A), with further improvements in 3GPP Release 11. LTE-A is the evolution of LTE, aiming to achieve increased peak and user experienced data rates, improved spectrum and network efficiency and an overall better performance of the system [54]. The main requirements proposed by 3GPP for LTE-A are the following:

- Peak data rates of up to 1 Gbps when considering low mobility and up to 100 Mbps when considering high mobility, for DL. For UL, up to 500 Mbps;
- Peak spectrum efficiency of 30 bit/s/Hz for DL and 15 bit/s/Hz for UL;

- Capacity and cell-edge throughput increase between 1.4 and 1.6 when compared to LTE.

The main Radio Access Network (RAN) features introduced in 3GPP Release 10 for LTE-A, in order to be able to reach the above-mentioned key requirements, are as follows [55] [56]:

- Carrier Aggregation (CA): a technique that allows spectrum aggregation in order to have a wider bandwidth, resulting in a throughput increase and hence higher peak data rates and more spectrum flexibility;
- Extended Multiple Input Multiple Output (MIMO): the use of multiple antennas at both the transmitter and receiver side extended to 8x8 MIMO for DL and 4x4 MIMO for UL, improving peak data rates, throughput and capacity;
- Coordinated Multi Point (CoMP) transmission for both UL and DL, increasing cell edge user throughput and enhancing coverage;
- Enhancements in Self Organizing Network (SON): enhancements of automatization and configuration of networks, leading to a more flexible network and more adaptable to varying radio conditions.

The development of mobile communication systems continuously delivers new features, improvements and increased target values. Figure 13 depicts the predicted traffic grow from 2010 to 2030. The next mobile generation, the Fifth Generation (5G), is expected to revolutionize our society, having extremely high expectations and demands from both users and operators' point of view.

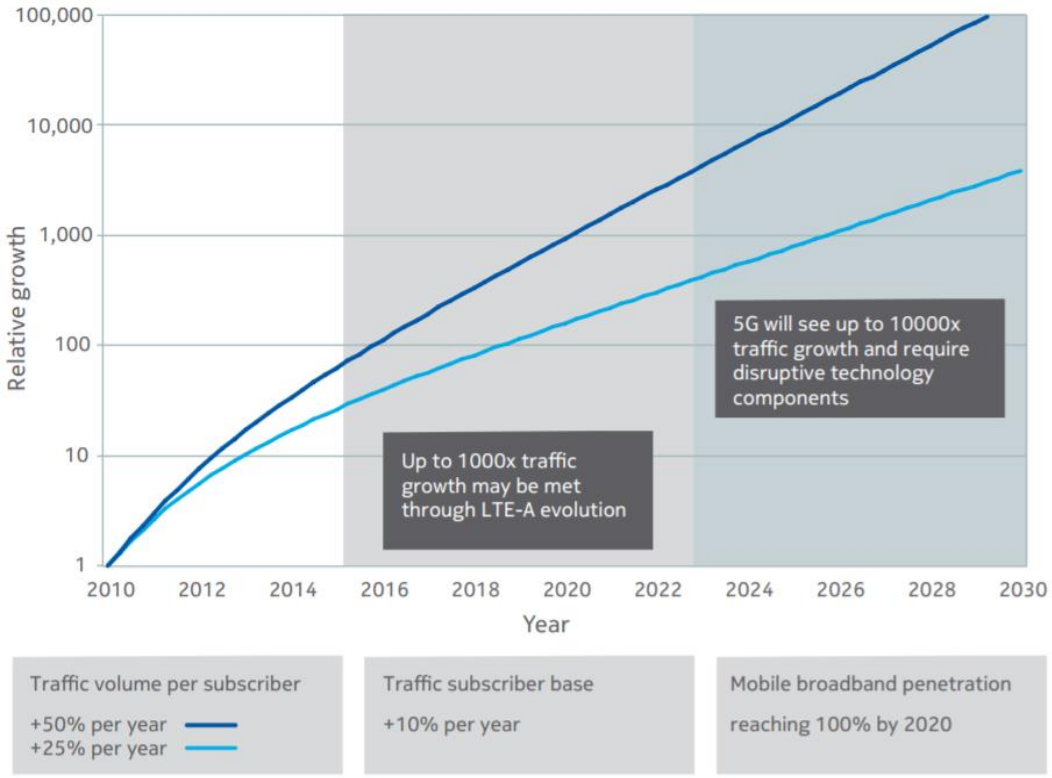

Figure 13: Predicted traffic growth towards 2030. Source: Nokia white paper [57]

1.2 Objectives and Motivations

Since the appearance of the first mobile phone and the first mobile generation, there has been a continuous increase on the number of mobile users, connected devices, new modulation techniques, features and other improvements within the mobile communication research field.

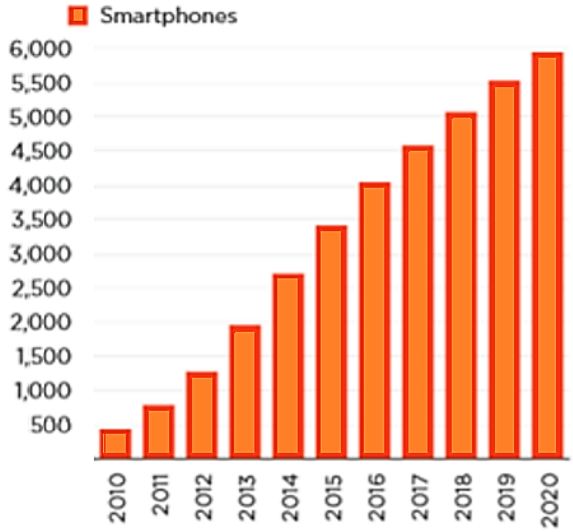

Figure 14: Global connections (in million). Source: GSMA Intelligence [58]

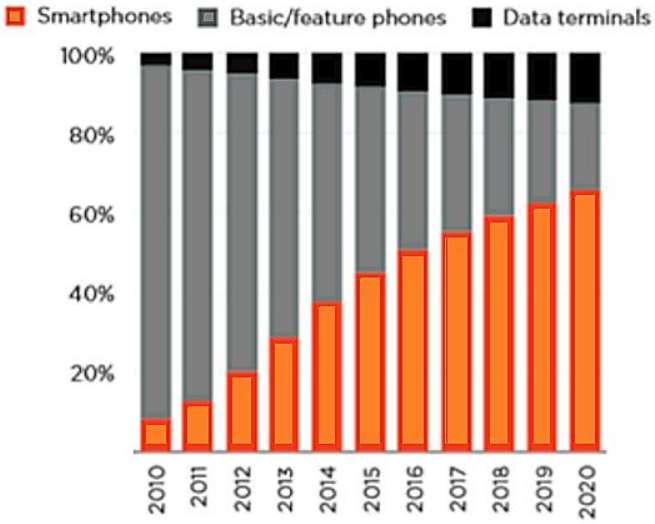

Figure 15: Percentage of global connections. Source: GSMA Intelligence [58]

Figures 14 and 15 portray the continuous grow from the last 10 years. It is noticeable how the smartphone has become a necessity in society. This trend is going to continue, and the number will continuously increase with the appearance of the next generation, 5G. Therefore, research on 5G is tremendously significant, the topic is novel with several sub-domains and in constant development.

The objectives of this thesis is to further contribute on the research of 5G communication systems. Specifically, it focuses on the study of proposed channel models for 5G systems, the use of digital beamforming techniques and massive MIMO, the evaluation of the multi-numerology proposed for 5G, and the study of dynamic

spectrum sharing, a 5G novel feature that improves spectrum efficiency and reduces cost from the operator's point of view. All these topics have the major goal of optimizing the performance of 5G communication systems. The research is realized with the support of Nokia Networks, using equipment and simulation tools from Nokia.

1.3 Thesis Outline

This thesis started with an introduction of the background and evolution of mobile communication systems and stated the objectives and motivations of the research. The remaining chapters are structured as follows:

Chapter 2 introduces the next mobile generation, 5G. It discusses the proposed requirements, challenges and key technologies of 5G communication systems. It performs a comparison between the actual mobile generation, 4G, and 5G, in terms of requirements and performance, multiplexing techniques, spectrum use, network architecture and applications.

In chapter 3, we discuss channel modeling for 5G systems. Specifically, two channel profiles proposed by 3GPP for the next generation systems are studied. The performance of a 5G system is evaluated using the respective channel models. Additionally, the influence of delay spread on the 5G system is investigated.

In chapter 4, we focus on digital beamforming techniques for 5G. Firstly, the eigen based beamforming and grid of beams beamforming techniques are described. Following, we analyze the performance in different 5G environment scenarios of these two beamforming techniques and perform a comparison of their performance.

Chapter 5 focuses on 5G numerology. The concept of multi-numerology is explained and the performance evaluation of an OFDM multi-numerology for 5G communication systems is analyzed.

Following, in chapter 6, we introduce the concept of dynamic spectrum sharing in 4G/5G networks. Two phases of the feature are studied, and their impact on the network is evaluated, analyzing how it can improve the spectrum efficiency and other target values of 5G communication systems.

Lastly, chapter 7 provides the thesis concluding remarks, contributions and future research work guidelines.

1.4 Research Publications

The main contributions of this thesis originated the following published articles:

1. **G. Barb** and M. Otesteanu, "5G: An Overview on Challenges and Key Solutions," 2018 International Symposium on Electronics and Telecommunications (ISETC), Timisoara, 2018, pp. 207-210, ISBN: 978-1-5386-5925-0.
2. **G. Barb**, M. Otesteanu, G. Budura and C. Balint, "Performance Evaluation of TDL Channels for Downlink 5G MIMO Systems," 2019 International Symposium on Signals, Circuits and Systems (ISSCS), Iasi, Romania, 2019, ISBN: 978-1-7281-3896-1.
3. A. Mamane, M. E. Ghazi, **G. Barb** and M. Oteșteanu, "5G Heterogeneous Networks: An Overview on Radio Resource Management Scheduling Schemes," 2019 7th Mediterranean Congress of Telecommunications (CMT), Fès, Morocco, 2019, ISBN: 978-1-7281-4420-7.
4. **G. Barb** and M. Otesteanu, "On the Influence of Delay Spread in TDL and CDL Channel Models for Downlink 5G MIMO Systems," 2019 IEEE 10th Annual Ubiquitous Computing, Electronics & Mobile Communication Conference (UEMCON), New York City, NY, USA, 2019, pp. 958-962, ISBN: 978-1-7281-3885-5.
5. **G. Barb** and M. Otesteanu, "4G/5G: A Comparative Study and Overview on What to Expect from 5G," *2020 43rd International Conference on Telecommunications and Signal Processing (TSP)*, Milan, Italy, 2020, pp. 37-40, ISBN: 978-1-7281-6376-5.
6. **G. Barb**, M. Otesteanu, F. Alexa and A. Ghiulai, "Digital Beamforming Techniques for Future Communications Systems," *2020 12th International Symposium on Communication Systems, Networks and Digital Signal Processing (CSNDSP)*, Porto, Portugal, 2020, ISBN: 978-1-7281-6743-5.
7. **G. Barb**, M. Otesteanu, F. Alexa and F. Danuti, "OFDM Multi-Numerology for Future 5G New Radio Communication Systems," 2020 International Conference on Software, Telecommunications and Computer Networks (SoftCOM), Split, Hvar, Croatia, 2020, ISBN: 978-953-290-099-6.
8. **G. Barb**, M. Otesteanu and M. Roman, "Dynamic Spectrum Sharing for LTE-NR Downlink MIMO Systems," 2020 International Symposium on Electronics and Telecommunications (ISETC), Timisoara, 2020, ISBN: 978-1-7281-9513-1.
9. **G. Barb** and M. Otesteanu, "Digital GoB-based Beamforming for 5G Communication Systems," 2020 International Symposium on Antennas and Propagation (ISAP), Osaka, Japan, 2020.

From the above presented papers, all of them are IEEE indexed, 4 are WoS indexed, and the remaining 5 papers were published at conferences that were in previous years WoS indexed. In addition, one of the papers published with this research was quoted in IEEE Access (magazine ISI indexed Q1).

2. The 5th Generation of Mobile Communication Systems

It is well known that presently our society strives for a more and more connected world, with the number of devices, users and traffic growing exponentially. Furthermore, mobile communications are no longer focused only for users, but also for machines, industry and things. It is clear that the actual generation cannot sustain the changes, requirements, and new technologies that are being introduced.

5G New Radio (NR) is the next generation of mobile communication systems which has started to be commercially available by the end of 2020. Unlike the previous generations, 5G will revolutionize our society and the expectations are extremely high. It is expected that 5G will be accompanied by massive changes, interconnect billions of users and devices and support enormously high data transfer rates [59].

This chapter discusses the 5th generation of mobile communication systems. The need for 5G is explained, the timeline of the standardization procedure is described, the principal use cases, key requirements and technologies are detailed. Furthermore, the network architecture and respective functions are presented.

2.1 5G Use Cases

There are 3 main potential use cases defined for the next mobile generation, see figure 16 [60]:

- Extreme Mobile Broadband: offering improved end-user experience and extremely high data transfer rates;
- Critical Machine Communication: offering ultra-reliability and availability for critical missions and enabling remote control over machines/robots;
- Massive Machine Communication: connecting billions of objects, devices and sensors.

Extreme mobile broadband or also known as Enhanced Mobile Broadband (eMBB) focuses on delivering gigabytes of data whenever necessary, on demand. In addition, it aims at offering an improved end-user experience regardless of the user location. The necessity for this use case is justified by the fact that the need for further mobile broadband is continuously increasing. This will lead to new applications and technologies on the market, a better performance of the system and improved user experience.

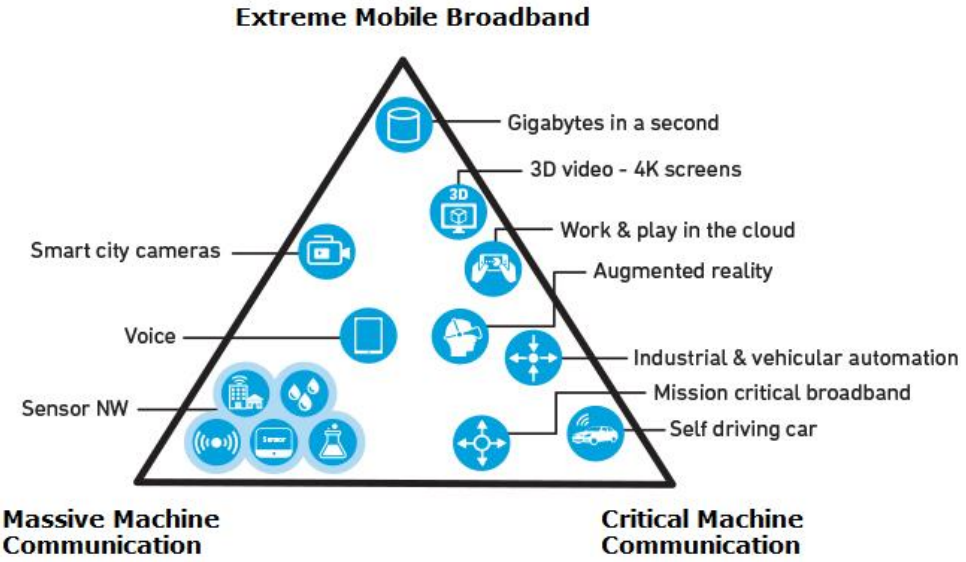

Figure 16: 5G potential use cases [61].

Critical machine communication or also known as Ultra-Reliable and Low Latency Communication (URLLC) focuses on instant availability, extreme low latency and an ultra-reliable communication, in order to control remote devices, sensors and robots, for applications such as medical surgery, emergency communication, connected cars and automated industry robots [62].

Massive machine communication or also known as Massive Machine Type Communication (mMTC) focuses on the massive connection between billions of machines and sensors. These objects will typically transmit low quantities of data with no delay and are expected to be low cost with a long battery life. An example of its application could be the positioning of fire sensors in areas where the danger of forest fires is high or the positioning of water sensors for inspecting and managing water quality [63].

New use cases will appear in the near future, demanding additional requirements and even more flexibility.

2.2 Proposed Requirements

The above-mentioned use cases proposed for the next mobile generation led to the creation of a variety of system requirements that need to be respected and achieved. The definition of these requirements by the standardization bodies is already completed, and they include high data transfer rates, high spectral and energy efficiency, low latency, increased capacity and mobility, low energy consumption and reduced costs.

The key requirements established for 5G are depicted in the spider chart of figure 17, with a comparison with the requirements of LTE-A, so we can have an idea of the improvements imposed. These target values can be further modified, depending on the advances in research and investigations. The main 8 5G performance requirements proposed are [64] [65]:

- Peak data rates: it represents the maximum value for the data transfer rates that can be achieved in an ideal environment. It is expected to reach values up to 20 Gbps. Figure 18 depicts the exponential increase of peak data rates compared to the actual and previous generations;
- User experienced data rates: it represents the average value for the data transfer rates in a certain coverage area of a mobile user. Around 100 Mbps are expected to be achieved. See figure 18 for the increase of the user experience data rates in comparison to previous mobile generations;
- Spectrum efficiency: measured in bits/s/Hz, it represents the amount of data transmitted per unit of spectrum resource and it is expected to be 3 times higher than the value reached by LTE-A;
- Mobility: it represents the maximum speed that can be obtained, according to a certain QoS and it is expected to reach values up to 500 km/h;
- Latency: it is defined as the time needed from when a data packet is sent until it reaches the destination. 5G will support latency values lower than 1 ms;
- Connection density: it represents the total number of connected devices per km^2;
- Network energy efficiency: measured in bit/J, it represents the amount of information bits that can be transmitted per unit of energy consumption and it is expected to be 100 times higher than for LTE-A;
- Area traffic capacity: it represents the generated traffic over a defined geographical area, with expected values up to 10 $Mbps/m^2$.

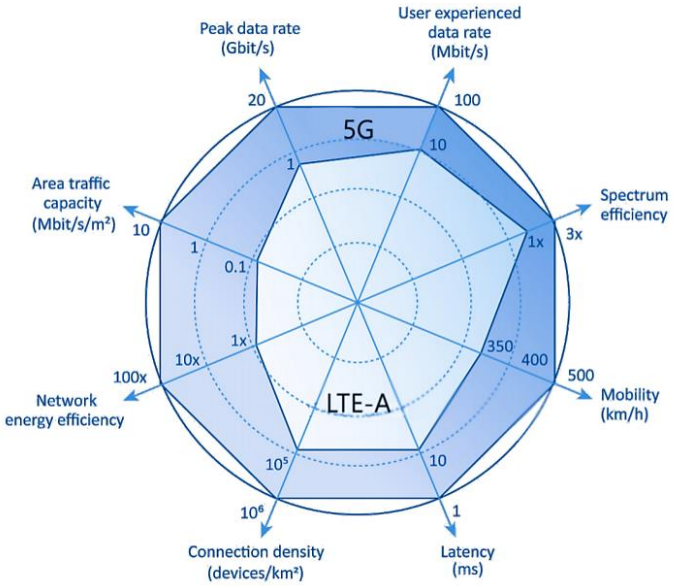

Figure 17: 5G Performance Requirements. Source: European Telecommunications Standards Institute

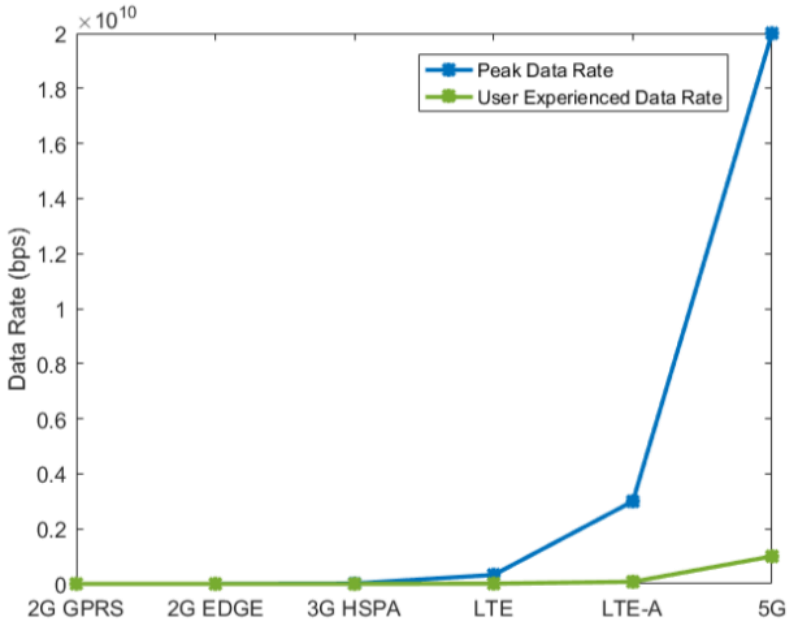

Figure 18: Peak and user experience data rate [66].

2.3 Standardization and Roll-Out

2020 is the year 5G is having its roll-out. The standardization process has been divided into two releases, in order to facilitate the entire procedure – 3GPP Release 15 and 3GPP Release 16 – representing Phase 1 and Phase 2, respectively [67].

Phase 1 contains the technical specifications of the network architecture of 5G communication systems. Furthermore, it contains specifications associated with the eMBB and URLLC use cases. Phase 2 is dedicated to the specifications for the mMTC use cases but also introduces further enrichments to Phase 1 specifications.

Figure 19 depicts the roadmap and timeline of the standardization process. Even though the research on 5G started in 2012, the interest for the next mobile generation started growing around 2014. Between the end of 2017 and end of 2019, 3GPP investigated and established the first set of standards regarding system requirements, key target values and network architecture, defined in the 3GPP Release 15 Phase 1. Following, between 2019 and June 2020, the second set of standards was finalized, accompanied with enhancements regarding Release 15 [68].

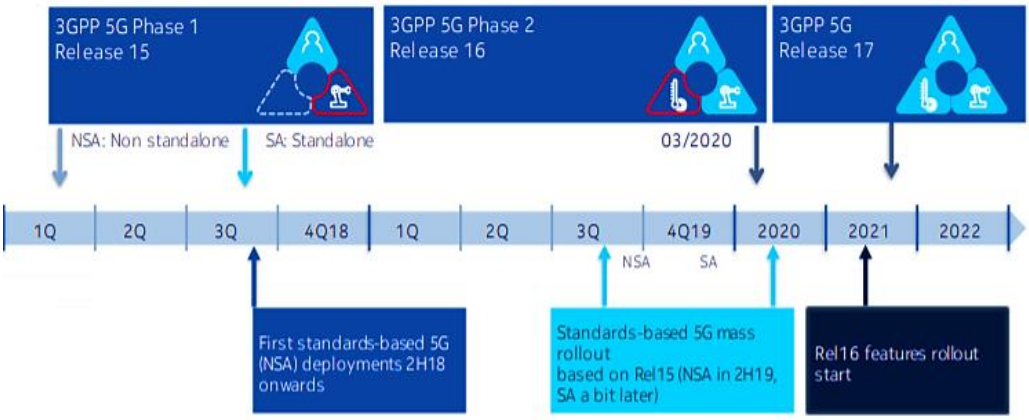

Figure 19: 5G Timeline. Source: Nokia [69]

The list of the main 3GPP specifications with the associated technical specification report are presented in table 3.

System Requirements	Service requirements for next generation new services and markets	TS 22.261
System Architecture	System architecture for the 5G system	TS 23.501
	Procedures for the 5G system	TS 23.502
	Security architecture and procedures for 5G system	TS 33.501
	NRL NR and NG-RAN overall description	TS 38.300
	NR; Multi-connectivity; Overall description	TS 37.340
	NG-RAN architecture description	TS 38.401
Protocols	NG-RAN; NG Application protocol	TS 38.413
	Non-access-stratum protocol	TS 24.501

Table 3: 3GPP Specifications [70].

2.4 Network Architecture

The current network architecture is known as a "one-size-fits-all" solution, and it is not suitable for the next mobile generation, since it cannot accommodate all the system requirements, target data values, new technologies and capabilities that 5G will support.

3GPP has designed new architectures options to help achieve extremely high data transfer rates, low latency, increased spectrum and energy efficiency, high mobility, for the new services and applications to be deployed. There are two main options for the 5G network architecture proposed by 3GPP: Non-standalone (NSA) and Standalone (SA). Each is described individually below [71].

NSA solution

The NSA architecture solution is based on the legacy EPC of LTE and uses LTE interfaces. It is not a full 5G network as it relays on the LTE core network. It is viewed as an intermediary solution to satisfy operator's short-term objectives, with low impact on the existing network architecture [72]. The main variations of the NSA solution are option 3, 3a, 3x, 4, 4a, 7 and 7a.

Figure 20 depicts the option 3 family options. It can be observed that:

- The core network is the legacy LTE EPC;
- Control plane and user plane use LTE S1 interface;
- 5G base station, referred to as 5G gNodeB or gNB, needs to support the LTE interfaces;
- The LTE eNodeB acts as a master node and the 5G gNodeB as secondary/slave node;
- Control plane is routed through master eNodeB towards secondary gNodeB;
- User plane is routed either directly to the secondary gNodeB (option 3x) or via master eNodeB (options 3,3a).

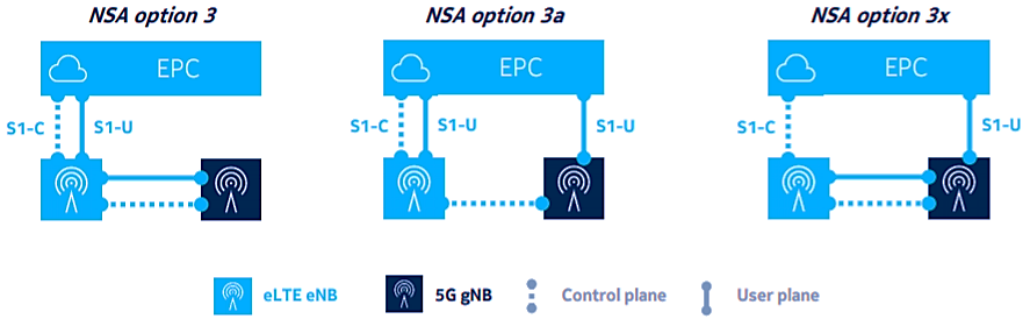

Figure 20: NSA option 3,3a and 3x [44].

Figure 21 depicts the options 4 and 4a. It can be observed that:

- The core network is the 5G Next Generation Core (NGC);
- Control plane and user plane use 5G Next Generation (NG) interfaces;
- LTE eNodeB needs to support 5G interfaces;
- The 5G gNodeB acts as a master node and the LTE eNodeB as secondary/slave node;
- Control plane is routed through master gNodeB towards secondary eNodeB;
- User plane is routed either through master gNodeB towards secondary eNodeB (option 4) or directly to secondary eNodeB (option 4a).

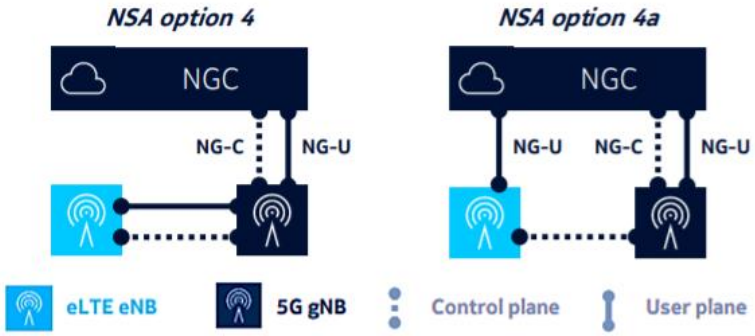

Figure 21: NSA option 4 and 4a [44].

Figure 22 depicts the options 7 and 7a, which are similar to options 4 and 4a. It can be observed that:

- The core network is the 5G NGC;
- Control plane and user plane use 5G NG interfaces;
- LTE eNodeB needs to support 5G interfaces;
- The LTE eNodeB acts as a master node and the 5G gNodeB as secondary/slave node;
- Control plane is routed through master eNodeB towards secondary gNodeB.
- User plane is routed either through master eNodeB towards secondary gNodeB (option 7) or directly to secondary gNodeB (option 7a) [73].

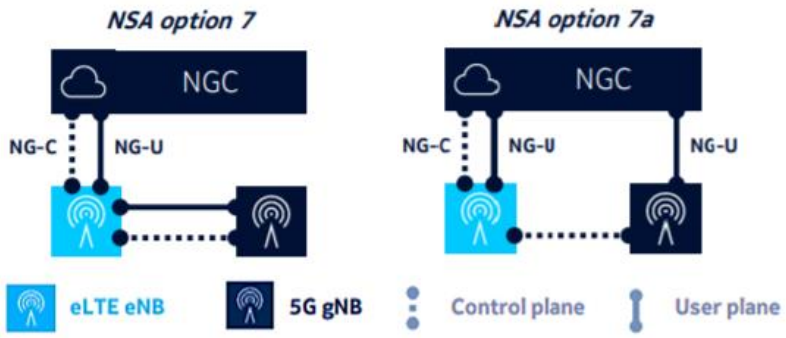

Figure 22: NSA options 7 and 7a [44].

SA solution

The SA architecture solution, contrary to the NSA solution, does not depend on the LTE legacy architecture and uses the NGC core with 5G interfaces. 3GPP has defined two main SA solutions: option 2 and 5, depicted in figure 23. As it can be observed, the network architecture is much simpler, which leads to an improvement on its efficiency [74].

Figure 23: SA options 2 and 5 [44].

For both types of architecture solutions, 5G NR brings new channels and signals for the physical layer. The physical channels defined for DL are:

- Physical Downlink Shared Channel (PDSCH);
- Physical Downlink Control Channel (PDCCH);
- Physical Broadcast Channel (PBCH).

As for the physical signals defined for DL, they are as follows:

- Demodulation reference signals (DMRS), for PDSCH and PBCH;
- Phase-tracking reference signals (PTRS);
- Channel-state information reference signal (CSI-RS);
- Primary synchronization signal (PSS);
- Secondary synchronization signal (SSS).

For UL, the defined physical channels are:

- Physical Random Access Channel (PRACH);
- Physical Uplink Shared Channel (PUSCH);
- Physical Uplink Control Channel (PUCCH).

The following UL physical channels are defined:

- Demodulation reference signals, DMRS;
- Phase-tracking reference signals, PTRS;
- Sounding reference signal (SRS).

2.5 5G Key Technologies and Principles

2.5.1 5G Spectrum Options

The frequency spectrum is a scarce and limited resource that is becoming saturated. In order to reach the key requirements proposed for 5G, or to handle the exponentially growing traffic, number of connected devices, and the new and future applications, there is the need for new available spectrum. Presently, the frequency spectrum used for mobile communications is mainly located between 300 MHz and 3 GHz [75]. It is expected for 5G to use frequency bands between 300 MHz and up to 90 GHz or even higher.

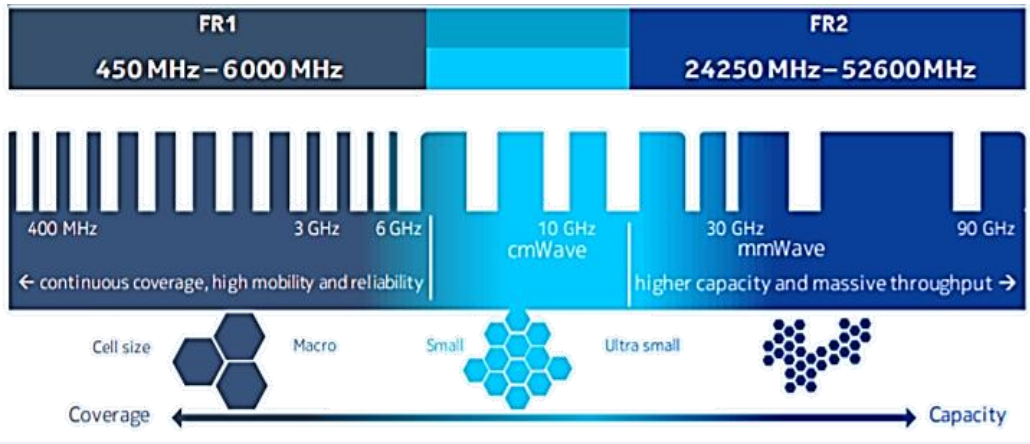

Figure 24: Frequency range designation [69].

3GPP has defined in Release 15 two types of Frequency Range (FR) for 5G systems: FR 1, below 6 GHz, and FR 2, between 24 and 52 GHz. As it can be observed in figure 24, operating bands in FR 1 are intended for use cases that need to provide continuous wide area coverage and high mobility and reliability. The cell size decreases as the frequency spectrum increases. Hence, operating bands in FR 2 are intended to provide increased capacity and higher data transfer rates.

The millimeter waves (mmW), consisting on spectrum between 30 and 300 GHz, are being widely investigated due to the massive frequency spectrum that could potentially be used for the next mobile generation. However, not all the spectrum can be utilized for mobile systems. In particular, the bands 57-64 GHz and 164-200 GHz are not suitable to be used, due to the propagation characteristics of mmW, as they suffer from atmospheric and molecular absorption. The main advantages of mmW consist on the substantial available frequency spectrum that can potentially be used for 5G systems, the ultra small antenna size and the narrow beam width that offers interference resistance [76] [77]. There is already a vast number of defined operating

frequency bands for 5G systems. The tables 4 and 5 depict the operating bands specified in the 3GPP Release 15.

	Operating Band	Uplink	Downlink	Duplex Mode
FR 1	1	1920 – 1980 MHz	2110 – 2170 MHz	FDD
	2	1850 – 1910 MHz	1930 – 1990 MHz	FDD
	3	1710 – 1785 MHz	1805 – 1880 MHz	FDD
	5	824 – 849 MHz	869 – 894 MHz	FDD
	7	2500 – 2570 MHz	2620 – 2690 MHz	FDD
	8	880 – 915 MHz	925 – 960 MHz	FDD
	20	832 – 862 MHz	791 – 821 MHz	FDD
	28	703 – 748 MHz	758 – 803 MHz	FDD
	38	2570 – 2620 MHz	2570 – 2620 MHz	TDD
	41	2496 – 2690 MHz	2496 – 2690 MHz	TDD
	50	1432 – 1517 MHz	1432 – 1517 MHz	TDD
	51	1427 – 1432 MHz	1427 – 1432 MHz	TDD
	66	1710 – 1780 MHz	2110 – 2200 MHz	FDD
	70	1695 – 1710 MHz	1995 – 2020 MHz	FDD
	71	663 – 698 MHz	617 – 652 MHz	FDD
	74	1427 – 1470 MHz	1475 – 1518 MHz	FDD
	75	N/A	1432 – 1517 MHz	SDL
	76	N/A	1427 – 1432 MHz	SDL
	77	3.3 – 4.2 GHz	3.3 – 4.2 GHz	TDD
	78	3.3 – 3.8 GHz	3.3 – 3.8 GHz	TDD
	79	4.4 – 5.0 GHz	4.4 – 5.0 GHz	TDD
	80	1710 – 1785 MHz	N/A	SUL
	81	880 – 915 MHz	N/A	SUL
	82	832 – 862 MHz	N/A	SUL
	83	703 – 748 MHz	N/A	SUL
	84	1920 – 1980 MHz	N/A	SUL

Table 4: FR 1 operating bands for 5G systems.

	Operating Band	Uplink	Downlink	Duplex Mode
FR 2	257	26.5 – 29.5 GHz	26.5 – 29.5 GHz	TDD
	258	24.25 – 27.5 GHz	24.25 – 27.5 GHz	TDD
	260	37 – 40 GHz	37 -40 GHz	TDD

Table 5: FR 2 operating bands for 5G systems.

To note that in both tables, besides the well-known duplex modes FDD and TDD, there are some operating bands that use Supplementary Downlink (SDL) bands and Supplementary Uplink (SUL) bands.

2.5.2 Massive MIMO and Beamforming

Multiple input multiple output is a technique that is vastly used in mobile communication systems, that is defined by the use of several antennas at both the

transmitter and receiver side. The main advantages of using MIMO systems are the major increase on capacity and robustness. Presently, the majority of MIMO systems have up to 8 antennas [78].

Massive MIMO is an extension of the MIMO technique, comprising a much higher number of antennas, reaching up to 100. The network capacity and robustness are increased dramatically, and hence it is viewed as a promising technique for the future mobile generations. The use of massive MIMO in 5G communication systems has two main goals, see figure 25. The first one consists on providing the necessary coverage when using frequency bands over 6 GHz, since the propagation loss is much higher than in the case of frequency bands below 6 GHz. If we compare a LTE system transmitting over the 3 GHz band and a 5G system in the 28 GHz band, the attenuation suffered for the second case can be up to 100 times higher than in the LTE case [79]. The second goal of the use of massive MIMO with 5G systems is to increase the spectral efficiency up to 3 times compared to LTE systems [80].

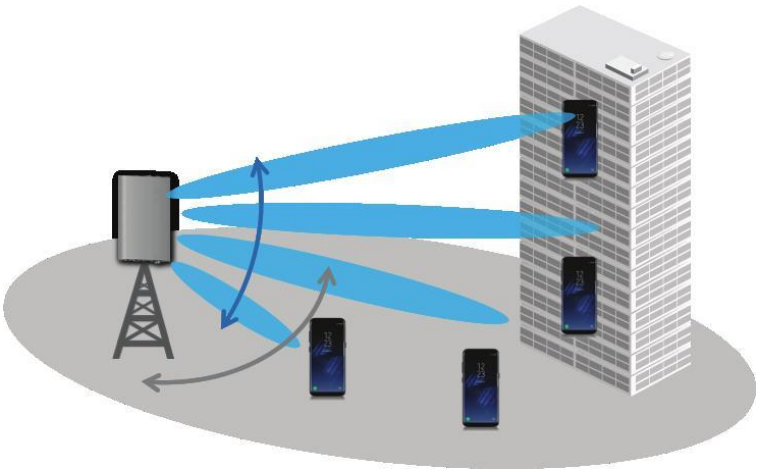

Figure 25: Massive MIMO and beamforming [81].

Beamforming is a well known technology that has recently attracted the interest of researchers for its usability in the mobile communications field, due to the fact that, together with massive MIMO, can bring several improvements and advantages [82]. Beamforming is defined as a signal processing technique that varies the amplitude and phase of one or more beams in order to direct the transmitting or receiving signal in a specific desired direction, so that we obtain the optimal gain. There are three types of beamforming [83]:

- Analog beamforming: the same signal is sent over the different antennas, although phase shifters are used so that the phases of the signal for each antenna are not equal. The variation of the amplitude and phase is performed on the transmitting side. At the receiver, the signals received from the different antennas are summed before the Digital-to-Analog Conversion (DAC);

- Digital beamforming: the variation of amplitude and phase is performed on the digital signal, at the transmitting side, before the Analog-to-Digital Conversion (ADC);
- Hybrid beamforming: a combination of analog and digital beamforming, where the different phases are combined in the analog domain, while the beam formation is performed in the digital domain [84] [85].

2.5.3 Multiple Access and Multiplexing Techniques

As introduced earlier, LTE uses OFMDA for downlink and SC-FDMA for uplink, as preferred multiple access schemes. Even though both of these techniques are stable, provide a good reliability and will be used for the first deployments of 5G communication systems, new techniques are being investigated and exploited to be used for the future mobile generation systems [86]. The techniques that have shown the most promising results are described individually below [44].

FBMC

Filter Bank Multicarrier (FBMC) is a multicarrier technique based on OFDM. In OFDM, the CP, a copy from the last part of the symbol that is added to the beginning of the symbol itself, is added in order to avoid ISI. The drawback is that the addition of the CP leads to an inefficient use of the frequency spectrum available. As the spectrum is already a scarce resource and represents a challenge for 5G systems, it is not at all desirable.

In order to solve the issue of the inefficient use of the spectrum due to the presence of the CP, FBMC adds to the OFDM structure two filtering blocks besides the IFFT/FFT blocks, one at the transmitter side and one at the receiver side. The filtering blocks represent a frequency-shifted variation of a low pass filter. At the transmitter side, a synthesis filter is used. At the receiver side, an analysis filter is applied. This way, ISI can be reduced significantly, without the need of using the CP [87]. In conclusion, spectrum efficiency is increased, at the cost of an increase of approximately 30% on complexity.

GFDM

Generalized Frequency Division Multiplexing (GFDM) is a multicarrier scheme, that, as OFDM, uses CP. The difference is that, in OFDM, the CP needs to be longer than the channel impulse response, while in GFDM, the CP needs to be longer than the impulse responses of the transmitter, receiver and channel filters. In order to reduce the length of the CP and hence improve spectrum efficiency, a technique denominated "tail-biting" is applied, which means that the impulse response of the transmitter filter is not considered. Consequently, the length of the CP needs to be longer than impulse responses of the receiver and the channel filters only. The GFDM technique allows the transmission of parallel streams of data on subcarriers that do not need to be necessarily adjacent. Therefore, it is a convenient technique to be used in environments with fragmented spectrum [88].

FTN

Faster-than-Nyquist (FTN) is a technique that reduces the spacing between adjacent symbols in the time domain. When considering the frequency domain, it envelops adjacent subcarriers, being no longer independent. This leads to an increase in the transmission rate. However, if the spacing between symbols is reduced, the orthogonality property is lost, which contributes to major ISI. The interference can be controlled with the addition of error coding algorithms at the receiver side [89].

CR and NOMA

Cognitive Radio (CR) is defined as a technology that uses dynamic spectrum access/sharing. It allows a secondary user to access and utilize licensed spectrum that is primordially intended for a primary user, when it is not being used by it.

Non-Orthogonal Multiple Access (NOMA) is a multiple access scheme based on multiplexing in the power domain. This means that the different users share the same resources, such as time, frequency and code, and each signal is distinguished at the receiver side by using successive interference cancellation.

Combining these two technologies together leads to a more efficient use of the available frequency spectrum [90] [91].

The information from this chapter resulted in the publication of two overview papers:

1. G. Barb and M. Otesteanu, "5G: An Overview on Challenges and Key Solutions," 2018 International Symposium on Electronics and Telecommunications (ISETC), Timisoara, 2018, pp. 207-210, ISBN: 978-1-5386-5925-0.

2. G. Barb and M. Otesteanu, "4G/5G: A Comparative Study and Overview on What to Expect from 5G," 2020 43rd International Conference on Telecommunications and Signal Processing (TSP), Milan, Italy, 2020, pp. 37-40, ISBN: 978-1-7281-6376-5.

3. Channel Modeling for 5G Systems

Channel modeling constitutes an important parameter when developing a 5G communication system and it is necessary in order to provide accuracy and to be intuitive, while being based on how the system would behave in a real-life environment scenario. These are important characteristics since the channels selected that are used to study and perform simulations are fundamental for the system design of 5G networks. Therefore, new channel models are being investigated in order to be used in the simulations for the research on 5G systems.

This chapter addresses two channel models proposed by 3GPP to be used for link-level simulations for the 5th generation of mobile communication systems. The channel models are initially described, then their performance is evaluated and analyzed in terms of Bit Error Rate (BER) and throughput. Following, the influence of the delay spread in these channels is investigated and the results obtained are evaluated. The simulations performed provide an understanding on how the performance of a 5G system is affected based on the channel model adopted.

3.1 Channel Models for Link-level Simulations

3GPP released a technical specification report for the Release 14 - TR. 138.901 - with the study on channel models for frequencies from 0.5 up to 100 GHz intended for 5G technology. The goal is to assist in the modeling and evaluation of physical layer techniques while using suitable channel models. Specifically, for link-level simulations, the technical specification report presents two main channel models: Tapped Delay Line (TDL) and Clustered Delay Line (CDL).

3.1.1 TDL Channel Model

The TDL channel model has 5 different profiles: TDL_A, TDL_B and TDL_C, intended for Non-Line-of-Sight (NLOS) scenarios, and TDL_D and TDL_E, designed for Line-of-Sight (LOS) environment scenarios.

The channel impulse response of the TDL model with *N* number of taps can be defined as [92]

$$H(t,\tau) = \sum_{i=1}^{N} a_i(t)\delta(\tau - \tau_i) \tag{3.1}$$

where $a_i(t)$ is the amplitude at the delay τ_i for the i^{th} tap and $\delta(.)$ is the Dirac's delta function. The Doppler spectrum regarding each tap is defined with a Jake's spectrum form, and the maximum Doppler shift, f_D, is given by

$$f_D = \frac{|\bar{v}|}{\lambda_0} \tag{3.2}$$

where $\bar{v}$ is the vector that represents the velocity and λ_0 is the wavelength of the carrier frequency. The TDL channel model is designed to be used in Single-Input-Single-Output (SISO) systems, although it can be extended for MIMO link-level simulations. For such, the extension can be obtained by adding a correlation matrix to the TDL model [93]. The tables 6, 7 and 8 present the characteristics of the three TDL models designed for NLOS scenarios.

Tap #	Normalized delay	Power in [dB]	Fading distribution
1	0.0000	-13.4	Rayleigh
2	0.3819	0	Rayleigh
3	0.4025	-2.2	Rayleigh
4	0.5868	-4	Rayleigh
5	0.4610	-6	Rayleigh
6	0.5375	-8.2	Rayleigh
7	0.6708	-9.9	Rayleigh
8	0.5750	-10.5	Rayleigh
9	0.7618	-7.5	Rayleigh
10	1.5375	-15.9	Rayleigh
11	1.8978	-6.6	Rayleigh
12	2.2242	-16.7	Rayleigh
13	2.1718	-12.4	Rayleigh
14	2.4942	-15.2	Rayleigh
15	2.5119	-10.8	Rayleigh
16	3.0582	-11.3	Rayleigh
17	4.0810	-12.7	Rayleigh
18	4.4579	-16.2	Rayleigh
19	4.5695	-18.3	Rayleigh
20	4.7966	-18.9	Rayleigh
21	5.0066	-16.6	Rayleigh
22	5.3043	-19.9	Rayleigh
23	9.6586	-29.7	Rayleigh

Table 6: TDL_A characterization. Source: 3GPP TR 138.901

Tap #	Normalized delay	Power in [dB]	Fading distribution
1	0.0000	0	Rayleigh
2	0.1072	-2.2	Rayleigh
3	0.2155	-4	Rayleigh
4	0.2095	-3.2	Rayleigh
5	0.2870	-9.8	Rayleigh
6	0.2986	-1.2	Rayleigh
7	0.3752	-3.4	Rayleigh
8	0.5055	-5.2	Rayleigh
9	0.3681	-7.6	Rayleigh
10	0.3697	-3	Rayleigh
11	0.5700	-8.9	Rayleigh
12	0.5283	-9	Rayleigh
13	1.1021	-4.8	Rayleigh
14	1.2756	-5.7	Rayleigh
15	1.5474	-7.5	Rayleigh
16	1.7842	-1.9	Rayleigh
17	2.0169	-7.6	Rayleigh
18	2.8294	-12.2	Rayleigh
19	3.0219	-9.8	Rayleigh
20	3.6187	-11.4	Rayleigh
21	4.1067	-14.9	Rayleigh
22	4.2790	-9.2	Rayleigh
23	4.7834	-11.3	Rayleigh

Table 7: TDL_B characterization. Source: 3GPP TR 138.901

Tap #	Normalized delays	Power in [dB]	Fading distribution
1	0	-4.4	Rayleigh
2	0.2099	-1.2	Rayleigh
3	0.2219	-3.5	Rayleigh
4	0.2329	-5.2	Rayleigh
5	0.2176	-2.5	Rayleigh
6	0.6366	0	Rayleigh
7	0.6448	-2.2	Rayleigh
8	0.6560	-3.9	Rayleigh
9	0.6584	-7.4	Rayleigh
10	0.7935	-7.1	Rayleigh
11	0.8213	-10.7	Rayleigh
12	0.9336	-11.1	Rayleigh
13	1.2285	-5.1	Rayleigh
14	1.3083	-6.8	Rayleigh
15	2.1704	-8.7	Rayleigh
16	2.7105	-13.2	Rayleigh
17	4.2589	-13.9	Rayleigh
18	4.6003	-13.9	Rayleigh
19	5.4902	-15.8	Rayleigh
20	5.6077	-17.1	Rayleigh
21	6.3065	-16	Rayleigh
22	6.6374	-15.7	Rayleigh
23	7.0427	-21.6	Rayleigh
24	8.6523	-22.8	Rayleigh

Table 8: TDL_C characterization. Source: 3GPP TR 138.901

TDL_A and TDL_B are composed by 23 taps, while TDL_C has 24 taps. All three profiles follow Rayleigh distribution. The normalized delay and relative power differ for each channel profile. For TDL_A, the relative power varies between -29.7 dB and 0 dB, being 0 dB at tap number 2, with a normalized delay of 0.3819. For TDL_B, the power varies between -12.2 dB and 0 dB, the latter being reached at the first tap, with a normalized delay of 0. Lastly, for TDL_C, the power varies between -22.8 dB and 0 dB, reaching 0 dB at tap number 6, with a normalized delay of 0.6366.

Tap #	Normalized delay	Power in [dB]	Fading distribution
1	0	-0.2	LOS path
	0	-13.5	Rayleigh
2	0.035	-18.8	Rayleigh
3	0.612	-21	Rayleigh
4	1.363	-22.8	Rayleigh
5	1.405	-17.9	Rayleigh
6	1.804	-20.1	Rayleigh
7	2.596	-21.9	Rayleigh
8	1.775	-22.9	Rayleigh
9	4.042	-27.8	Rayleigh
10	7.937	-23.6	Rayleigh
11	9.424	-24.8	Rayleigh
12	9.708	-30.0	Rayleigh
13	12.525	-27.7	Rayleigh
NOTE:	The first tap follows a Ricean distribution with a K-factor of K_1 = 13.3 dB and a mean power of 0dB.		

Table 9: TDL_D characterization. Source: 3GPP TR 138.901

Tap #	Normalized delay	Power in [dB]	Fading distribution
1	0	-0.03	LOS path
	0	-22.03	Rayleigh
2	0.5133	-15.8	Rayleigh
3	0.5440	-18.1	Rayleigh
4	0.5630	-19.8	Rayleigh
5	0.5440	-22.9	Rayleigh
6	0.7112	-22.4	Rayleigh
7	1.9092	-18.6	Rayleigh
8	1.9293	-20.8	Rayleigh
9	1.9589	-22.6	Rayleigh
10	2.6426	-22.3	Rayleigh
11	3.7136	-25.6	Rayleigh
12	5.4524	-20.2	Rayleigh
13	12.0034	-29.8	Rayleigh
14	20.6519	-29.2	Rayleigh
NOTE:	The first tap follows a Ricean distribution with a K-factor of K_1 = 22 dB and a mean power of 0dB.		

Table 10: TDL_E characterization. Source: 3GPP TR 138.901

TDL_D and TDL_E, designed for LOS environments, have 13 and 14 taps, respectively. The characteristics can be observed in tables 9 and 10. For TDL_D, the relative power varies between -30 dB and -0.2 dB, while for TDL_E the relative power varies between -29.8 dB and -0.03 dB. Since we are dealing with LOS scenarios, the first tap of both TDL_D and TDL_E profiles follows a Ricean fading distribution. Therefore, the Doppler spectrum for those taps has an additional peak at [94]

$$f_s = 0.7 f_D \tag{3.3}$$

where f_s is the additional Doppler shift, with an amplitude so that the Ricean distribution has a certain specified K-factor, that can be modified to a desired factor value. If this is the case, firstly there is the need to determine the tap relative power, P_{n_scaled}, for the taps that follow Rayleigh distribution [94]

$$P_{n\_scaled} = P_{n\_inital} - K_{desired} + K_{initial} \tag{3.4}$$

where P_{n_inital} is the power of the *n* tap as specified in the tables above. The $K_{initial}$ is calculated by [94]

$$K_{initial} = P_{1\_initial}^{LOS} - 10log_{10}\left(\sum_{n=1}^{N} 10^{\frac{P_{n\_initial}}{10}}\right) \tag{3.5}$$

3.1.2 CDL Channel Model

The CDL channel model is an extension of the TDL model, intended for 3D channel simulations. Therefore, instead of referring to taps, for the CDL channel model there are clusters. Just as the TDL model, it has 5 different channel profiles: CDL_A, CDL_B and CDL_C, envisioned for NLOS environments, and CDL_D and CDL_E, envisioned for LOS environment scenarios [95]. Tables 11-15 present the characteristics of each CDL channel profile.

Cluster #	Normalized delay	Power in [dB]	AOD in [°]	AOA in [°]	ZOD in [°]	ZOA in [°]
1	0.0000	-13.4	-178.1	51.3	50.2	125.4
2	0.3819	0	-4.2	-152.7	93.2	91.3
3	0.4025	-2.2	-4.2	-152.7	93.2	91.3
4	0.5868	-4	-4.2	-152.7	93.2	91.3
5	0.4610	-6	90.2	76.6	122	94
6	0.5375	-8.2	90.2	76.6	122	94
7	0.6708	-9.9	90.2	76.6	122	94
8	0.5750	-10.5	121.5	-1.8	150.2	47.1
9	0.7618	-7.5	-81.7	-41.9	55.2	56
10	1.5375	-15.9	158.4	94.2	26.4	30.1
11	1.8978	-6.6	-83	51.9	126.4	58.8
12	2.2242	-16.7	134.8	-115.9	171.6	26
13	2.1718	-12.4	-153	26.6	151.4	49.2
14	2.4942	-15.2	-172	76.6	157.2	143.1
15	2.5119	-10.8	-129.9	-7	47.2	117.4
16	3.0582	-11.3	-136	-23	40.4	122.7
17	4.0810	-12.7	165.4	-47.2	43.3	123.2
18	4.4579	-16.2	148.4	110.4	161.8	32.6
19	4.5695	-18.3	132.7	144.5	10.8	27.2
20	4.7966	-18.9	-118.6	155.3	16.7	15.2
21	5.0066	-16.6	-154.1	102	171.7	146
22	5.3043	-19.9	126.5	-151.8	22.7	150.7
23	9.6586	-29.7	-56.2	55.2	144.9	156.1
Per-Cluster Parameters						
Parameter	c_{ASD} in [°]	c_{ASA} in [°]	c_{ZSD} in [°]	c_{ZSA} in [°]	XPR in [dB]	
Value	5	11	3	3	10	

Table 11: CDL_A characterization. Source: 3GPP TR 138.901

Cluster #	Normalized delay	Power in [dB]	AOD in [°]	AOA in [°]	ZOD in [°]	ZOA in [°]
1	0.0000	0	9.3	-173.3	105.8	78.9
2	0.1072	-2.2	9.3	-173.3	105.8	78.9
3	0.2155	-4	9.3	-173.3	105.8	78.9
4	0.2095	-3.2	-34.1	125.5	115.3	63.3
5	0.2870	-9.8	-65.4	-88.0	119.3	59.9
6	0.2986	-1.2	-11.4	155.1	103.2	67.5
7	0.3752	-3.4	-11.4	155.1	103.2	67.5
8	0.5055	-5.2	-11.4	155.1	103.2	67.5
9	0.3681	-7.6	-67.2	-89.8	118.2	82.6
10	0.3697	-3	52.5	132.1	102.0	66.3
11	0.5700	-8.9	-72	-83.6	100.4	61.6
12	0.5283	-9	74.3	95.3	98.3	58.0
13	1.1021	-4.8	-52.2	103.7	103.4	78.2
14	1.2756	-5.7	-50.5	-87.8	102.5	82.0
15	1.5474	-7.5	61.4	-92.5	101.4	62.4
16	1.7842	-1.9	30.6	-139.1	103.0	78.0
17	2.0169	-7.6	-72.5	-90.6	100.0	60.9
18	2.8294	-12.2	-90.6	58.6	115.2	82.9
19	3.0219	-9.8	-77.6	-79.0	100.5	60.8
20	3.6187	-11.4	-82.6	65.8	119.6	57.3
21	4.1067	-14.9	-103.6	52.7	118.7	59.9
22	4.2790	-9.2	75.6	88.7	117.8	60.1
23	4.7834	-11.3	-77.6	-60.4	115.7	62.3
Per-Cluster Parameters						
Parameter	c_{ASD} in [°]	c_{ASA} in [°]	c_{ZSD} in [°]	c_{ZSA} in [°]	XPR in [dB]	
Value	10	22	3	7	8	

Table 12: CDL_B characterization. Source: 3GPP TR 138.901

Cluster #	Normalized delay	Power in [dB]	AOD in [°]	AOA in [°]	ZOD in [°]	ZOA in [°]
1	0	-4.4	-46.6	-101	97.2	87.6
2	0.2099	-1.2	-22.8	120	98.6	72.1
3	0.2219	-3.5	-22.8	120	98.6	72.1
4	0.2329	-5.2	-22.8	120	98.6	72.1
5	0.2176	-2.5	-40.7	-127.5	100.6	70.1
6	0.6366	0	0.3	170.4	99.2	75.3
7	0.6448	-2.2	0.3	170.4	99.2	75.3
8	0.6560	-3.9	0.3	170.4	99.2	75.3
9	0.6584	-7.4	73.1	55.4	105.2	67.4
10	0.7935	-7.1	-64.5	66.5	95.3	63.8
11	0.8213	-10.7	80.2	-48.1	106.1	71.4
12	0.9336	-11.1	-97.1	46.9	93.5	60.5
13	1.2285	-5.1	-55.3	68.1	103.7	90.6
14	1.3083	-6.8	-64.3	-68.7	104.2	60.1
15	2.1704	-8.7	-78.5	81.5	93.0	61.0
16	2.7105	-13.2	102.7	30.7	104.2	100.7
17	4.2589	-13.9	99.2	-16.4	94.9	62.3
18	4.6003	-13.9	88.8	3.8	93.1	66.7
19	5.4902	-15.8	-101.9	-13.7	92.2	52.9
20	5.6077	-17.1	92.2	9.7	106.7	61.8
21	6.3065	-16	93.3	5.6	93.0	51.9
22	6.6374	-15.7	106.6	0.7	92.9	61.7
23	7.0427	-21.6	119.5	-21.9	105.2	58
24	8.6523	-22.8	-123.8	33.6	107.8	57

Per-Cluster Parameters					
Parameter	c_{ASD} in [°]	c_{ASA} in [°]	c_{ZSD} in [°]	c_{ZSA} in [°]	XPR in [dB]
Value	2	15	3	7	7

Table 13: CDL_C characterization. Source: 3GPP TR 138.901

Cluster #	Cluster PAS	Normalized Delay	Power in [dB]	AOD in [°]	AOA in [°]	ZOD in [°]	ZOA in [°]
1	Specular(LOS path)	0	-0.2	0	-180	98.5	81.5
	Laplacian	0	-13.5	0	-180	98.5	81.5
2	Laplacian	0.035	-18.8	89.2	89.2	85.5	86.9
3	Laplacian	0.612	-21	89.2	89.2	85.5	86.9
4	Laplacian	1.363	-22.8	89.2	89.2	85.5	86.9
5	Laplacian	1.405	-17.9	13	163	97.5	79.4
6	Laplacian	1.804	-20.1	13	163	97.5	79.4
7	Laplacian	2.596	-21.9	13	163	97.5	79.4
8	Laplacian	1.775	-22.9	34.6	-137	98.5	78.2
9	Laplacian	4.042	-27.8	-64.5	74.5	88.4	73.6
10	Laplacian	7.937	-23.6	-32.9	127.7	91.3	78.3
11	Laplacian	9.424	-24.8	52.6	-119.6	103.8	87
12	Laplacian	9.708	-30.0	-132.1	-9.1	80.3	70.6
13	Laplacian	12.525	-27.7	77.2	-83.8	86.5	72.9

Per-Cluster Parameters					
Parameter	c_{ASD} in [°]	c_{ASA} in [°]	c_{ZSD} in [°]	c_{ZSA} in [°]	XPR in [dB]
Value	5	8	3	3	11

Table 14: CDL_D characterization. Source: 3GPP TR 138.901

Cluster #	Cluster PAS	Normalized Delay	Power in [dB]	AOD in [°]	AOA in [°]	ZOD in [°]	ZOA in [°]
1	Specular (LOS path)	0.000	-0.03	0	-180	99.6	80.4
	Laplacian	0.000	-22.03	0	-180	99.6	80.4
2	Laplacian	0.5133	-15.8	57.5	18.2	104.2	80.4
3	Laplacian	0.5440	-18.1	57.5	18.2	104.2	80.4
4	Laplacian	0.5630	-19.8	57.5	18.2	104.2	80.4
5	Laplacian	0.5440	-22.9	-20.1	101.8	99.4	80.8
6	Laplacian	0.7112	-22.4	16.2	112.9	100.8	86.3
7	Laplacian	1.9092	-18.6	9.3	-155.5	98.8	82.7
8	Laplacian	1.9293	-20.8	9.3	-155.5	98.8	82.7
9	Laplacian	1.9589	-22.6	9.3	-155.5	98.8	82.7
10	Laplacian	2.6426	-22.3	19	-143.3	100.8	82.9
11	Laplacian	3.7136	-25.6	32.7	-94.7	96.4	88
12	Laplacian	5.4524	-20.2	0.5	147	98.9	81
13	Laplacian	12.0034	-29.8	55.9	-36.2	95.6	88.6
14	Laplacian	20.6419	-29.2	57.6	-26	104.6	78.3

Per-Cluster Parameters					
Parameter	c_{ASD} in [°]	c_{ASA} in [°]	c_{ZSD} in [°]	c_{ZSA} in [°]	XPR in [dB]
Value	5	11	3	7	8

Table 15: CDL_E characterization. Source: 3GPP TR 138.901

In order to generate the channel coefficients for the CDL channel model, firstly the azimuth angles of departure and arrival need to be calculated. Hence, the angles for the m^{th} ray of the n^{th} cluster are given by

$$\emptyset_{n,m,AoD} = \emptyset_{n,AoD} + c_{ASD}\alpha_m \tag{3.6}$$

where $\emptyset_{n,m,AoD}$ is the Azimuth Angle of Departure (AoD), c_{ASD} represents the azimuth spread of the departure angle and α_m is the ray offset angle for the m^{th} ray. A similar equation is used for the angles of arrival

$$\emptyset_{n,m,AoA} = \emptyset_{n,AoA} + c_{ASA}\alpha_m \tag{3.7}$$

where $\emptyset_{n,m,AoA}$ is the Azimuth Angle of Arrival (AoA) and c_{ASA} represents the azimuth spread of the arrival angle. In addition, to generate the $\theta_{n,m,ZoA}$ Zenith Angle of Arrival (ZoA) and $\theta_{n,m,ZoD}$ Zenith Angle of Departure (ZoD), the equations are identical to equations (3.6) and (3.7), respectively.

The $\emptyset_{n,m,AoD}$ AoD angles and the $\emptyset_{n,m,AoA}$ AoA angles are randomly coupled within a cluster *n.* Similarly, the $\theta_{n,m,ZoD}$ ZoD angles are coupled with the $\theta_{n,m,ZoA}$ ZoA angles, and the $\emptyset_{n,m,AoD}$ AoD angles are also coupled with the $\theta_{n,m,ZoD}$ ZoD angles.

The next step is to generate the Cross Polarization Power Ratio (XPR), k, for each ray of each cluster

$$k = 10^{\frac{C}{10}} \tag{3.8}$$

where C is the XPR for each cluster n, represented in dB.

In conclusion, for a NLOS environment scenario, the channel coefficients for the *n* cluster and the pair of transmitter and receiver *(t,r)* antenna elements are defined by

$$H_{r,t,n}^{NLOS}(t) = \sqrt{\frac{P_n}{M}} \sum_{m=1}^{M} \begin{bmatrix} F_{rx,r,\theta}(\theta_{n,m,ZoA},\emptyset_{n,m,AoA}) \\ F_{rx,r,\emptyset}(\theta_{n,m,ZoA},\emptyset_{n,m,AoA}) \end{bmatrix}^T \times \begin{bmatrix} e^{j\Phi_{n,m}^{\theta\theta}} & \sqrt{k_{n,m}^{-1}} e^{j\Phi_{n,m}^{\theta\emptyset}} \\ \sqrt{k_{n,m}^{-1}} e^{j\Phi_{n,m}^{\emptyset\theta}} & e^{j\Phi_{n,m}^{\emptyset\emptyset}} \end{bmatrix} \begin{bmatrix} F_{tx,t,\theta}(\theta_{n,m,ZoD},\emptyset_{n,m,AoD}) \\ F_{tx,t,\emptyset}(\theta_{n,m,ZoD},\emptyset_{n,m,AoD}) \end{bmatrix} \times e^{\frac{j2\pi(\hat{r}_{rx,n,m}^T \cdot \bar{d}_{rx,r})}{\lambda_0}} \times e^{\frac{j2\pi(\hat{r}_{tx,n,m}^T \cdot \bar{d}_{tx,t})}{\lambda_0}} \times e^{\frac{j2\pi(\hat{r}_{rx,n,m}^T \cdot \bar{v})}{\lambda_0} t} \tag{3.9}$$

where $F_{tx,t,\theta}$ and $F_{tx,t,\emptyset}$ define the field patters of radiation of the transmit antenna element *t*, and $F_{rx,r,\theta}$ and $F_{rx,r,\emptyset}$ represent the field patters of radiation of the receive antenna element *r*.

The three elements from the last line of the equation (3.9) represent the phase array offset of the mobile terminal, the gNodeB phase array offset and the Doppler phase shift, respectively. The elements $\bar{d}_{rx,r}$ and $\bar{d}_{tx,t}$ represent the vector location of the receiver and transmitter antenna element, respectively. The wavelength of the carrier frequency is defined by λ_0. The $\hat{r}_{rx,n,m}$ is the spherical unit vector with the zenith angle of arrival $\theta_{n,m,ZoA}$ and the azimuth angle of arrival $\emptyset_{n,m,AoA}$. It is given by [96]

$$\hat{r}_{rx,n,m} = \begin{bmatrix} sin\,\theta_{n,m,ZoA} & cos\,\emptyset_{n,m,AoA} \\ sin\,\theta_{n,m,ZoA} & sin\,\emptyset_{n,m,AoA} \\ cos\,\theta_{n,m,ZoA} & \end{bmatrix} \tag{3.10}$$

The $\hat{r}_{tx,n,m}$ is the spherical unit vector with the zenith angle of departure $\theta_{n,m,ZoD}$ and the azimuth angle of departure $\emptyset_{n,m,AoD}$. The expression is similar to (3.10) and it is given by [96]

$$\hat{r}_{tx,n,m} = \begin{bmatrix} sin\,\theta_{n,m,ZoD} & cos\,\emptyset_{n,m,AoD} \\ sin\,\theta_{n,m,ZoD} & sin\,\emptyset_{n,m,AoD} \\ cos\,\theta_{n,m,ZoD} & \end{bmatrix} \tag{3.11}$$

In a LOS environment scenario, the channel coefficients are given by [97]

$$H_{r,t,1}^{LOS}(t) = \begin{bmatrix} F_{rx,r,\theta}(\theta_{LOS,ZoA},\emptyset_{LOS,AoA}) \\ F_{rx,r,\emptyset}(\theta_{LOS,ZoA},\emptyset_{LOS,AoA}) \end{bmatrix}^T \begin{bmatrix} 1 & 0 \\ 0 & -1 \end{bmatrix} \times \begin{bmatrix} F_{tx,t,\theta}(\theta_{LOS,ZoD},\emptyset_{LOS,AoD}) \\ F_{tx,t,\emptyset}(\theta_{LOS,ZoD},\emptyset_{LOS,AoD}) \end{bmatrix} e^{\frac{j2\pi(\hat{r}_{rx,LOS}^T \cdot \bar{d}_{rx,r})}{\lambda_0}} \times e^{\frac{j2\pi(\hat{r}_{tx,LOS}^T \cdot \bar{d}_{tx,t})}{\lambda_0}} \times e^{\frac{j2\pi(\hat{r}_{rx,LOS}^T \cdot \bar{v})}{\lambda_0} t} \times e^{\frac{-j2\pi d_{3D}}{\lambda_0}} \quad (3.12)$$

3.2 Performance Evaluation Using TDL Channels for 5G MIMO Systems

In this sub-section we evaluate the performance of a downlink single-user 5G MIMO system, using the TDL channel model for different modulation schemes. We study the three profiles of the TDL channel that are intended for NLOS environments (TDL_A, TDL_B and TDL_C). The parameters considered are BER and throughput for a selected range of Signal-to-Noise-Plus-Interference Ratio (SNIR). Link-level simulation results show how the different channel profiles impact the system performance and are extremely valuable to be used in the design of 5G systems. The link-level simulations are performed using Nokia's internal link-level simulator: 5GMax.

Table 16 illustrates the Modulation and Coding Scheme (MCS) index table and the associated target code rate and spectral efficiency used in the physical downlink shared channel. As it can be observed, there are 28 values for the MCS index. The second column of the table represents the modulation order. Between 0 and 4 MCS index, the modulation type is QPSK. From 5 to 10 MCS index, the modulation type is 16QAM. From 11 to 19, the modulation is 64QAM and from 20 to 27 the modulation is 256QAM. The third column presents the target code rate, that increases as the MCS index increases. The last column presents the spectral efficiency, with values between 0.2344 and 7.4063. To note that the actual values obtained will be lower than the ones presented in the table, due to the presence of reference signals and overhead, which is around 25%. The current mobile generation uses up to 64QAM as modulation type, although 256QAM is envisioned to be used in future 5G systems.

MCS Index I_{MCS}	Modulation Order Q_m	Target code Rate R x [1024]	Spectral efficiency
0	2	120	0.2344
1	2	193	0.3770
2	2	308	0.6016
3	2	449	0.8770
4	2	602	1.1758
5	4	378	1.4766
6	4	434	1.6953
7	4	490	1.9141
8	4	553	2.1602
9	4	616	2.4063
10	4	658	2.5703
11	6	466	2.7305
12	6	517	3.0293
13	6	567	3.3223
14	6	616	3.6094
15	6	666	3.9023
16	6	719	4.2129
17	6	772	4.5234
18	6	822	4.8164
19	6	873	5.1152
20	8	682.5	5.3320
21	8	711	5.5547
22	8	754	5.8906
23	8	797	6.2266
24	8	841	6.5703
25	8	885	6.9141
26	8	916.5	7.1602
27	8	948	7.4063
28	2	reserved	
29	4	reserved	
30	6	reserved	
31	8	reserved	

Table 16: MCS index table for PDSCH. Source: 3GPP TS 38.214 version 15.2.0 Release 15

3.2.1 System Model Characterization

The system model adopted for the link-level simulations is as follows. We consider a downlink single-user MIMO system with 1 BS and 1 MS in a NLOS environment. The BS is equipped with 4 transmitter antennas and the MS is equipped with 4 receiver antennas, moving at a speed of 3 km/h. The carrier frequency adopted is of 3.5 GHz with a bandwidth of 100 MHz. The duplex mode used is TDD and the number of Physical Resource Blocks (PRB) allocated is 256. On the receiver side, the MS uses the Minimum Mean Square Error (MMSE) algorithm, therefore, real channel estimation is applied to the environment scenario. Furthermore, a Precoding Matrix Indicator (PMI) is added to the system. A delay spread of 32 ns is added in order to

simulate an indoor office environment. The summarized parameters are depicted in table 17.

Simulation Parameters	Values
Carrier frequency	3.5 GHz
Bandwidth	100 MHz
Duplex mode	TDD
Number of PRB allocated	256
Delay Spread	32 ns
MS velocity	3 km/h
Channel estimation	Real
Tx/Rx antenna number	4/4
Shadow specification	3GPP release 15.3 September 2018 Baseline
Diversity scheme	CLSM1 (DMRS port 0)

Table 17: Adopted parameters for the link-level simulations [98].

3.2.2 Performance Results

The performance of the 5G MIMO system is evaluated by comparing three different channel models: TDL_A, TDL_B and TDL_C. Different MCS index values and modulation schemes are used for the link-level simulations. Particularly, for 16QAM we use the MCS index values of 5 and 9, for 64QAM we use MCS index values of 13 and 17, and for 256QAM we use MCS values of 25 and 27. We chose these values since we wanted to obtain results for a lower and a higher MCS value for each modulation type, each with different target code rates and a reasonable increase on the spectral efficiency from one to another. For 16QAM, the SNIR range of [-10,8] dB is considered, for 64QAM the SNIR ranges between [2,20] dB and for 256QAM the SNIR range is [12,28] dB.

Figures 26, 27 and 28 depict the BER and throughput performance of the three channel profiles studied while using 16QAM, 64QAM and 256QAM modulation, respectively. It is possible to conclude that the performance of the 5G system is better when we use 256QAM modulation scheme with the MCS index value of 27, the maximum value achievable. Additionally, we can also observe that, even though higher MCS index values lead to higher throughput values, the required SNIR also increases, which leads to the need of better environment conditions in order to achieve high values for the throughput.

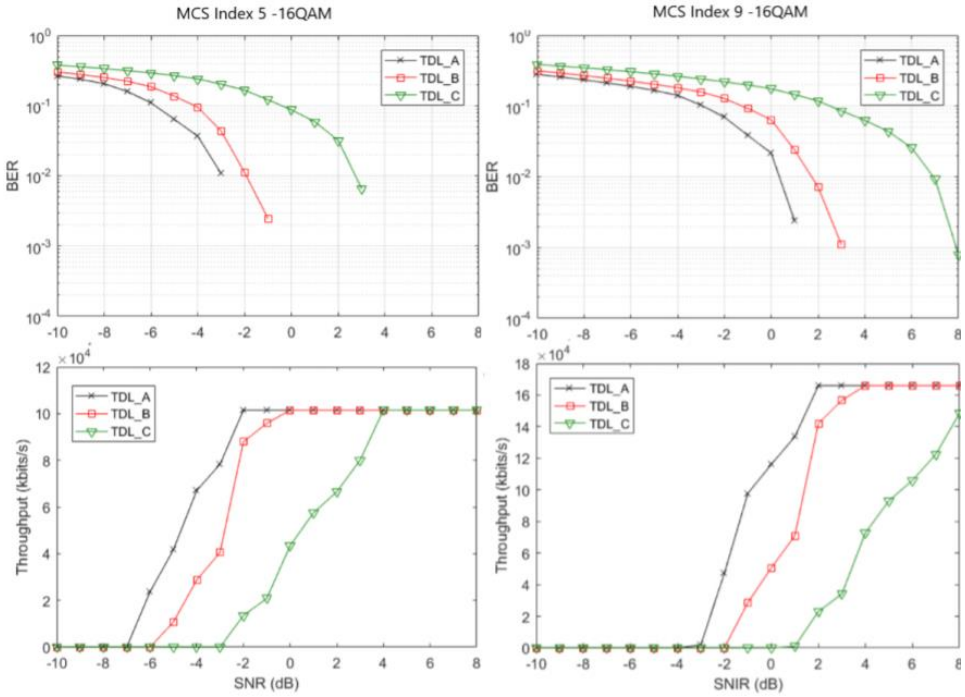

Figure 26: BER and throughput results for 16QAM modulation.

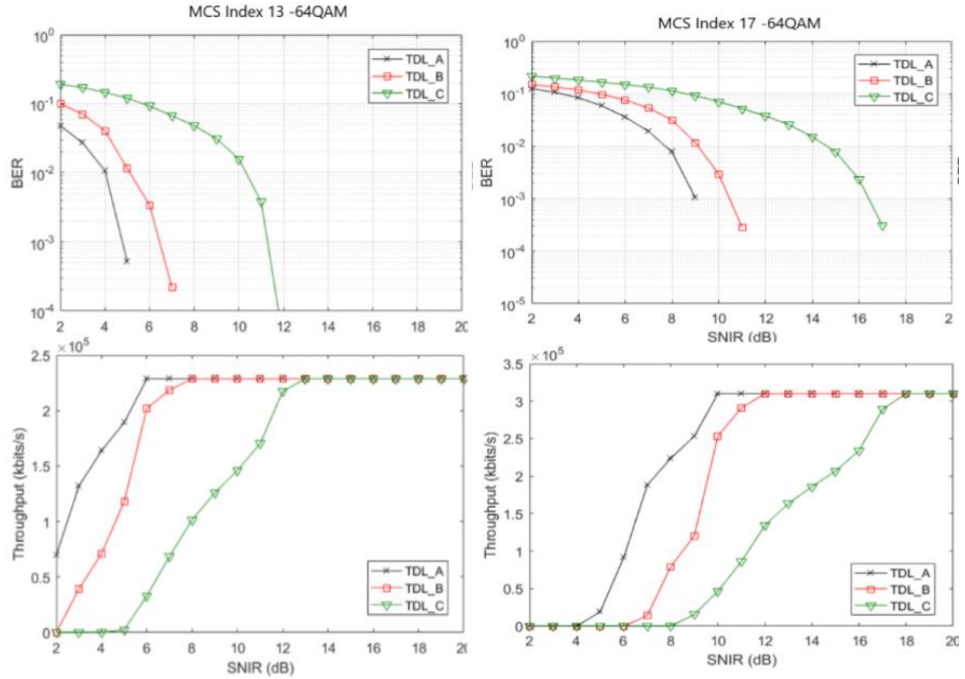

Figure 27: BER and throughput results for 64QAM modulation.

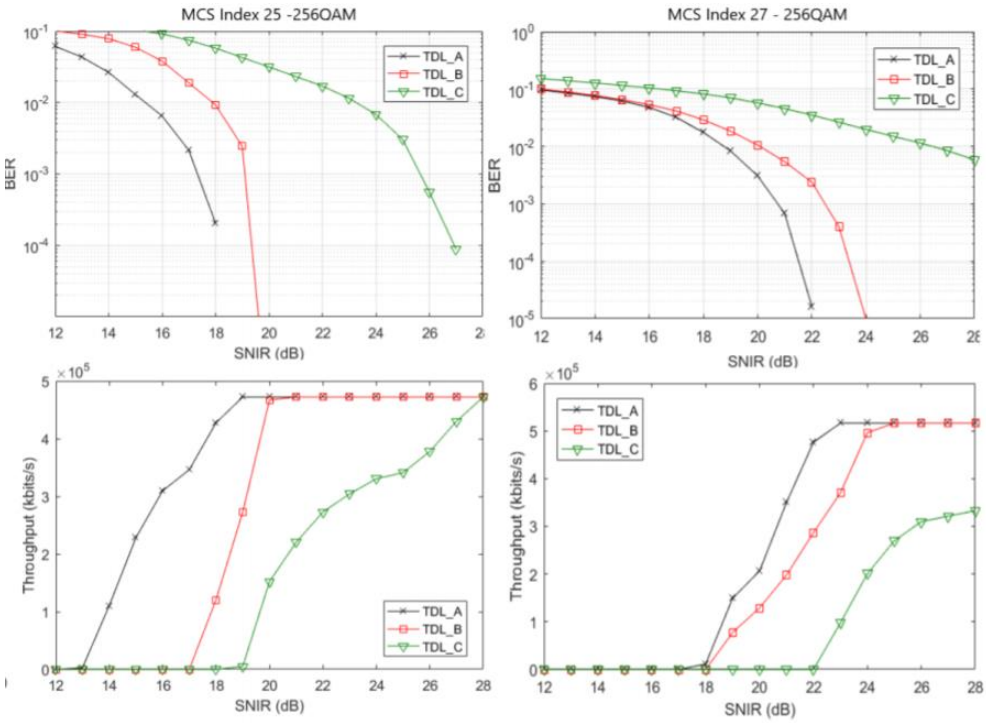

Figure 28: BER and throughput results for 256QAM modulation.

The maximum throughput obtained for 16QAM is 165,960 Mbps, with an MCS index of 9. For 64QAM modulation, the maximum throughput is increased by 131%, reaching up to 383,720 Mbps, with the MCS index value of 17. For 256QAM modulation, the increase is of 35% when compared to 64QAM, with a maximum throughput of 516,560 Mbps. We assessed that in scenarios with poorer conditions, the channel profile that performs better is the TDL_A, due to the fact that the required SNIR in order to achieve better throughput values or to minimize BER, is smaller, out of the three profiles investigated. Consequently, when comparing the three channel profile models, link-level simulation results show that the profile that achieves a better overall system performance, regardless of the MCS index value and modulation scheme adopted, is the TDL_A profile, followed by TDL_B and lastly TDL_C.

Specifically, for the MCS index of 9 (16QAM modulation), TDL_B reaches the maximum throughput of 165,960 Mbps with a SNIR of 2 dB more when compared to TDL_A. For TDL_C, the difference is even higher, needing 7 dB more to reach the same maximum throughput. For the MCS index of 17 (64QAM modulation), the maximum throughput of 309,920 Mbps is reached by TDL_B with 2 dB after TDL_A, while for TDL_C a difference of 8 dB is perceived, in comparison with TDL_A. Lastly, for 256QAM modulation and MCS index of 27, TDL_B reaches the maximum throughput of 516,560 Mbps 2 dB after TDL_A, while TDL_C is not able to reach it within the stated SNIR range.

For 256QAM modulation, the channel model TDL_C necessitates very good conditions (higher SNIR values) in order to reach maximum throughput values and minimize BER. Figure 28 depicts that for the MCS index value of 27, the maximum throughput is not attained when using the TDL_C profile. Subsequently, for this channel profile, a higher SNIR range is needed in order to reach the maximum throughput and minimize BER. Another observation is that, for lower MCS index values, the curves for TDL_A and TDL_B are positioned closer one to another, while TDL_C is more distant.

The study of the three channel models and their performance evaluation, in terms of BER and throughput, allows a better understanding on how a 5G system behaves using the respective channels with different scenario conditions. The link-level simulation results are valuable in the design of future 5G communication systems. In addition, from the simulation results, we can conclude that we can greatly minimize the values for the BER if we adopt the TDL_A profile with a higher modulation type and a higher MCS value from the ones presented in table 15. As for the throughput, it can be increased by similarly adopting the TDL_A profile instead of the TDL_B or TDL_C and by selecting MCS values that have a higher target code rate and hence an increased spectral efficiency.

3.3 Influence of Delay Spread in TDL and CDL Channel Models

In this sub-section we evaluate the influence of the Delay Spread (DS) in a 5G communication system that uses the TDL and CDL channel models. We study how different values for the DS affect the system's performance, in terms of BER and throughput. We use Nokia's internal link-level simulator 5GMax. The simulation results obtained provide an insight on the understanding on how the TDL and CDL channels affect the system's performance in different environment scenarios with specific values for the DS selected.

The DS represents an important factor that characterizes a frequency selective channel. Thus, it is a parameter that needs to be taken into consideration when dealing with these types of channels. The DS can be obtained from the Power Delay Profile (PDP). Precisely, it computes the difference, in time, between the arrival of the first multipath component and the arrival of the last multipath component. It is defined as being the second central moment of the PDP [99]. The delay scaling factor is introduced to the TDL and CDL channel models. The value of the Root Mean Square (RMS) DS is normalized and scaled in delay, being given by

$$\tau_{n,scaled} = \tau_{n,model} \cdot DS_{desired} \tag{3.13}$$

where $DS_{desired}$ is the desired DS, $\tau_{n,model}$ is the normalized delay value for the n^{th} tap or cluster, depending if we are dealing the TDL or CDL channel, respectively. The $\tau_{n,scaled}$ represents the new delay value for the n^{th} tap or cluster.

3.3.1 System Model Characterization

The system model adopted for the simulations is as follows. We consider a single-user MIMO DL system, with 1 BS composed with 4 transmitter antennas and 1 MS composed with 4 receiver antennas, moving at 3 km/h. We adopt a carrier frequency of 3.5 GHz with 100 MHz bandwidth. At the receiver side, we use MMSE estimation. The number of PRBs allocated is 256, the duplex mode adopted is TDD and the modulation scheme is 256QAM modulation. We simulate the performance of the 5G communication system using all 5 profiles from both the TDL and CDL channel models, with the following environment scenarios:

- Indoor office: DS 18, 32, 53 ns;
- Rural macro cell: DS 34, 39 ns;
- Urban micro cell street canyon: DS 47, 95, 318 ns;
- Urban macro cell: DS 365, 1150 ns.

Tables 18-20 present the 3 sets of environment scenarios simulated.

#	Environment	Scenario	Channel Model	Proposed DS [ns]
1	NLOS	Indoor office	TDL_A	18
2	NLOS	Indoor office	TDL_B	18
3	NLOS	Indoor office	TDL_C	18
4	LOS	Indoor office	TDL_D	18
5	LOS	Indoor office	TDL_E	18
6	NLOS	Indoor office	CDL_A	18
7	NLOS	Indoor office	CDL_B	18
8	NLOS	Indoor office	CDL_C	18
9	LOS	Indoor office	CDL_D	18
10	LOS	Indoor office	CDL_E	18

Table 18: First set of environment scenarios.

#	Environment	Scenario	Channel Model	Proposed DS [ns]
11	LOS	Indoor office	TDL_E	18
12	LOS	Indoor office	TDL_E	32
13	LOS	Indoor office	TDL_E	53
14	LOS	RMa	TDL_E	34
15	LOS	RMa	TDL_E	39

Table 19: Second set of environment scenarios.

#	Environment	Scenario	Channel Model	Proposed DS [ns]
16	NLOS	UMi Street-canyon	CDL_A	47
17	NLOS	UMi Street-canyon	CDL_A	95
18	NLOS	UMi Street-canyon	CDL_A	318
19	NLOS	UMa	CDL_A	365
20	NLOS	UMa	CDL_A	1150

Table 20: Third set of environment scenarios.

3.3.2 Performance Results

Initially, we selected a DS of 18 ns, representing an indoor office environment scenario, as is the lower value of the set of values that we investigated. The performance results, in terms of BER and throughput, of all the TDL and CDL channel models are presented below.

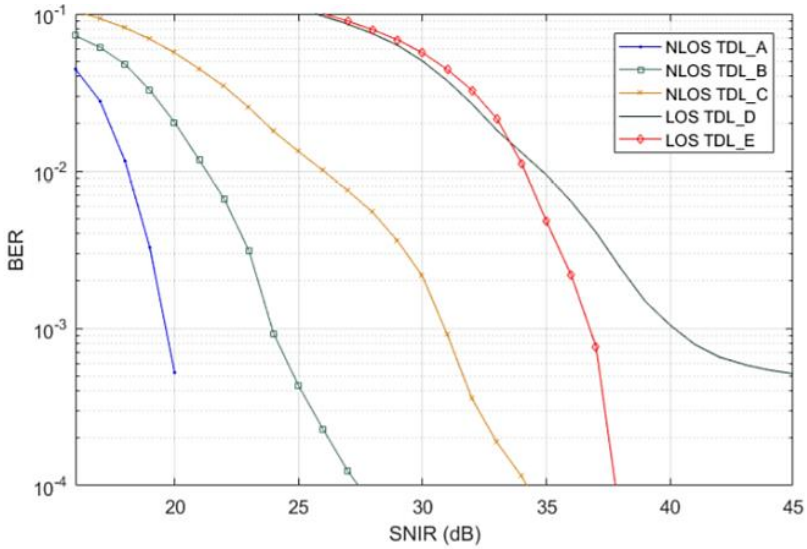

Figure 29: BER results for all TDL profiles using a DS of 18 ns.

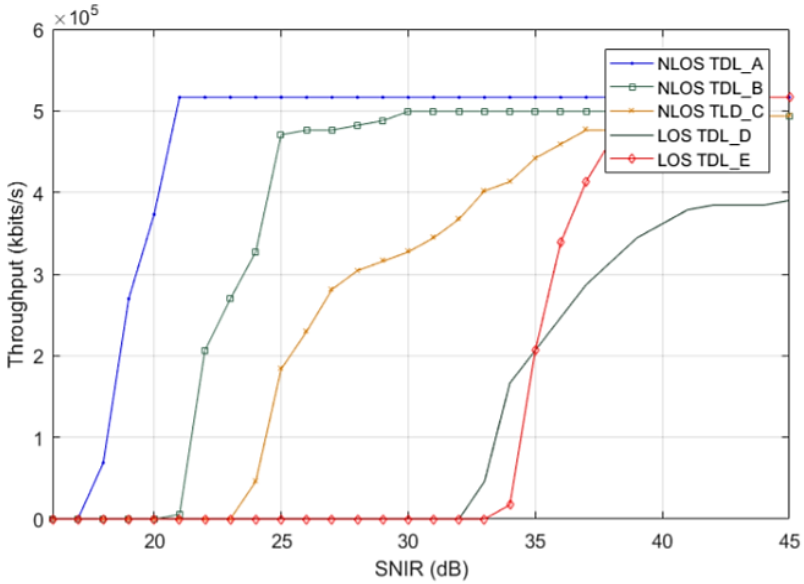

Figure 30: Throughput results for all TDL profiles using a DS of 18 ns.

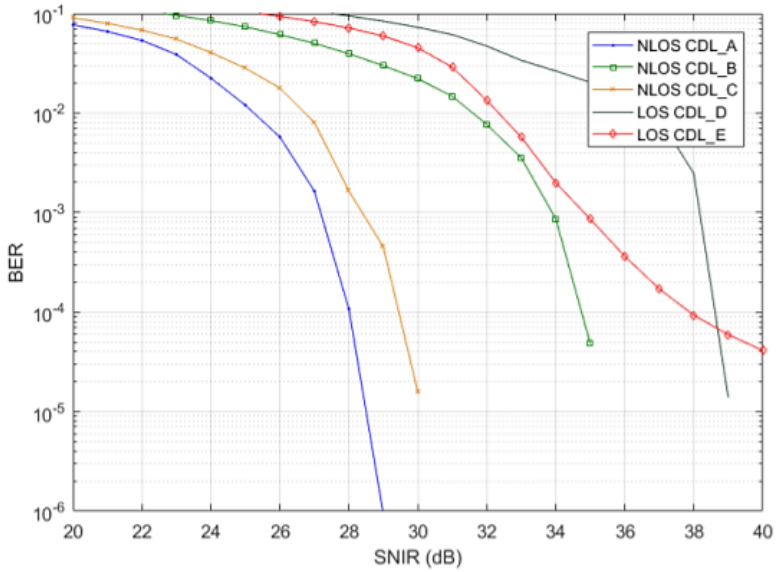

Figure 31: BER results for all CDL profiles using a DS of 18 ns.

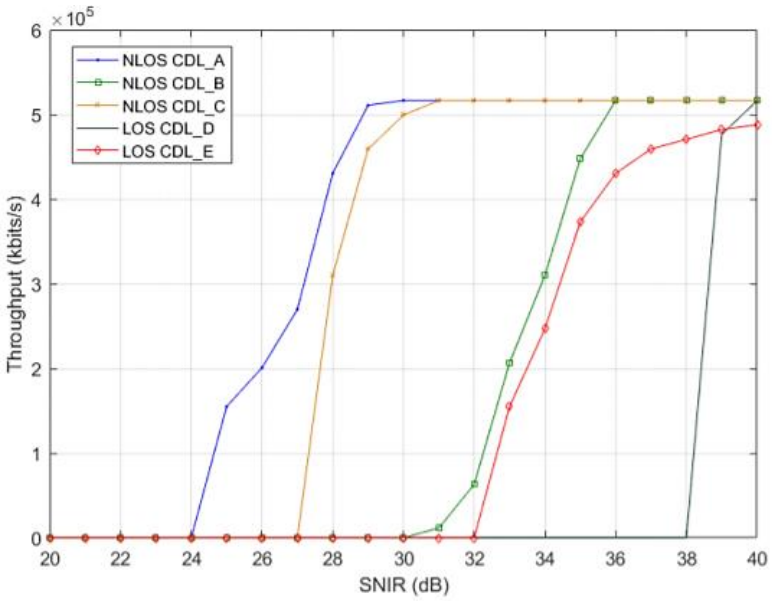

Figure 32: Throughput results for all CDL profiles using a DS of 18 ns.

Figure 29 depicts BER results for all TDL profiles. We can observe that for NLOS scenarios, the TDL profile that performs best is the TDL_A model, followed by TDL_B and TDL_C. For LOS scenarios, for SNIR values up to 34 dB, TDL_D performs better than the TDL_E model, notwithstanding as we increase SNIR values, TDL_E has an overall improved performance when compared to the TDL_D profile. Figure 30 depicts

throughput results for all TDL profiles. We can observe that the first profile that reaches maximum throughput of 516,5 Mbps from the NLOS profiles is the TDL_A, while for LOS scenarios, the profile TDL_E has a better performance than TDL_D, for higher values of SNIR than 35 dB, with a maximum throughput of approximately 500 Mbps.

Figures 31 and 32 present the BER and throughput results for the CDL channel profiles, that were simulated using the exact environment conditions as the TDL profiles. For NLOS scenarios, the best performing profile is the CDL_A, while for LOS the profile is the CDL_E. An important aspect to retain, for both TDL and CDL models, the profiles designated for NLOS environments have a better performance than the LOS profiles. The reason is that the number of taps/clusters of the NLOS profiles is higher than in the case of LOS profiles, which consequently leads to an increased number of reflexions. Furthermore, the reception and reconstruction of the signal, when we are using multipath channels as is the case, is easier if we have a higher number of reflexions, as the probability of encountering constructive interference will be higher.

The next step is to study the influence of the DS. Therefore, we have chosen the TDL_E profile for LOS environments and CDL_A for NLOS, as they are the best performing profiles for each category. Firstly, we performed the link-level simulations with the TDL_E channel profile using two environments: indoor office, with short DS values of 18, 32 and 53 ns, and rural macro cell, also with short DS values of 34 and 39 ns. Figures 33 and 34 present BER and throughput results, respectively. As we can observe, the system has an expected behavior, for both BER and throughput, in the two environments. However, we can note that the influence of the DS stops being pertinent above the threshold of 35 dB for the SNIR. Thus, it would be much harder to obtain the signal's level in a real environment scenario, since higher SNIR values correspond to practically ideal environment conditions.

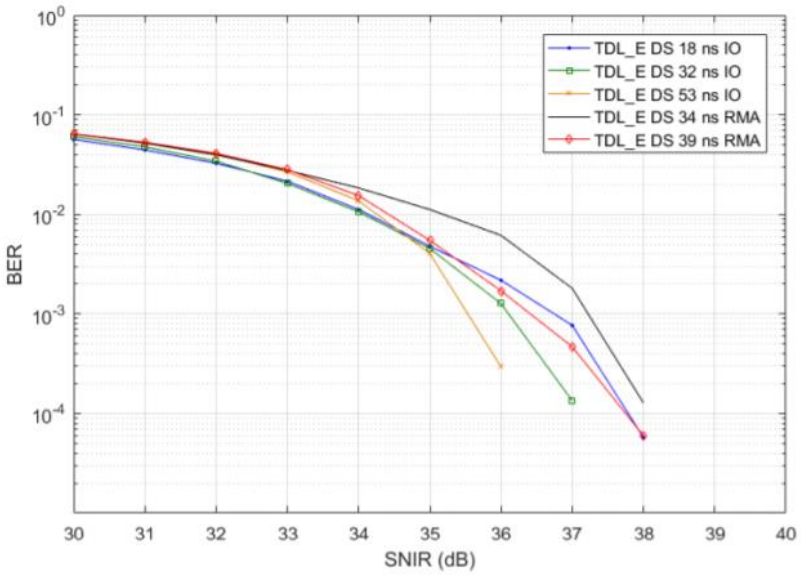

Figure 33: BER results for the TDL_E profile using different values for the DS.

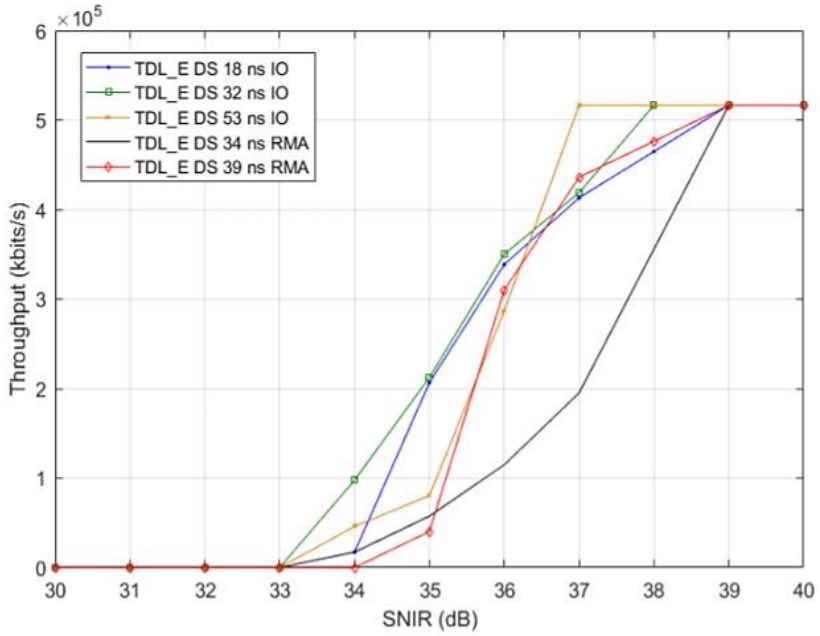

Figure 34: Throughput results for the TDL_E profile using different values for the DS.

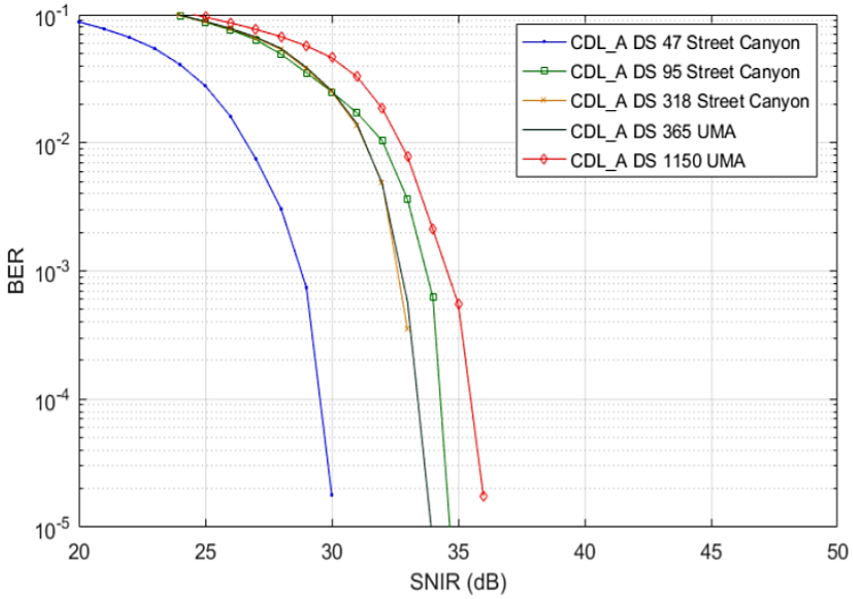

Figure 35: BER results for the CDL_A profile using different values for the DS.

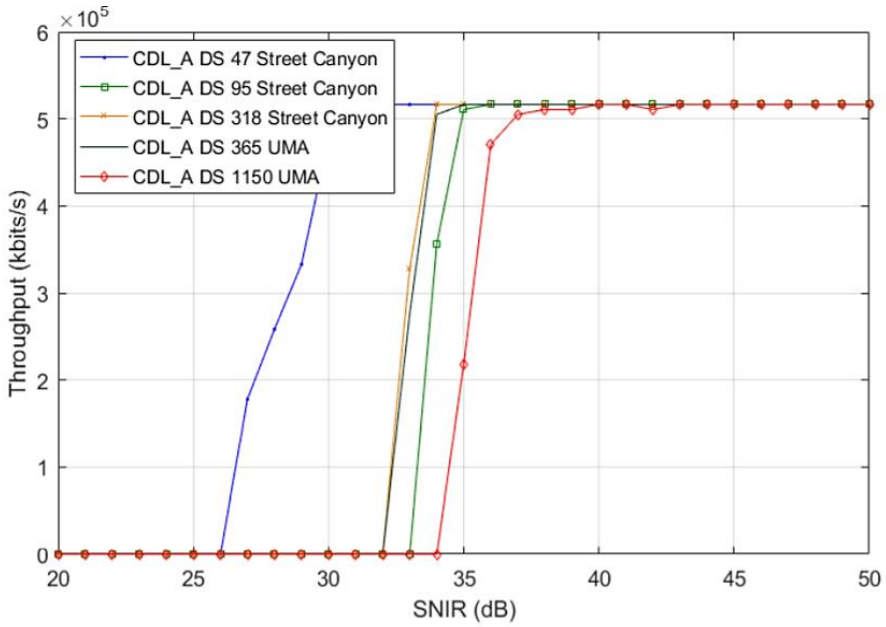

Figure 36: Throughput results for the CDL_A profile using different values for the DS.

Following, we simulated with the CDL_A profile using normal and long DS values in two different environments. For the first environment, urban micro cell street canyon, we selected DS values of 47, 95 and 318 ns. For the second environment, urban macro cell, the values of DS studied were 365 and 1150 ns. From figures 35 and 36, that present BER and throughput results, respectively, we can observe that the system has an increased performance when we consider the urban micro cell street canyon environment compared to the urban macro cell environment, that has higher values for the DS. We can also observe that the influence of the DS is not so relevant after the threshold of 32 dB of SNIR. The worst performance is seen when using a DS of 1150 ns, with the urban macro cell environment.

In conclusion, if we consider the TDL_E channel profile, which simulates a LOS environment, in order to obtain an optimized performance of the 5G communication system it is recommended to adopt short DS values, specifically 18 and 32 ns, that refer to an indoor office scenario. On the other hand, if we are dealing with a NLOS environment, it is recommended to use the CDL_A profile, since is the channel model that reaches firstly the maximum throughput and minimum BER values. For this case, it is recommended to implement a DS of 47 ns, referring to an urban micro cell street canyon scenario in order to optimize the performance of the system.

The results obtained on the influence of the DS in TDL and CDL channels for 5G MIMO systems are useful for the understanding on the behavior and performance of the respective channels in the different environments simulated and while using different DS values. In addition, the results obtained let to the publication of the following papers:

1. G. Barb, M. Otesteanu, G. Budura and C. Balint, "Performance Evaluation of TDL Channels for Downlink 5G MIMO Systems," 2019 International Symposium on Signals, Circuits and Systems (ISSCS), Iasi, Romania, 2019, ISBN: 978-1-7281-3896-1.

2. G. Barb and M. Otesteanu, "On the Influence of Delay Spread in TDL and CDL Channel Models for Downlink 5G MIMO Systems," 2019 IEEE 10th Annual Ubiquitous Computing, Electronics & Mobile Communication Conference (UEMCON), New York City, NY, USA, 2019, pp. 958-962, ISBN: 978-1-7281-3885-5.

4. Digital Beamforming Techniques for 5G

Beamforming is a technology that is viewed as a key enabler to be used simultaneously with massive MIMO in order to reach the target requirements proposed for the next mobile generation systems. The beamforming technology is utilized to transmit and receive directional signals. It is defined by changing the phase and amplitude of the emitted beam in order to direct it to a specific direction, instead of emitting the signal in all directions. Figure 37 depicts two antenna systems that emit the same amount of energy. On the left side, there is no beamforming, henceforth, the energy is emitted in all directions. On the right side, with beamforming, beams are formed and directed in the specific direction of the intended mobile terminal [100]. There are three beamforming types: analog, digital and hybrid beamforming.

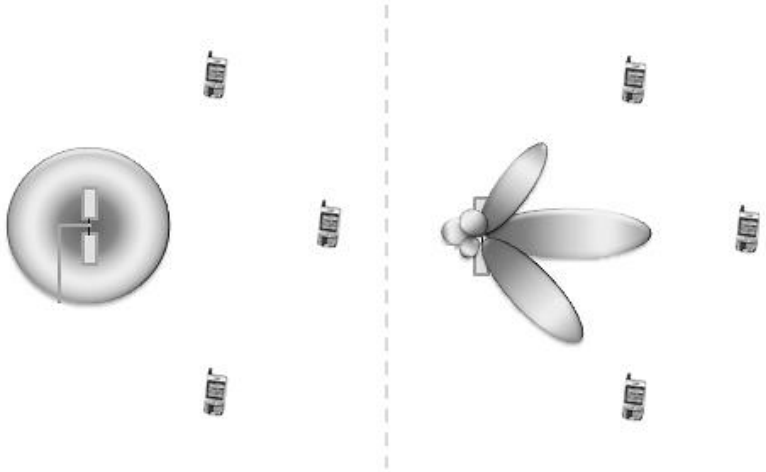

Figure 37: On the left side, no beamforming is used. On the right side, beamforming is applied.

This chapter addresses the use of digital beamforming in 5G communication systems. Two different techniques of digital beamforming are investigated: Grid of Beams (GoB) beamforming and Eigen Based Beamforming (EBB). Primarily, their definitions are explained. Then, a comparison between the performance of a 5G communication system using these techniques is performed. The system model used for the link-level simulations is presented, followed by the performance results and analysis.

4.1 Grid of Beams Beamforming

The schematics of grid of beams beamforming is presented in figure 38. The transmission flows/user signals are represented by the QAM symbols d_n, with $n = 1,2,\dots N$. These need to be sent using the same time and frequency allocation and are weighted at the BS using a precoding matrix $P = [P_1, \dots, P_n]$ with precoding vectors P_n , that represent the set of predefined vectors that are going to be transmitted as the fixed beams, each one in a defined polarizing direction, forming a beam network.

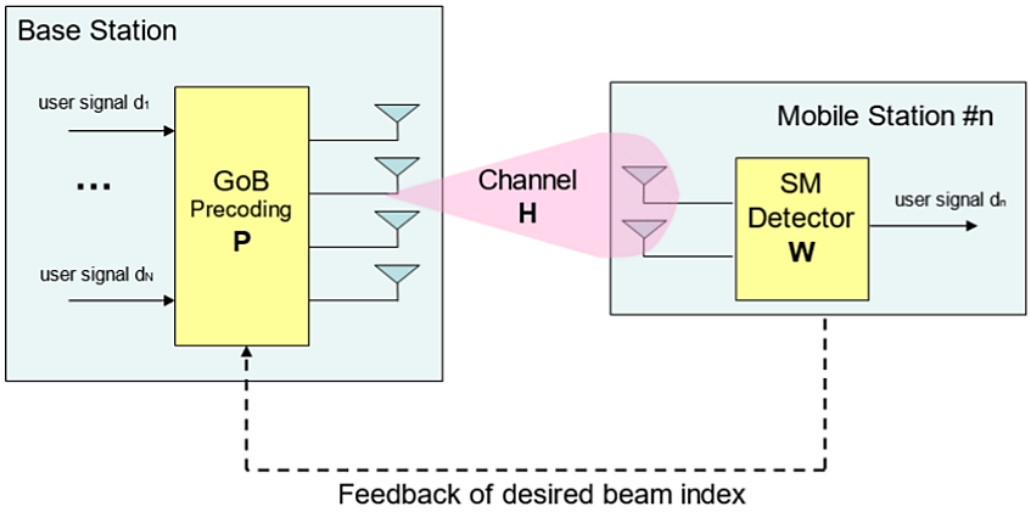

Figure 38: Schematics of GoB beamforming [101].

The beam network is composed by the precoded beams. Each beam is allocated to a mobile terminal taking in account the position of the user in the cell. Figure 38 presents an example of a GoB network with eight different beams. The beams have a specific spatial separation. In order to minimize intra cell interference beam subgroups are formed. For example, beam number 2 and beam number 6 can form a beam subgroup. In that case, two mobile terminals that favor the subgroup of beams are set on the same OFDMA allocation. Each beam index is assigned at the BS side. The MS measures and evaluates test signals that are sent for each precoded beam in order to choose the beams with the strongest transmitted power.

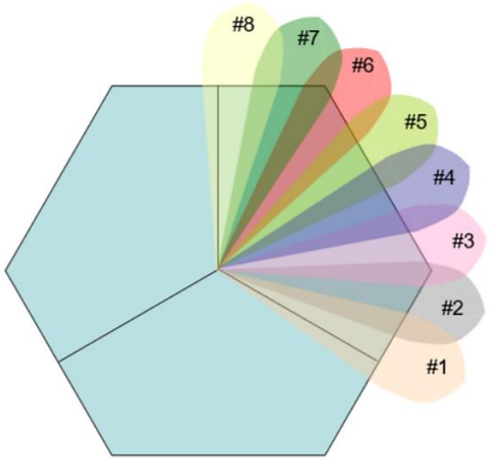

Figure 39: GoB beam network example [101].

4.2 Eigen Based Beamforming

In the EBB technique, the precoding matrix is attained from the decomposition of the single values. Therefore, the BS is modeled by a uniform rectangular matrix, where d_V and d_H represent the vertical and horizontal antennas, respectively [102]. The uniform rectangular matrix can have single or dual polarization. Figure 40 presents an example of the matrix with dual polarization. The colors blue and red characterize the horizontal and vertical polarization direction of the antennas, respectively.

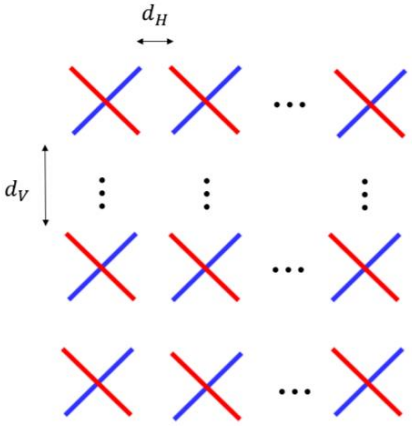

Figure 40: Uniform rectangular matrix with the positioning of antennas [82].

Figure 41 illustrates the EBB diagram and how the beams are formed. u_0 is a column vector that is attained by selecting the eigenvector that corresponds to the strongest eigenvalue. $a(i)$ controls the beam mapping for both polarization directions.

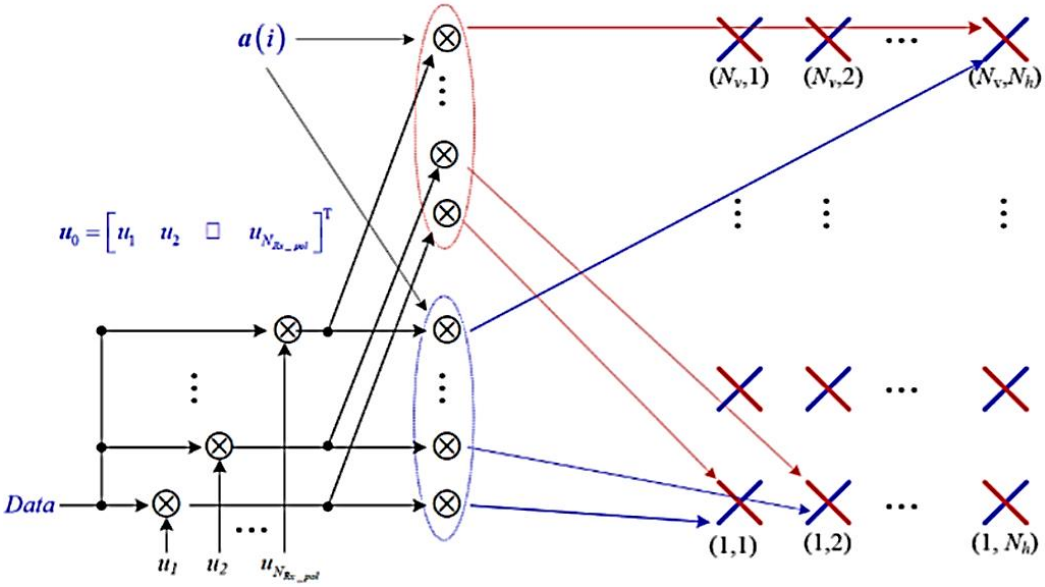

Figure 41: EBB schematics. Source: Nokia

4.3 Performance Analysis of EBB and GoB Beamforming in 5G Systems

In this sub-section we evaluate the performance of the EBB and GoB beamforming in 5G communication systems using Nokia's internal link-level simulator, in terms of BER and throughput. Firstly, we present the system model adopted for the simulations followed by the performance results and analysis. We perform a comparison between both beamforming techniques that are envisioned to be used with 5G communication systems, enabling a better understanding on their behavior.

4.3.1 System Model Characterization

For the link-level simulations, we consider 1 BS equipped with 64 antennas and 1 MS equipped with 4 antennas, moving at 3 km/h. We consider a carrier frequency of 3.5 GHz with a bandwidth of 100 MHz. The number of PRBs allocated is 256, the duplex mode selected is the TDD and the channel assumed is the Extended Pedestrian A channel model.

We simulate two different scenarios, one using 64QAM modulation and one using 256QAM modulation. For both modulation types, we choose the maximum MCS value for each one, 28 and 27, respectively, so that we obtain the best values for throughput and BER. For the SNIR range, we selected between 1 and 35 dB, in order to simulate a real environment scenario. Table 21 summarizes the adopted scenarios.

Scenario	*Modulation Type*	*MCS*	*SNIR Range (dB)*
1	64-QAM	28	[1,35]
2	256-QAM	27	[1,35]

Table 21: Scenarios adopted for the simulations.

4.3.2 Performance Results

A comparison on the performance, in terms of BER and throughput, between EBB and GoB beamforming, is evaluated, using 64QAM and 256QAM modulation. Figures 42 and 43 depict BER and throughput results for 64QAM modulation, correspondingly.

In terms of BER, we can observe that GoB beamforming has a lower error rate than EBB. For example, if we consider a SNIR of 10 dB, the BER for GoB beamforming is 10^{-2}, while for EBB the BER is of 10^{-1}, registering a difference of 10 between both techniques. Moreover, with GoB beamforming, the minimum value for BER is reached sooner than for EBB, stabilizing at a SNIR of 15 dB for GoB and 24 dB for EBB.

In terms of throughput, the maxim value reached for GoB beamforming is approximately 620 Mbps, starting at a SNIR of 16 dB. As for EBB, the maximum throughput value is slightly higher than for GoB, with an increase of 30 Mbps. Nevertheless, the maximum throughput for EBB is reached 7 dB of SNIR later, compared to GoB beamforming.

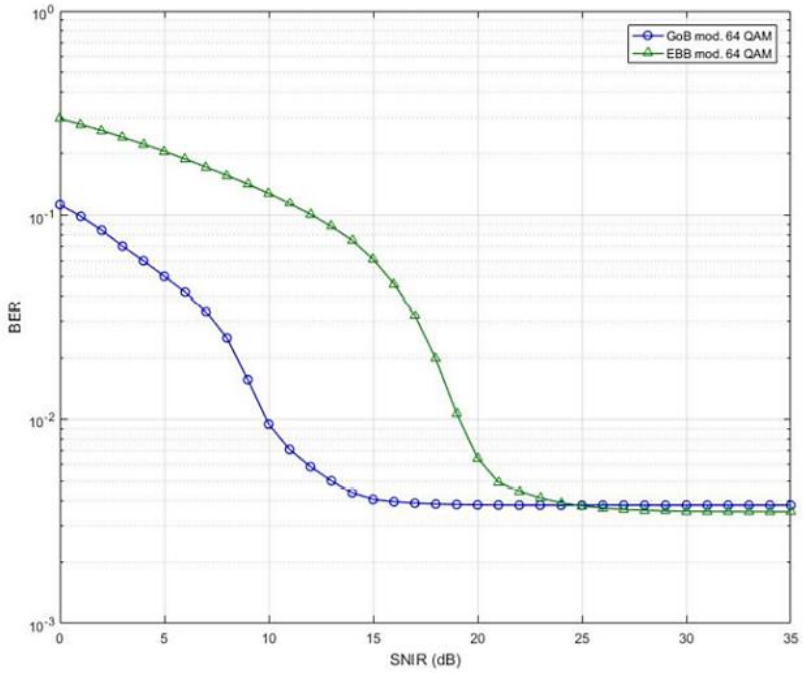

Figure 42: BER simulation results for 64QAM modulation.

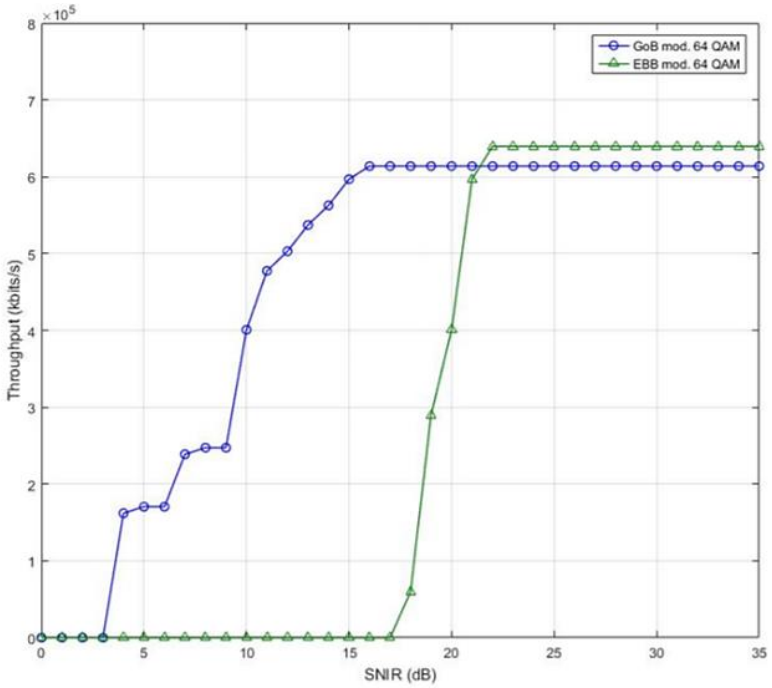

Figure 43: Throughput simulation results for 64QAM modulation.

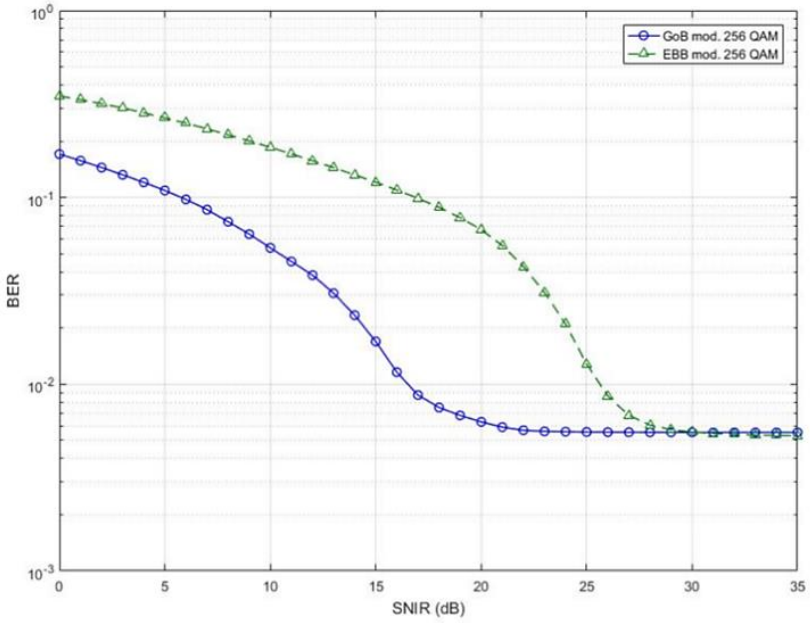

Figure 44: BER simulation results for 256QAM modulation.

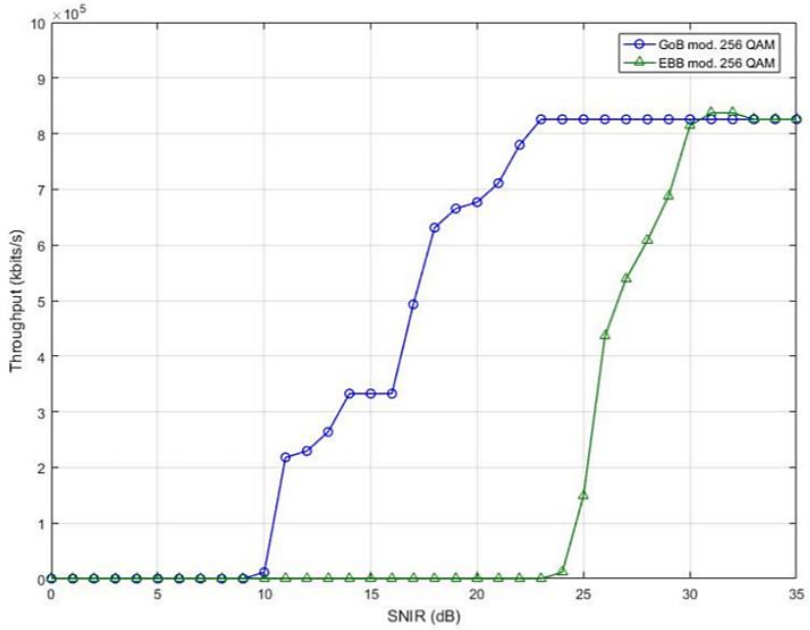

Figure 45: Throughput simulation results for 256QAM modulation.

Figures 44 and 45 present BER and throughput simulation results for 256QAM modulation, respectively. Regarding BER, it can be observed that similarly to 64QAM modulation, BER is lower for GoB beamforming than for EBB. For example, if we consider a SNIR of 15 dB, the BER for GoB beamforming is 10^{-2}, while for EBB the BER is greater than 10^{-1}.

In terms of throughput, the maximum value is reached primarily by GoB beamforming, achieving up to 820 Mbps for a SNIR of 23 dB. For EBB, there is a delay of 7 dB until the maximum value is reached.

Comparing the throughput simulation results with 64QAM modulation, we can observe an increase of 200 Mbps regarding the maximum throughput value. The increase is according to theoretical values. The reason is that with 64QAM modulation we transmit 6 bits/symbol, while with 256QAM we transmit 8 bits/symbol. Therefore, an expected increase of around 33% should be observed. Practically, we observe an increase from approximately 620 Mbps of maximum throughput to 820 Mbps with 256QAM modulation.

Taking in account both BER and throughput results, we evaluate that the GoB method is preferable to be used with 5G systems in comparison to EBB method, as it brings better results. If we compare the results obtained in this chapter with the results from the previous chapter that do not make use of beamforming, and even though we use different channel models (TDL and CDL channels), there is a visible and relevant difference. When not using beamforming, we reach a maximum of approximately 500 Mbps, while with beamforming we reach a maximum of 820 Mbps. The increase is of around 64%. It is evident that there is an increase on complexity when adding beamforming to the system, however it is compensated with the extremely high values of achievable throughput, which is one of the main requirements of the next generation mobile systems.

In conclusion, the use of beamforming techniques in 5G communication systems leads to an increase of performance. In this chapter we studied two beamforming techniques envisioned for the next mobile generation systems. From the results obtained with both 64QAM and 256QAM modulation, we conclude that the use of GoB beamforming leads to an overall increased performance, in terms of BER and throughput, compared to the use of EBB. The results obtained led to the publication of the following paper:

1. G. Barb, M. Otesteanu, F. Alexa and A. Ghiulai, "Digital Beamforming Techniques for Future Communications Systems," 2020 12th International Symposium on Communication Systems, Networks and Digital Signal Processing (CSNDSP), Porto, Portugal, 2020, ISBN: 978-1-7281-6743-5.

2. G. Barb and M. Otesteanu, "Digital GoB-based Beamforming for 5G Communication Systems," 2020 International Symposium on Antennas and Propagation (ISAP), Osaka, Japan, 2020.

5. Multi-Numerology for 5G Communication Systems

5G communication systems are being designed to be able to work with wider frequency ranges than the current mobile communication systems, ranging from 1 GHz and reaching up to 100 GHz. The adopted structure of the physical layer in LTE systems is based on fixed parameters, leaving little room for flexibility, which constitutes an important feature for the future mobile generation. Consequently, one major characteristic of 5G communication systems is the ability to support different and scalable numerologies [103]. The definition of numerology, as described by 3GPP, is based on a set of parameters required when configuring a waveform, from which a Subcarrier Spacing (SCS) in the frequency domain is built. The SCS is conditioned by the CP value and the symbol length of the OFDM frame structure. The information data is sent over the PRBs, each one accommodating 12 subcarriers separated with a fixed SCS value. The number of PRBs used depends of the channel bandwidth of the system.

This chapter studies the new OFDM multiple numerologies proposed by 3GPP for 5G systems. The definition of 5G NR numerology is initially provided, followed by the performance analysis of a 5G communication system, in terms of BER and throughput, when using the different numerologies proposed for the next mobile generation. The link-level simulation results, consisting on a comparison of the multiple numerologies, provide an understanding on how these affect the behavior of the investigated 5G system, using different environment scenarios.

5.1 5G New Radio Numerology

5G NR numerology is one of the main characteristics of the next mobile generation as it introduces the necessary flexibility in the frame structure that LTE is not able to offer. The OFDM numerology has its flexibility implemented in the frequency domain, but it can also be implemented in the time domain with Transmission Time Interval (TTI) [104].

There are multiple variations for the 5G numerology, as presented in table 22, where each one is defined by certain values for the SCS, CP duration, symbol and slot duration and the number of slots per subframe.

Numerology (μ)	Sub-Carrier Spacing (kHz)	Cyclic Prefix Duration (μs)	OFDM Symbol Duration (μs)	OFDM Symbol Duration+CP (μs)	OFDM Slot Duration (ms)	Slots per Subframe
0	15	4.69	66.67	71.35	1	1
1	30	2.34	33.33	35.68	0.5	2
2	60	1.17	16.67	17.84	0.25	4
3	120	0.57	8.33	8.92	0.125	8
4	240	0.29	4.17	4.46	0.0625	16

Table 22: 5G NR numerology [104].

Each numerology is defined by μ, ranging between 0 and 4. The numerology with μ=0 represents the LTE numerology, with a SCS value of 15 kHz. The values for the remaining SCS are calculated by

$$\Delta f = 2^{\mu} \times 15\ kHz \tag{5.1}$$

From equation 5.1, we can observe that the SCS values are a multiple integer of the fixed SCS value of the LTE numerology. 5G NR multi-numerology will support SCS values ranging between 15 kHz and 240 kHz. A SCS of 15 kHz is mostly preferred for wide area coverage. SCS values of 30 and 60 kHz are intended for dense urban areas and 120 and 240 kHz are considered when adopting higher frequencies such as bands above 10 GHz.

Regarding the frame structure, one main difference between the LTE and 5G network is the number of OFDM symbols in a slot. In the LTE frame structure, one slot is composed by 7 OFDM symbols, while in the 5G frame structure one slot has 14 OFDM symbols.

Figure 46 depicts the different frame structures according to the SCS values. One frame is composed by 10 subframes, with a duration of 10 ms and 1 ms, respectively. Each subframe is formed by slots composed with 14 OFDM symbols each. As it can observed, the number of slots and its duration in a subframe depend on the SCS value selected. For 15 kHz, a subframe contains 1 slot with a duration of 1 ms, while for 240 kHz, a subframe contains 16 slots, each with a duration of 0.0625 ms. However, this case is only used for synchronization, not for data.

An important aspect to consider is the time alignment of the slots. In order to avoid ISI, the delay spread value must be set lower than the CP duration. If there is a decrease on the cell size, the delay spread also decreases. Due to propagation characteristics of the environment, higher carrier frequencies are used when considering small cells [105].

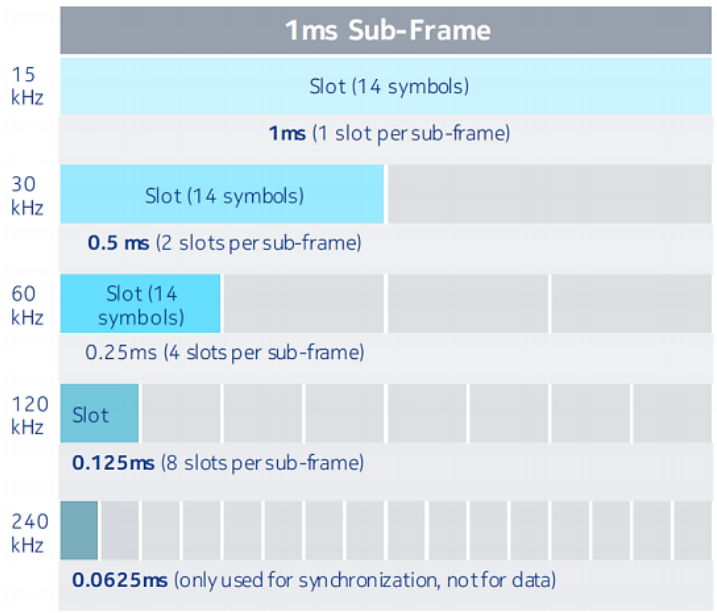

Figure 46: Frame structure of the 5G multi-numerology [69].

A slot is regarded as the fundamental transmission unit. Nevertheless, there is the possibility of complementing the transmission with mini-slots, so that a shorter and prompter transmission is achieved. The mini-slots have variable lengths, depending on the number of OFDM symbols adopted. 3GPP established that a mini-slot can be composed by 2,4 or 7 OFDM symbols, providing this way a faster transmission with lower latency [106].

5.2 Performance Evaluation of OFDM Multi-Numerology for 5G

In this sub-section we evaluate the performance of a 5G communication system using the different OFDM numerologies proposed for the next mobile generation systems. The performance is analyzed in terms of BER and throughput, using Nokia's internal link-level simulator.

5.2.1 System Model Characterization

The system model used to perform the simulations is a single-user DL massive MIMO 5G system. It is composed by 1 BS equipped with 64 transmitted antennas and 1 MS equipped with 4 receiver antennas, moving at 3 km/h. The system uses digital beamforming at the transmitter side. The modulation type adopted is 64QAM modulation and the SNIR range selected is between 15 and 40 dB, reproducing a real environment scenario. The channel model adopted is the CDL_A profile. The list of

parameters and scenarios adopted are described in table 23. We consider 3 main scenarios. Scenario 1 uses a carrier frequency of 6 GHz, comprised in FR1, and a SCS of 30 kHz. Scenarios 2 and 3 use both a carrier frequency of 28 GHz, comprised in FR2, and SCS values of 60 and 120 kHz, respectively. All 3 scenarios are simulated with 2 environments: indoor office with a DS of 18 ns representing environment a, and urban micro cell street canyon with a DS of 95 ns representing environment b.

Parameters	Carrier Frequency (GHz)	Frequency Range (FR)	Sub-Carrier Spacing (kHz)	Environment
Scenario 1a	6	FR 1	30	Indoor Office
Scenario 1b	6	FR 1	30	UMi Street Canyon
Scenario 2a	28	FR 2	60	Indoor Office
Scenario 2b	28	FR 2	60	UMi Street Canyon
Scenario 3a	28	FR 2	120	Indoor Office
Scenario 3b	28	FR 2	120	UMi Street Canyon

Table 23: List of parameters for the simulations [107].

5.2.2 Performance Results

Figures 47 and 48 present the performance results in terms of BER and throughput using the indoor office environment with a DS of 18 ns. On the other side, figures 49 and 50 present the results using the street canyon environment with a DS of 95 ns.

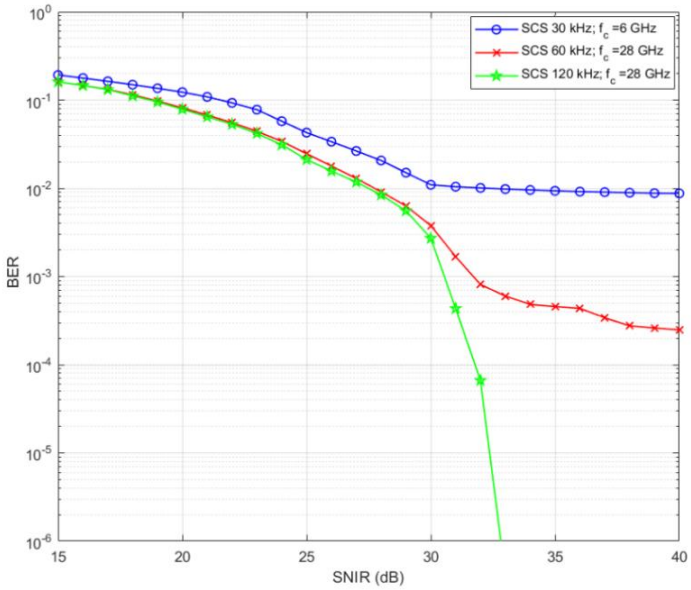

Figure 47: BER results with indoor office environment.

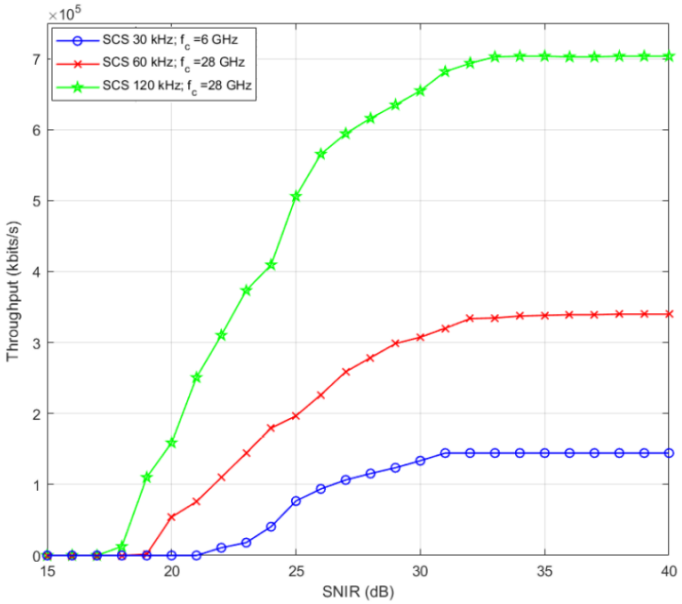

Figure 48: Throughput results with indoor office environment.

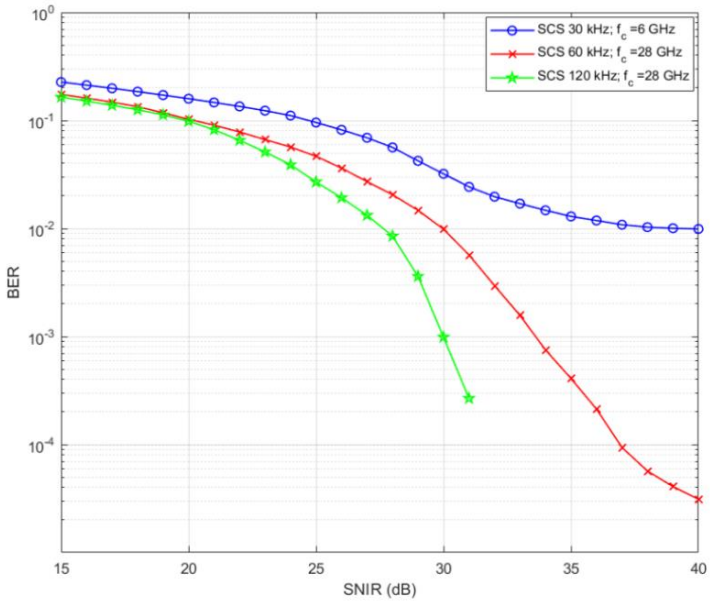

Figure 49: BER results with street canyon environment.

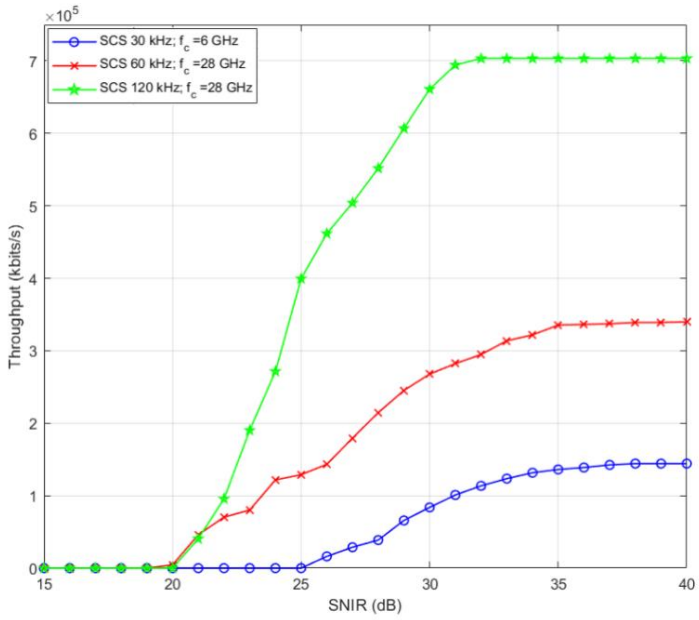

Figure 50: Throughput results with street canyon environment.

As it can be observed in the figures above, in terms of BER, for both indoor office and street canyon environments, the best performance is observed when using a SCS of 120 kHz with a carrier frequency of 28 GHz, followed by the case with a SCS of 60 kHz and a carrier frequency of also 28 GHz. The system performs the worst when using a SCS of 30 kHz with a carrier frequency of 6 GHz. Normally, since we are dealing with a fading channel (CDL_A model), it should be expected that as we increase the carrier frequency the BER to get worse. This indicates that there is an error with the BER simulation results that are due to issues with simulation parametrization or in the simulator itself. The enormous difference for the curves after 30 dB can be explained by having a short simulation time, where the statistics get quite worse.

In terms of throughput, for the worst case scenario, represented by the blue curve, with a SCS of 30 kHz and a carrier frequency of 6 GHz, the maximum throughput reached is approximately 140 Mbps at 31 dB of SNIR. For the second scenario, represented by the red curve, having the SCS doubled to 60 kHz with a carrier frequency of 28 GHz, an increase of 142% is observed on the maximum throughput achieved, reaching up to 340 Mbps. Lastly, for the best case scenario, represented by the green curve, with the SCS of 120 kHz, a maximum throughput of 700 Mbps is achieved, increasing with 106% in comparison to the case when using a SCS of 60 kHz. It is important to discuss that theoretically we would expect the throughput values to double from the case with 30 kHz SCS and 60 kHz SCS. Practically, we observed that the increase was slightly higher than 2x more. The same thing can be observed when comparing the 60 kHz SCS case with the 120 kHz SCS case. The reason why the throughput is slightly higher than the one expected theoretically is due to the presence of additional sweeping slots. There is 1 sweeping slot dedicated to synchronization that occurs every half frame. During the simulations,

we settled that for the first scenario (30 kHz) there was 1 sweeping slot every 10 slots, for the second scenario (60 kHz) there was 1 sweeping slot every 20 slots and for the last scenario (120 kHz) there was 1 sweeping slot every 40 slots. This means that as we increased the SCS value, we had less sweeping slots for synchronization and therefore some additional ones for data transmission, leading to the small difference on throughput values.

Moreover, it was demonstrated that increasing the value for the SCS while using higher values for the carrier frequency, leads to an improvement on the performance of the 5G system, which translates to a lower BER and a higher throughput. The considerable improvement reflects how important is to have a flexible numerology for the next mobile generation, as one of the principal requirements for 5G systems is to be able to provide extremely high data rates. Additionally, we verified that selecting a DS of 18 ns, for the indoor office environment, the maximum throughput is achieved faster than for the case with a DS of 95 ns, representing the street canyon environment. As for the BER, a lower value is obtained for the indoor office environment, which reflects reality. In conclusion, a flexible numerology constitutes an important feature for 5G NR communication systems, as it brings a considerate increase in data rates and therefore it is viewed as one of the technologies that will allow 5G systems to reach the target values agreed and proposed by the standardization bodies. The results obtained led to the publication of the following paper:

1. G. Barb, M. Otesteanu, F. Alexa and F. Danuti, "OFDM Multi-Numerology for Future 5G New Radio Communication Systems," 2020 International Conference on Software, Telecommunications and Computer Networks (SoftCOM), Split, Hvar, Croatia, 2020, ISBN: 978-953-290-099-6.

6. Dynamic Spectrum Sharing in 4G/5G Networks

The requirements established for the next mobile generation are extremely ambitious with high target values. As detailed in previous chapters, the current architecture, equipment and spectrum utilized do not support these requirements. One major factor that needs to be taken into consideration is the use of the available spectrum, as it is a limited and expensive resource, specially from the operator's perspective. The current mobile frequency spectrum used is mostly saturated, comprised between 300 MHz and 6 GHz. The need for new available frequency spectrum is mandatory for the next mobile generation. Thus, 5G will use not only frequency bands below 6 GHz, but also higher, reaching up to 300 GHz [108] [109]. The low band spectrum, with frequencies below 1 GHz, is intended for high coverage and penetration situations. The mid band spectrum and high band are intended for obtaining high data rates, reaching up to 1 Gbps in the case of the mid band spectrum and up to 20 Gbps with very low latency in the case of the high band spectrum. However, for the last case, the high data rate comes with the inconvenience that the high band spectrum offers low coverage and penetration. Therefore, it is only suitable to be used in closed or indoor environments.

Being that the frequency spectrum is a scarce resource, in order to improve spectrum efficiency and to reduce its associated cost for the operator, a new solution is introduced and is being investigated: Dynamic Spectrum Sharing (DSS).

This chapter discusses a new solution for improving spectrum efficiency and consequently being able to reach the target requirements for 5G communication systems. Firstly, the concept of DSS is explained, which is divided in two phases. The differences between Phase 1 and Phase 2 are detailed. Following, the performance of a LTE-NR system is evaluated in terms of throughput and bandwidth occupied using the DSS technology. Various possibilities for the resource allocation are proposed, and the performance is analyzed according to the different sharing ratios adopted.

6.1 Dynamic Spectrum Sharing

The official standardization procedure regarding shared spectrum principles of 5G NR systems started in March 2017 by 3GPP [110]. A solution for the allocation of the frequency spectrum for 5G communication systems consists in re-using the existing frequency spectrum bands that are being used by the "on-air" technologies, such as 2G, 3G and 4G.

DSS is a solution that allows operators to use simultaneously both LTE and NR technologies in the same frequency operating bands, although in an interleaved mode.

This brings a major advantage for the operator, since it assures the deployment of 5G systems without needing to buy additional dedicated spectrum bands.

Figure 51 portrays the concept of DSS with LTE and NR sharing the same frequency bands in comparison with the case of needing separate bands for each technology.

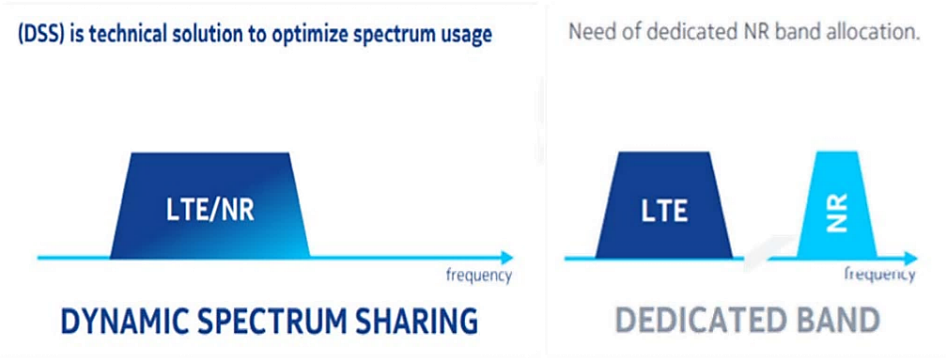

Figure 51: DSS concept [111].

The deployment of the DSS technology is divided in two phases: Phase 1 and Phase 2, in order to facilitate its deployment. Phase 1 contains some limitations that are expected to be solved with Phase 2, such as [112]:

- It can support only FDD;
- It is limited to 2x2 or 4x4 MIMO systems;
- It supports only the NSA architecture;
- It cannot be applied in a shared radio/multi-vendor solution.

In addition to the above-mentioned limitations, there are also some requirements that need to be respected. These are:

- Both LTE and NR need to operate in the same frequency band with the same bandwidth allocated;
- Timing over packet or Global Positioning System (GPS) is required;
- Both LTE and NR need to use the same time zone;
- Phase synchronization needs to be used.

6.1.1 Phase 1 DSS

Downlink

The downlink resource sharing for Phase 1 DSS is done on a subframe basis in Time Division Multiplexing (TDM). The allocation ratio for NR subframes can be between 20% and 60% of the total number of subframes. The allocations are done in 10% steps. In order to avoid the transmission of LTE symbols in dedicated subframes for NR, Multicast-Broadcast Single Frequency Network (MBSFN) subframes are implemented.

One frame is composed by 10 subframes, from which 2 to 6 can be used by NR, as it can be observed in figure 52, corresponding to a 20% to 60% sharing ratio of NR-LTE. The dedicated subframes for LTE are 0, 4, 5 and 9. If we consider the minimum sharing ratio of 20%, corresponding to 2 subframes for NR, these will be subframes 1 and 2. Subframes 6, 7 and 8 are allocated dynamically for either LTE or NR, according to the selected sharing ratio, and depending on the traffic conditions.

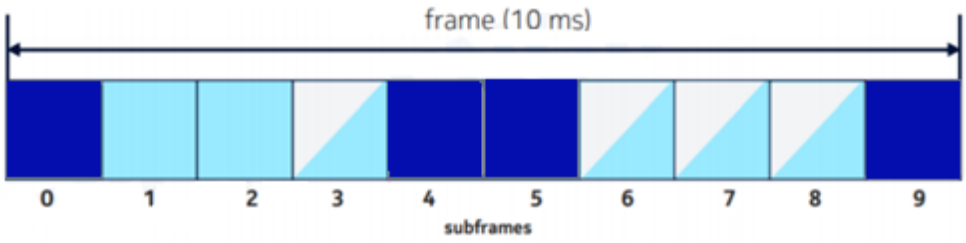

Figure 52: Subframes allocation for Phase 1 DSS [111].

The definition of the sharing ratio between LTE and NR is coordinated by a new system entity denominated Common Resource Manager (CRM). The CRM computes the sharing ratio allocated and modifies it according to traffic demands. Initially, the CRM gathers information from both LTE and NR sites and defines the parameters and resources that are shared between both technologies. Based on that, it selects the sharing ratio to be used and allocates the shared resources to LTE and NR. The CRM continuously receives information from both LTE and NR sites and according to traffic demands for a specific moment, it evaluates the optimal sharing ratio and updates it as needed.

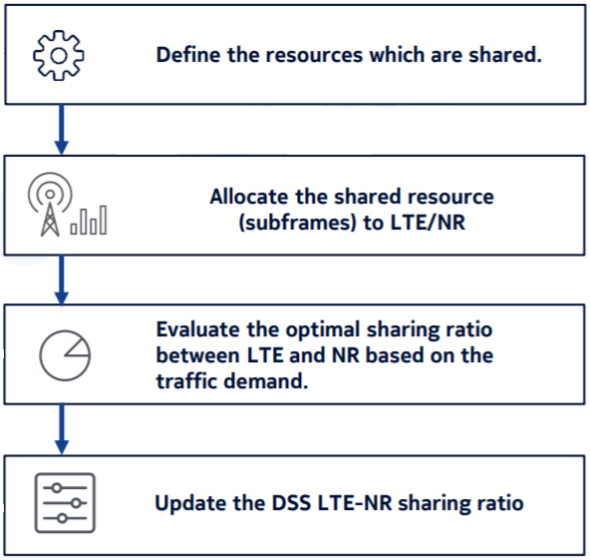

Figure 53: CRM main tasks [111].

The sharing ratio is calculated based on two main parameters:

- Average relative NR DSS PRB Load, $RB_{avg_{load}}$;
- Relative NR DSS PRB Load, RB_{load}.

The two parameters are calculated and then updated according to the following equations

$$RB_{avg_{load}}(n) = RD\alpha \times RB_{load}(n) + (1\text{-}RD\alpha) \times RB_{avg_{load}}(n\text{-}1) \quad (6.1)$$

$$RB_{load} = 100 \times \frac{NR_{load\_weighted}}{LTE_{load\_weighted} + NR_{load\_weighted}} \quad (6.2)$$

where $LTE_{load\_weighted}$ and $NR_{load\_weighted}$ are given by the following expressions, respectively

$$LTE_{load\_weighted} = \frac{\text{RBs used by LTE}}{\text{RBs available for LTE}} \times 100 \quad (6.3)$$

$$NR_{load\_weighted} = \frac{\text{RBs used by NR}}{\text{RBs available for NR}} \times 100 \quad (6.4)$$

Uplink

The uplink resource sharing for Phase 1 DSS is done on a subframe basis in Frequency Division Multiplexing (FDM). Therefore, the rule that is applied for uplink is that the direction UL is shared in a static way between LTE and NR, in the frequency domain. This means that both LTE and NR transmissions in the uplink direction take place in each TTI.

For the case of 10 MHz and 15 MHz bandwidth, the resources are allocated as presented in figure 54: the 6 PRBs that are located in the most outer region of the frequency spectrum are allocated to NR, while the remaining are granted to LTE.

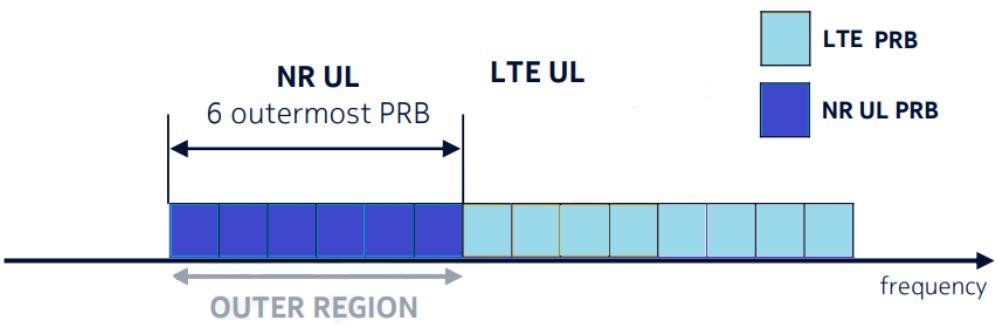

Figure 54: UL sharing resources for 10 and 15 MHz cell bandwidth.

For the case of 20 MHz cell bandwidth, the lower and upper 6 PRBs are blanked. Similarly, to the case of 10 and 15 MHz bandwidth, the lower 6 PRBs are granted to NR. However, the difference is that the upper 6 PRBs are not allocated to NR or LTE transmission, see figure 55.

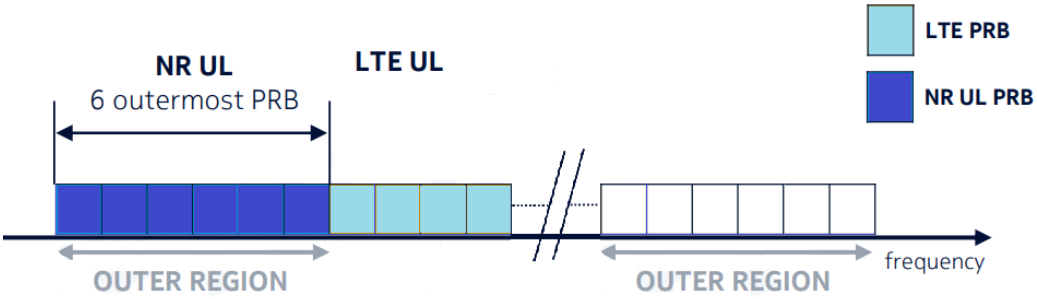

Figure 55: UL sharing resources for 20 MHz cell bandwidth.

Dimensioning Impact

LTE downlink

As NR and LTE share the resources from one frame, with NR using from 20% up to 60% of the TTIs, this leads to a decrease on the DL resources available for LTE. However, the number of PRBs in one TTI doesn't change, therefore there is no impact on the DL side regarding power. Notwithstanding, due to the lower number of TTIs that can be allocated to LTE, depending on the sharing ratio adopted, the LTE capacity is decreased, between 20% and 60%.

LTE uplink

In UL, NR has 6 PRBs granted in the lower outer region of the frequency carrier. Moreover, for 20 MHz bandwidth, an additional 6 PRBs on the upper edge side are left blanked. This leads to an impact on coverage for LTE, since the number of available PRBs for LTE UL is lower. In addition, due to the lower number of available PRBs for LTE, the capacity is reduced. The actual impact on the LTE capacity decrease depends on the bandwidth and number of PRBs allocated.

NR downlink

From the NR perspective, for DL, between 40% and 80% of the subframes can be allocated to LTE, hence, the capacity decrease depends on the allocated sharing ratio. However, it is expected a decrease of 50% up to approximately 80%.

NR uplink

Regardless the cell bandwidth, NR has granted the first 6 PRBs from the left outer edge of the carrier frequency. The allocation of the slots depends on the sharing ratio selected.

6.1.2 Phase 2 DSS

Phase 2 DSS constitutes the follow-up to Phase 1 DSS. The main differences and improvements/developments that Phase 2 DSS brings in comparison to Phase 1 are detailed in table 24.

Phase 1 DSS	Phase 2 DSS
Sharing ratio between 20 and 60%	Sharing ratio between 5 and 70%
UL sharing is fixed	UL sharing is dynamic
Supports only NSA architecture	Supports both NSA and SA architecture
Sharing ratio updates takes several minutes	Sharing ratio updates are fast, within 100 ms

Table 24: Differences between Phase 1 DSS and Phase 2 DSS.

Downlink

For downlink Phase 2 DSS, the allocation of the subframes is also TDM based as in Phase 1 DSS and is as shown in figure 55. In one frame, subframes 0, 5 and 9 are dedicated to LTE transmission only, regardless the sharing ratio adopted. The remaining subframes can be used for both LTE and NR transmission, depending on the architecture mode and sharing ratio selected, see figure 56.

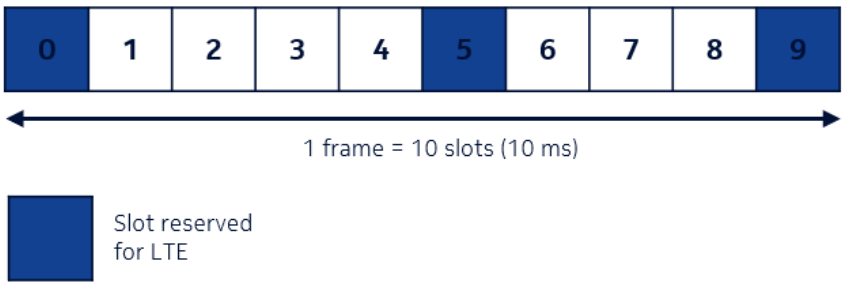

Figure 56: Downlink sharing allocation for Phase 2 DSS [113].

Depending on the sharing ratio, the allocation of the resources has different patterns. If we consider the NSA architecture mode, several patterns are depicted in figure 57. Regardless the sharing ratio, it can be observed that slots 0, 5 and 9 for all frames is dedicated to LTE transmission.

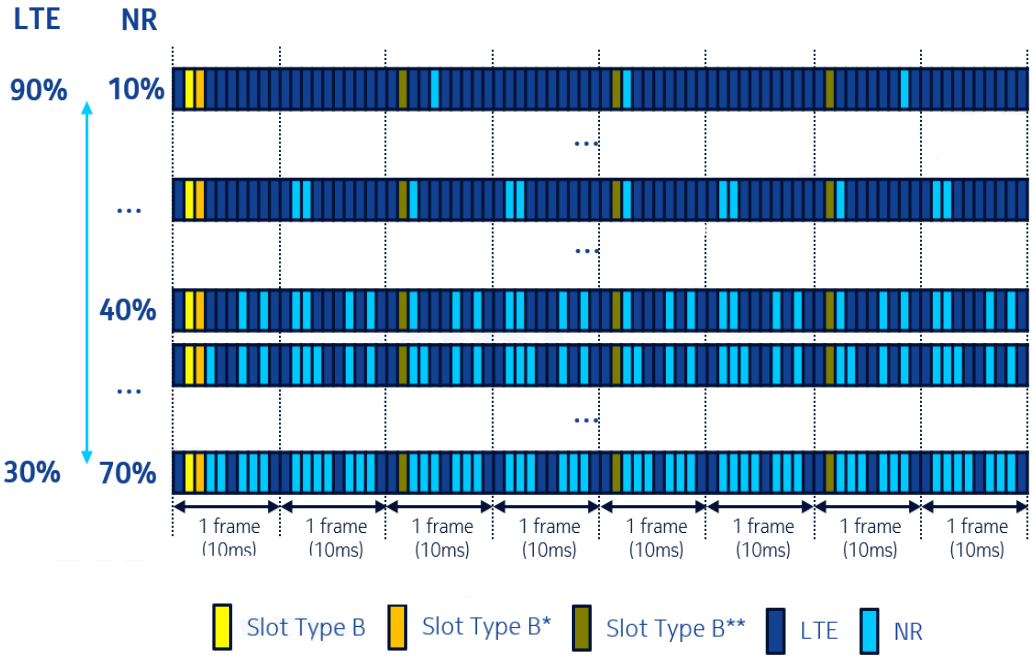

Figure 57: Examples for the resource sharing patterns for Phase 2 DSS [113].

Moreover, at the beginning of the first frame, slot 1 represented with the color yellow (Type B) and slot 2 represented with the color orange (Type B*) are used for the transmission of synchronization signals and CSI-RS signals, respectively. For the remaining frames, synchronization signals are sent with a periodicity of 20 ms in slot 1, represented by the color green (Type B**). The remaining slots are used for LTE and NR transmission.

Uplink

The uplink resource sharing of Phase 2 DSS is based on FDM, similarly to Phase 1 DSS. The sharing ratio for uplink is selected according to the number of available PRBs for LTE. The CRM selects an area for dynamic shared resources between LTE and NR, depending on the sharing ratio and carrier bandwidth adopted, represented by the color green in figure 58.

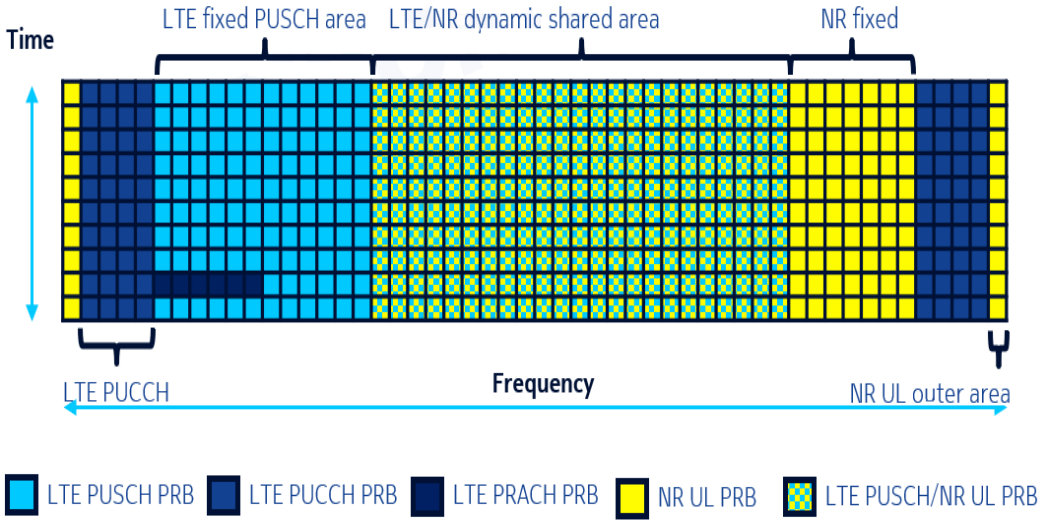

Figure 58: UL resource sharing for Phase 2 DSS [113].

The NR has guaranteed 7 PRBs that cannot be used by LTE, depicted in the upper outer edge of the frequency band in figure 58. However, the placement of the dedicated PRBs for NR UL depends on the position of the LTE PRACH PRBs, which in this case are positioned on the left outer region of the frequency band. If the LTE PRACH PRBs were located on the right outer area, then the NR UL PRBs would be positioned in the opposite side, on the left outer area.

In order to calculate the maximum available NR-LTE UL sharing ratio, the following expression is given

$$\text{Sharing ratio}_{\text{Max\_UL}} = 1 - \left(\frac{\text{N+ PUCCH}_{\text{Max\_LTE}}}{\text{LTE BW in PRBs}}\right) \quad (6.5)$$

where *N* constitutes the number of PRBs that are compulsory for LTE transmission, such as for LTE PRACH in the inner region of the carrier frequency.

Sharing Ratio Calculation

Downlink

The CRM receives information, depending on traffic demands, regarding the load indication, and it makes a decision on the DL sharing ratio that needs to be applied. In order to calculate the DL load, the following values need to be determined:

- Weighted load, based on the PRB occupancy;
- Average LTE DSS Guaranteed Bit Rate (GBR) load, NR DSS GBR load and NR PDCCH load.

The algorithm applied to calculate the sharing ratio is as depicted in figure 59. The first step of the algorithm consists on the CRM verifying the LTE GBR load and the NR PDCCH load against the threshold in order to decide on the resources assigned. If the first case is applied, with the average LTE GBR load being higher than 70% while the NR PDCCH load is lower than 70%, then the NR sharing ratio is reduced. If the second case is applied, with the average LTE GBR load being equal or lower than 70% and the NR PDCCH load is higher than 70%, then the NR sharing ratio is increased. For the last case, where both LTE and NR loads are higher than 70%, the following conditions are applied:

- If LTE GBR resource delta (n,n-1)>0, then the NR sharing ratio is reduced;
- If LTE GBR resource delta (n,n-1)≤0 and NR PDCCH resource delta (n,n-1)>0, then the NR sharing ratio is increased.

The second step takes in consideration the received load information from step 1. Based on it, the CRM determines the LTE weighted load and the NR weighted load, from which the LTE total load and NR total load are calculated.

In step 3, with the calculated values for the LTE total load and NR total load from step 2, the number of LTE subframes and NR subframes is determined, which corresponds to a specific sharing ratio.

Uplink

Similarly to the downlink procedure, based on the load information received and the traffic demands, the CRM decides on the UL sharing ratio that needs to be applied. In order to calculate the UL load, the following values need to be determined:

- Weighted load, based on PRB occupancy;
- Average LTE DSS GBR load.

The algorithm applied to calculate the sharing ratio is depicted in figure 60.

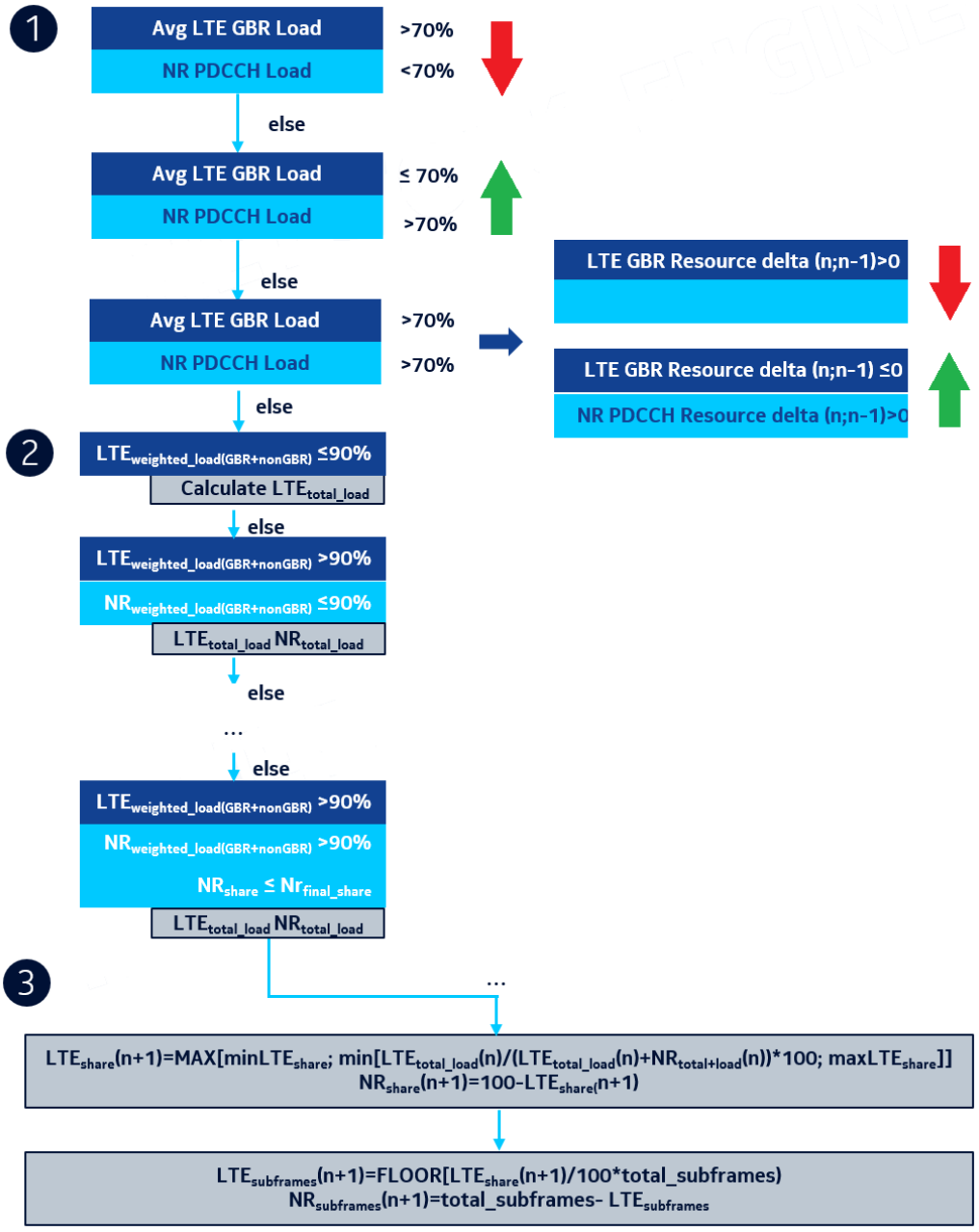

Figure 59: Algorithm to calculate DL sharing ratio [113].

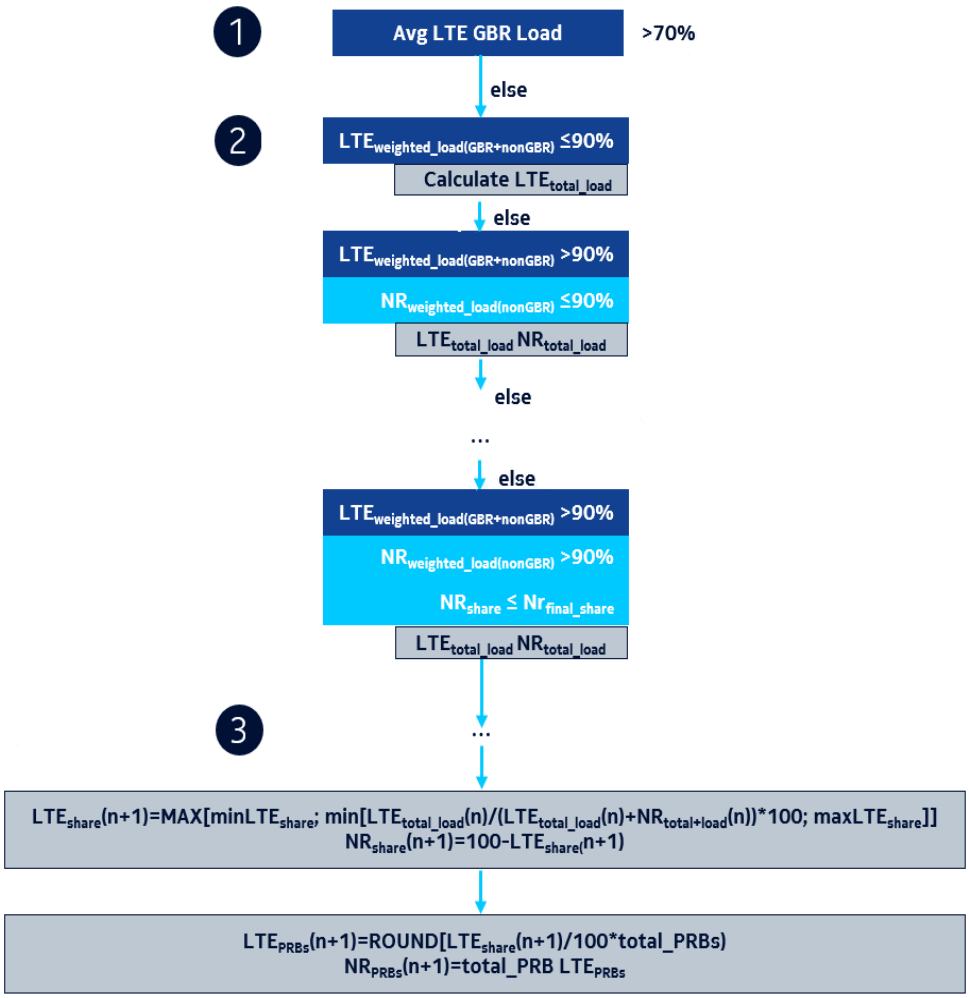

Figure 60: Algorithm to calculate UL sharing ratio [113].

In step 1, the CRM verifies the average LTE GBR load in order to decide on the resources assigned. If the average LTE GBR load is higher than 70%, then the NR sharing ratio is decreased.

In step 2, taking in consideration the received load information, the CRM determines the LTE weighted load and the NR weighted load, from which the LTE total load and NR total load are calculated.

Finally, in step 3, with the calculated values for the LTE total load and NR total load from step 2, the number of LTE subframes and NR subframes is determined, which corresponds to a specific sharing ratio.

Dimensioning Impact

LTE downlink

As NR and LTE share the resources from one frame, with NR using from 5% up to 70% of the available slots, this leads to a decrease on the DL resources available for LTE. However, the number of PRBs from one slot doesn't change, therefore there is no impact on the DL side regarding power, similarly to Phase 1 DSS.

LTE uplink

The dimensioning impact on LTE UL is as in Phase 1 DSS. Both coverage and capacity are decreased, due to the fact that the number of available PRBs is lower for LTE.

NR downlink

From the NR perspective, for DL, between 30% and 95% of the subframes can be allocated to LTE, hence, the capacity decrease depends on the allocated sharing ratio.

NR uplink

Due to the lower number of available PRBs in comparison to a NR only system, there is an impact on the NR UL coverage, as it is decreased. The NR UL capacity, depending on the sharing ratio adopted, has a decrease that can vary between 14% and 68%.

6.1.3 System Model Characterization for Phase 1 DSS

The system model adopted for investigating and measuring the impact of Phase 1 DSS for LTE-NR technologies consists on a downlink 2x2 MIMO system, composed by 1 BS and 1 MS. The modulations adopted are 64QAM and 256QAM modulations for LTE and 5G, respectively. For both technologies we selected a bandwidth of 10 MHz, using FDD duplex mode. The architecture for NR adopted is NSA, as is the only one supported by Phase 1 DSS. We perform throughput measurements using physical and static equipment from Nokia Networks R&D laboratory. We propose different resource allocation schemes for LTE and NR in a subframe, for several sharing ratio values. The allocation schemes and sharing ratio values are presented in table 25.

Sharing Ratio (%)	LTE Subframes Number	5G Subframes Number
20	0,3,4,5,6,7,8,9	1,2
30	0,3,4,5,7,8,9	1,2,6
40	0,3,4,5,7,9	1,2,6,8
50	0,4,5,7,9	1,2,3,6,8
60	0,4,5,9	1,2,3,6,7,8

Table 25: Proposed resource allocation schemes for LTE-NR Phase 1 DSS.

6.1.4 Performance Results for Phase 1 DSS

We start by analyzing the impact of DSS with the first scheme from the ones proposed in table 24, meaning that a sharing ratio of 20% is selected, with LTE occupying 80% of the available resources (subframes 0,3,4,5,6,7,8,9) while NR occupies 20% (subframes 1,2). In order to study the impact of DSS, we measured the throughput for 30 iterations, each one with a duration of 1 s. Figure 61 depicts the throughput results without using Phase 1 DSS technology.

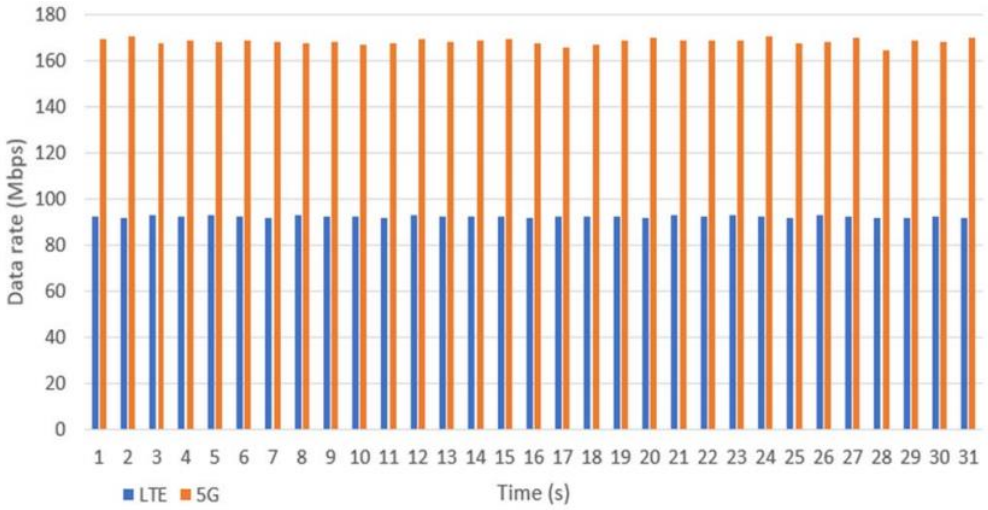

Figure 61: Throughput results without Phase 1 DSS for LTE-NR.

Both LTE and NR are served by the same radio modules, however with separate spectrum resources. The central frequency of LTE is 2155 MHz, while for NR is 2165 MHz. The average throughput value for LTE is 92.43 Mbps while for NR is 168.58 Mbps, with an increase of 82% compared to LTE.

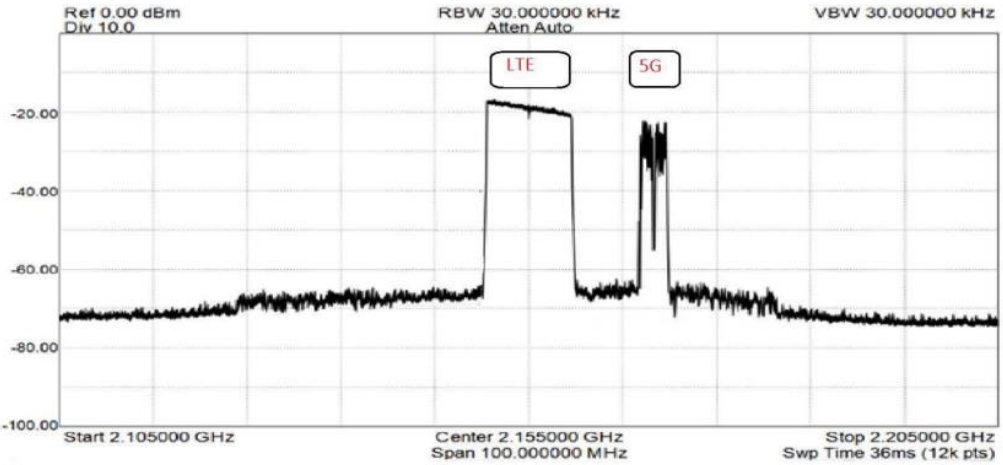

Figure 62: Spectrum usage for LTE and NR without Phase 1 DSS.

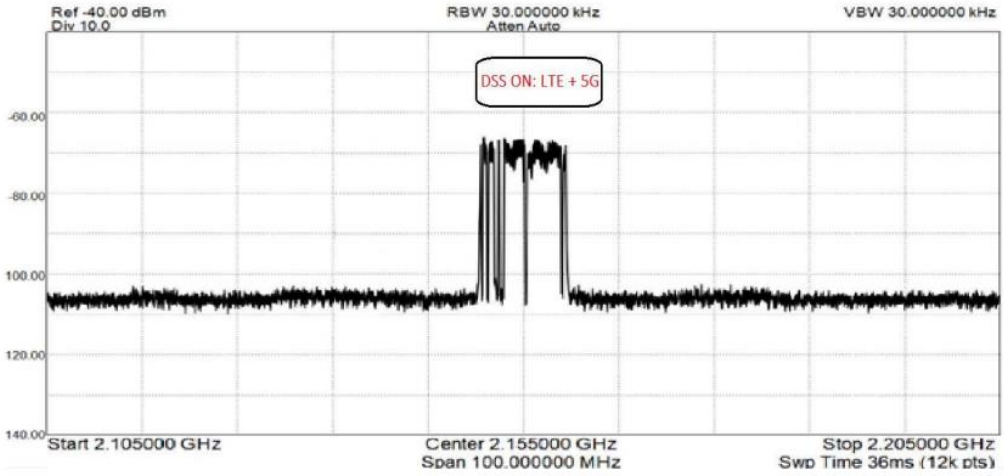

Figure 63: Spectrum usage for LTE and NR with Phase 1 DSS.

Figures 62 and 63 depict the spectrum usage for LTE-NR for both cases of not using the DSS technology and when using it, respectively. It can be observed, for the first case, that each technology has a separated and dedicated frequency spectrum. A number of peaks can be observed for 5G NR, which is due to the fact than even if the bandwidth used for both technologies is the same, 5G makes use of the spectrum more efficiently, leading to the appearance of peaks, and not being continuous as for the LTE case. For the second case, figure 63, it can be observed that both technologies share the same 10 MHz frequency spectrum.

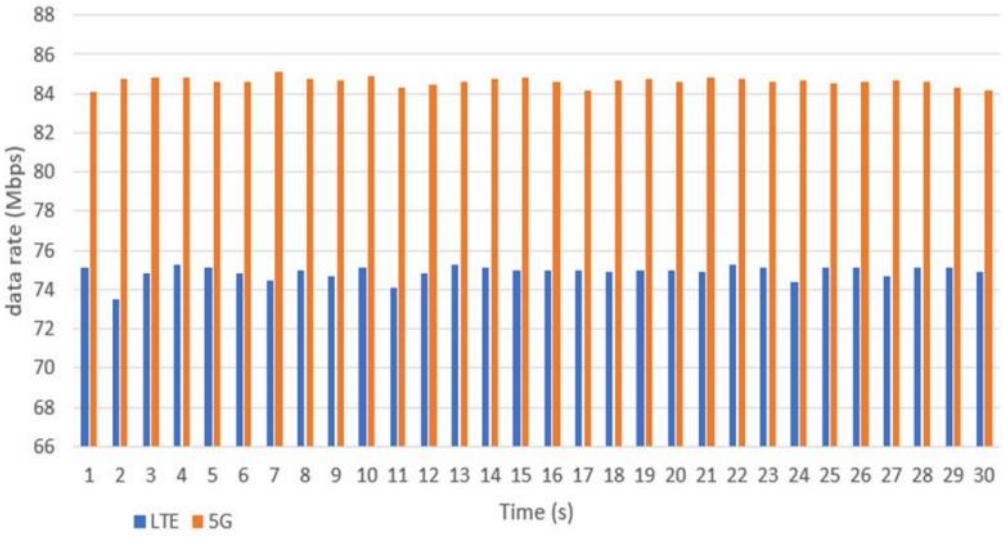

Figure 64: Throughput results with Phase 1 DSS for LTE-NR.

Figure 64 depicts the throughput results when using Phase 1 DSS. The difference from the case of figure 60 is that now the spectrum resources are shared between LTE and NR. The central frequency is shared between both technologies and it values 2155 MHz, with a sharing ratio of 20%, see figure 63. The average throughput reached by LTE is 74.88 Mbps, registering a decrease of approximately 19%. For NR, the average throughput achieved is 84.62 Mbps, with a decrease of approximately 50%. The decrease observed for the throughput values is expected for both technologies, since the available resources are now shared between LTE and NR, with NR using only 20% of them.

The same analysis is performed for the remaining sharing ratios with the proposed allocation schemes from table 24. Using a central frequency of 2155 MHz with a bandwidth of 10 MHz, figure 64 presents the average throughput for the sharing ratios of 20, 30, 40, 50 and 60%. As it can be observed, as the sharing ratio increases, the LTE average throughput decreases, which is expected since the number of subframes allocated decreases with the increase of sharing ratio. Meanwhile, the 5G NR throughput increases. For the last case of 60% sharing ratio, meaning that NR uses 60% of the available resources while LTE uses only 40%, the throughput achieved by NR is approximately 130 Mbps while LTE reaches up to 36 Mbps. If compared to the case where Phase 1 DSS is not used, a decrease in the NR throughput of 23% is observed.

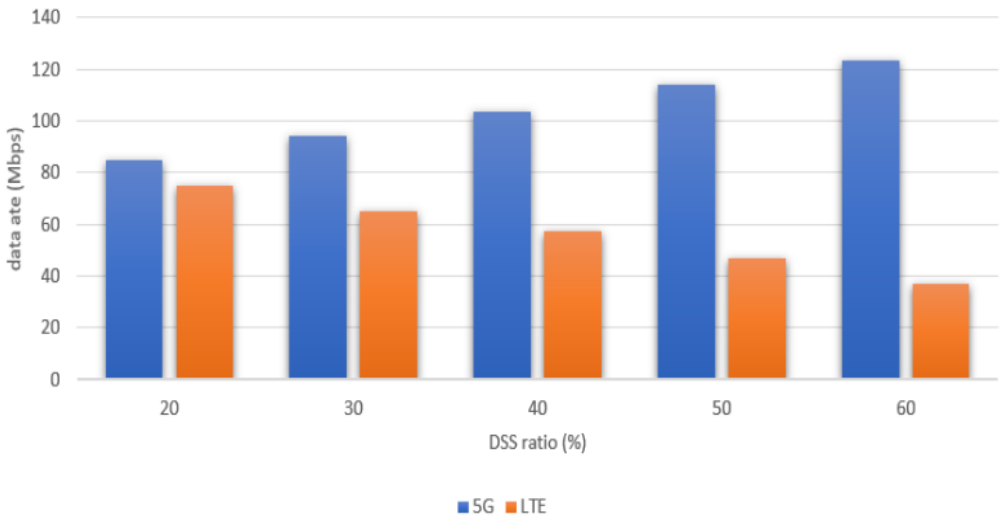

Figure 65: Throughput results for different sharing ratios using Phase 1 DSS.

It is clear that using Phase 1 DSS brings a compromise on data rates. Nevertheless, it brings a major advantage, specially from the mobile network operator point of view, which consists in the increase of spectrum efficiency. When using Phase 1 DSS, the operator does not need to buy new specific and dedicated spectrum in order to deploy the NR network, which leads to cost reductions and a more efficient use of the available frequency spectrum, while being able to offer 5G services. The disadvantage is the decrease in throughput, that can vary depending on the sharing

ratio adopted. However, the results obtained showed that the 5G throughput decrease is not extremely high. As observed, for a sharing ratio of 60%, NR suffers a decrease in throughput of 23%, but instead of needing two separate bandwidth of 10 MHz each, one for LTE and one for NR, the operator can re-use the 10 MHz bandwidth of LTE for NR also.

In conclusion, the Phase 1 DSS technology is an opportune solution to deploy 5G communication systems for the mobile network operators. The main advantage is that the MNO is able to introduce NR services without needing to buy dedicated frequency spectrum for it. Moreover, the sharing of the spectrum is dynamic, meaning that according to the traffic demands of a specific moment, the sharing ratio is updated in agreement to the user needs for that time or/and location.

6.2 System Model Characterization for Phase 2 DSS

The system model adopted for the measurements with Phase 2 DSS consists on a MIMO system, constituted by one base station and one mobile station. Both 64QAM and 256QAM modulation are used for the measurements. A bandwidth of 15 MHz is selected with a NR-ARFCN of 175800 for downlink and 166800 for uplink. For all cases we use FDD. Throughput measurements are investigated using physical and static equipment from Nokia Networks R&D laboratory. A SNIR higher than 25 dB and a Reference Signal Receive Power (RSRP) higher than -70 dBm with LoS and without the presence of fading are considered. We study both downlink and uplink directions, using the NSA and SA architectures. The sharing ratios considered for NSA architecture are between 20% and 70%, while for SA we consider between 30% and 70%. We use for DL 2x2 MIMO and 4x4 MIMO with 2 and 4 layers, respectively. The maximum number of layers possible is equal to the minimum number of antennas used for the transmitting or receiving side. For UL we use only 1 layer, as we only have 1 transmitting and one receiving antenna. Table 26 recapitulates the parameters adopted for the Phase 2 DSS measurements.

CASE	DIRECTION	BANDWIDTH	NR. OF LAYERS	MODULATION	MIMO
1	DL	15	2	64QAM	2x2
2	DL	15	2	256QAM	2x2
3	DL	15	4	64QAM	4x4
4	DL	15	4	256QAM	4x4
5	UL	15	1	64QAM	1x1

Table 26: List of parameters adopted.

Each type of architecture has several possible variations. The NSA architecture is based on the LTE core network and makes use of LTE based interfaces. For this case, the gNodeB needs to support these interfaces while behaving as a secondary node, since the eNodeB acts as primary/master node. There are different possibilities to deploy the NSA architecture – option 3, 3a, 3x, 4, 4a, 7 and 7a. The option selected for our measurements is the NSA option 3x, where the control plane is routed through primary eNodeB and user plane is directly routed through secondary gNodeB. The

eNodeB likewise connects directly with the gNodeB and both base stations communicate directly with the EPC.

On the other hand, the SA architecture is composed by 2 options – option 2 and 5. Option 2 is the one selected for our work and, as it can be seen in figure 66 (b), consists on a NGC and a gNodeB that communicates directly with it, without the need of any support of LTE equipment. For both network architectures studied, we consider two radio modules, each one having attached to it one attenuator, since the measurements are performed in a laboratory with close distance to the mobile user. We use either 2 or 4 antennas, depending on the case studied.

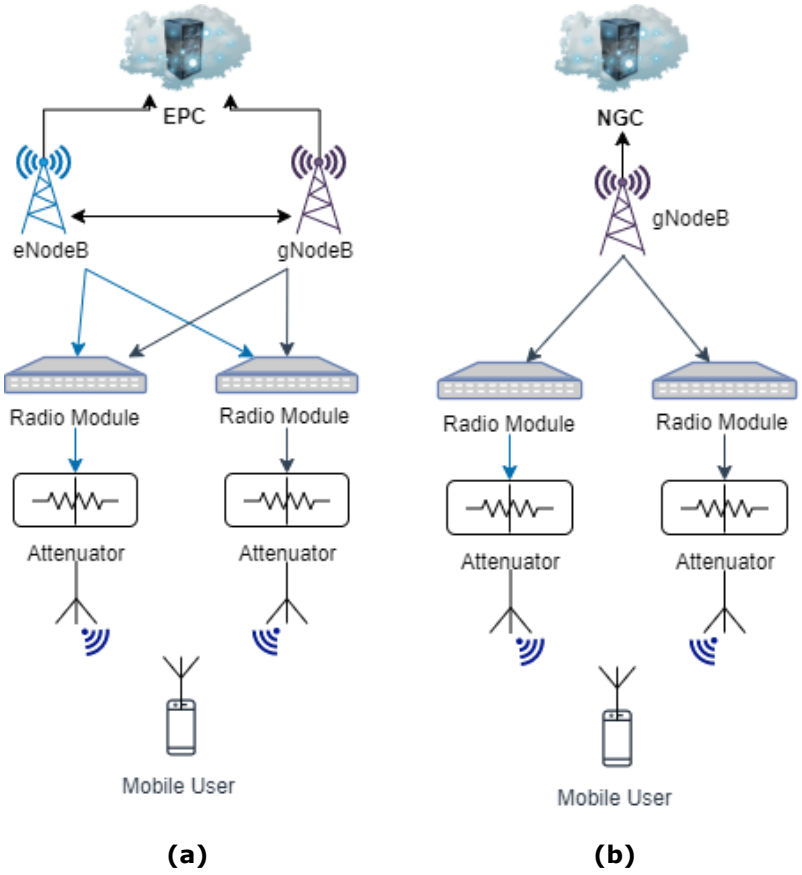

Figure 66: Architecture scheme adopted. (a) NSA architecture; (b) SA architecture.

6.2.1 Performance Results for Phase 2 DSS

We begin by presenting the downlink results, for the NSA and SA architecture, consisting on the first 4 cases from table 25.

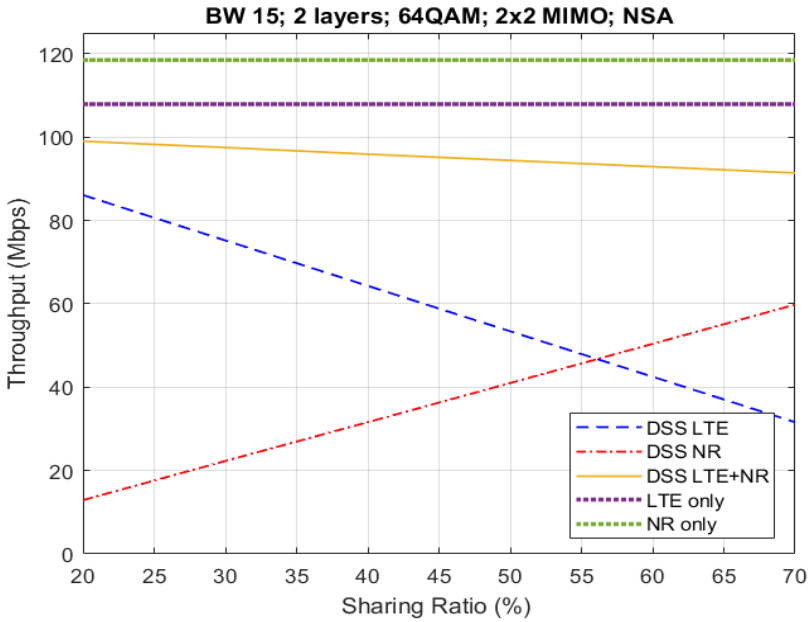

Figure 67: Throughput results for DL NSA architecture for case 1.

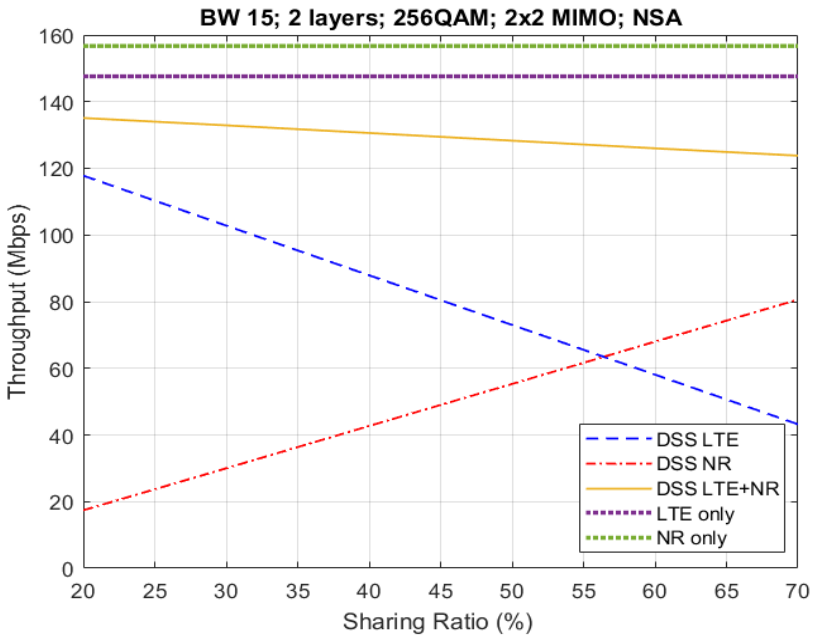

Figure 68: Throughput results for DL NSA architecture for case 2.

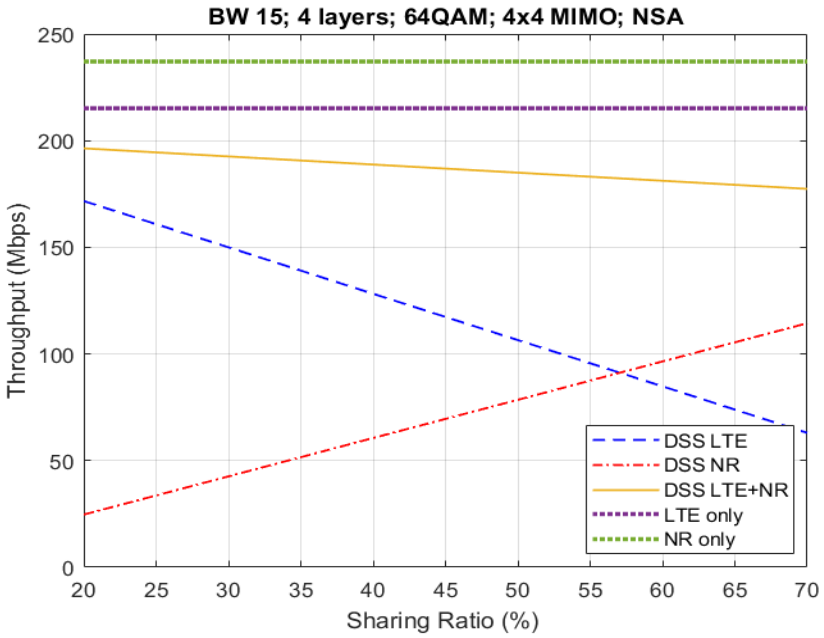

Figure 69: Throughout results for DL NSA architecture for case 3.

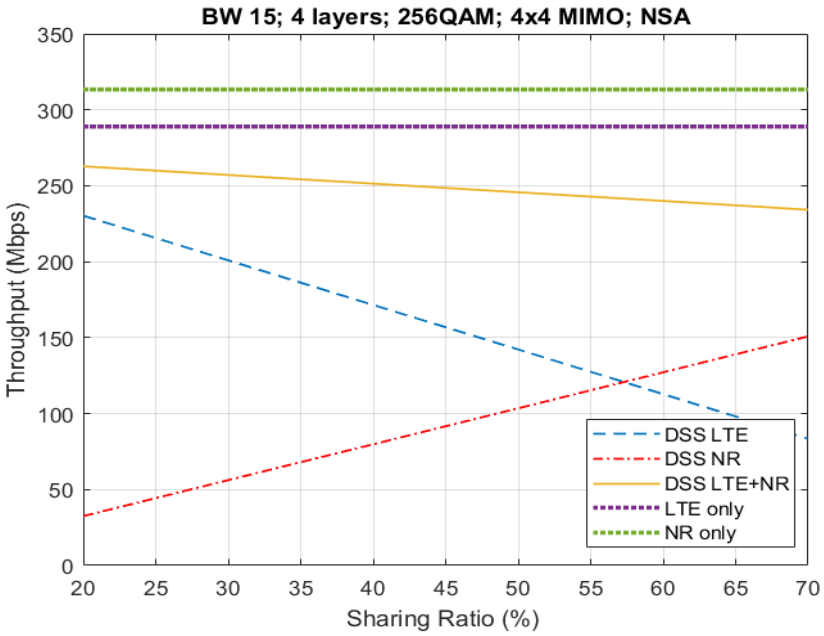

Figure 70: Throughput results for DL NSA architecture for case 4.

Figures 67-70 present the throughput results for the first 4 cases from table 25. The main characteristics that differ from one case to another consist on the modulation type adopted and the MIMO type, which is either 2x2 or 4x4 MIMO. Each figure present 5 different curves.

The purple (LTE only) and green (NR only) curves present the throughput obtained without using Phase 2 DSS. The blue (DSS LTE) and red (DSS NR) curves represent the individual throughput obtained for each technology with DSS. The most important curve is the yellow one (DSS LTE+NR) and it represents the total obtained throughput using DSS. To note that the DSS LTE+NR throughput constitutes the sum of the individual DSS NR and DSS LTE throughputs. We can observe that for every scenario/case, as the sharing ratio increases, the DSS NR throughput also increases while the DSS LTE throughput decreases. This behavior is expected due to the fact that the as we increase the sharing ratio, more resources will be available for NR transmission and fewer for LTE. Additionally, we can conclude that starting from a sharing ratio of approximately 57%, the DSS NR throughput surpasses the DSS LTE throughput. We can observe that, for all cases, the DSS LTE+NR throughput is slightly lower than the LTE only and NR only throughput (without DSS). This is comprehensible, since the available frame resources are shared among both technologies.

Regarding case 1 and case 2 from figures 65 and 66, with the main difference being the modulation type used (64QAM and 256QAM, respectively) we can observe a similar behavior although with different maximum throughput values. Depending on the sharing ratio selected, with case 1, a maximum throughput for the DSS LTE+NR between 90-100 Mbps is reached while for case 2 the maximum throughput varies between 120-135 Mbps. The increase from one case to another is of 35%. Regarding case 3 and case 4, the maximum DSS LTE+NR throughput values obtained are between 175-200 Mbps and 240-260 Mbps, respectively. The increase observed is of 37% for 20% sharing ratio and 30% for a sharing ratio of 70%.

Comparing case 1 and case 3, with the difference being the number of transmitter and receiver antennas (2x2 and 4x4 MIMO, respectively), the increase on all throughput values is of approximately 50%, with the downside of an increase in complexity and power consumption.

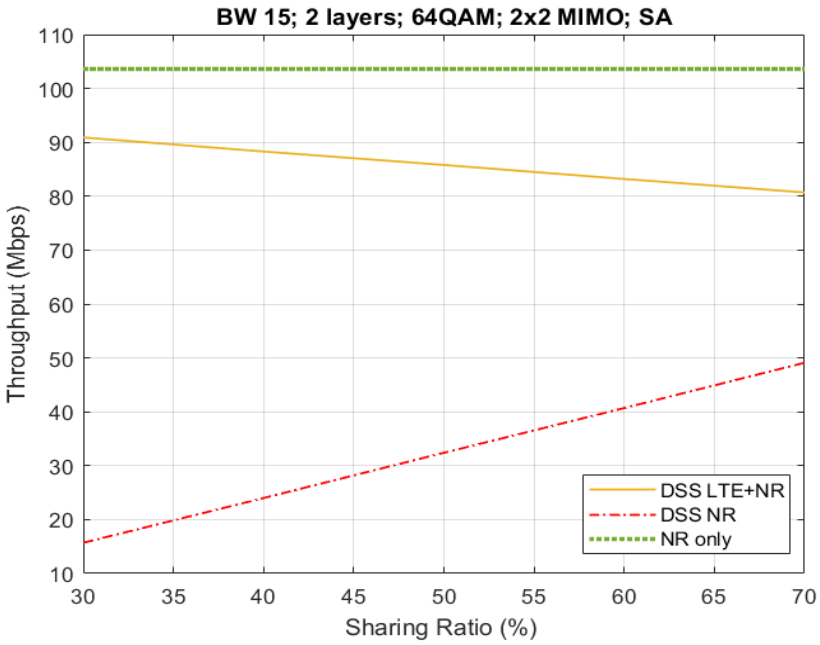

Figure 71: Throughput results for DL SA architecture for case 1.

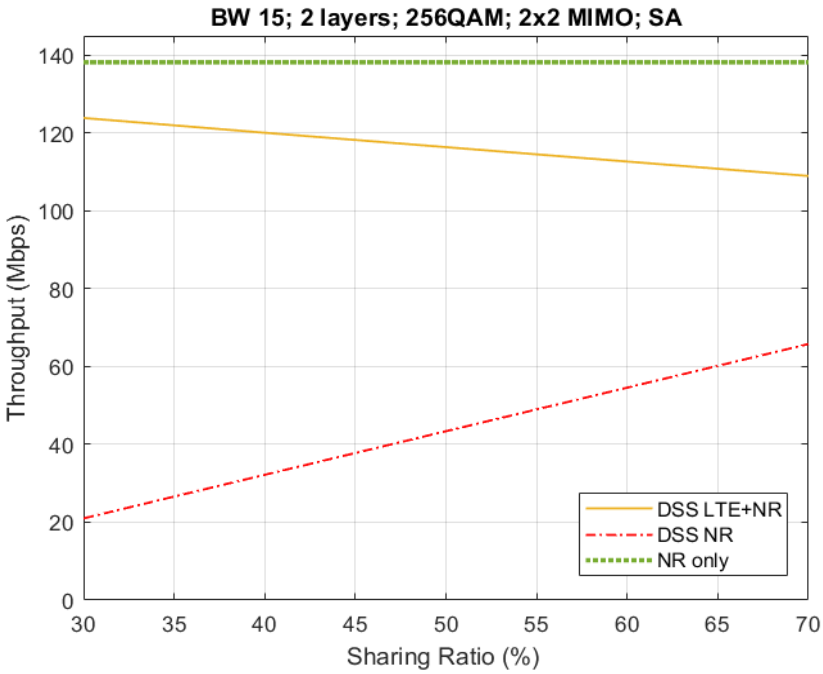

Figure 72: Throughput results for DL SA architecture for case 2.

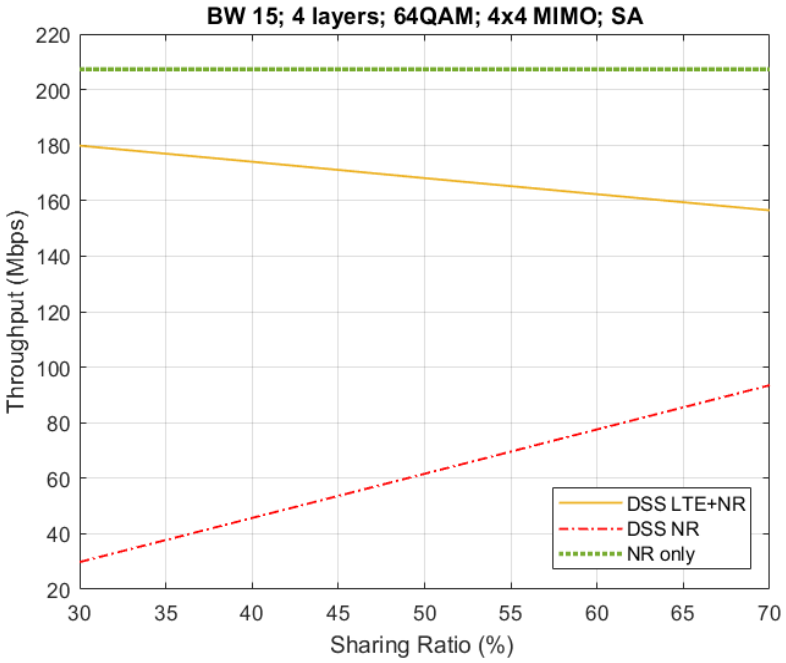

Figure 73: Throughput results for DL SA architecture for case 3.

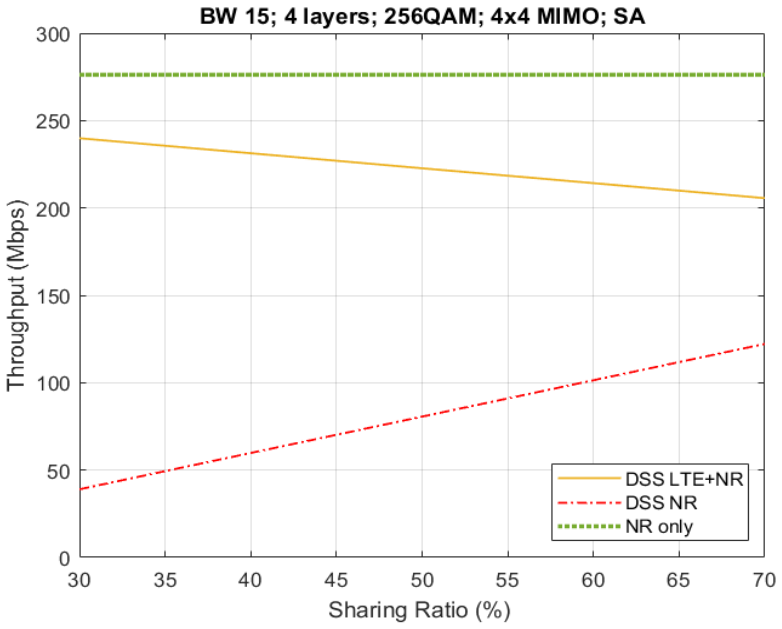

Figure 74: Throughput results for DL SA architecture for case 4.

Figures 71-74 present the throughput results for the first 4 cases from table 25, using the SA architecture. As explained in Chapter 2, the NSA architecture is based on the LTE network, being considered an intermediary solution to deploy the first NR systems. On the other side, the SA architecture does not depend on the LTE network and makes use of a new NGC core as well as NR protocols. In addition, the SA architecture offers improved efficiency with reduced complexity.

Regarding case 1 and case 2, it can be observed that the maximum DSS LTE+NR throughput achieved varies between 80-90 Mbps and 110-120 Mbps, respectively. An increase of 36% is observed from one case to the other. As for case 3 and case 4, the maximum DSS throughput value varies between 160-180 Mbps and 200-240 Mbps, respectively, depending on the sharing ratio adopted. For these cases, the increase observed if of approximately 29%. If we compare case 2 and case 4, we can observe that for both sharing ratios of 30% and 70% the increase on maximum DSS throughput is of approximately 87%.

Furthermore, an important remark is that regardless of the case, the values of the NR only throughput using the SA architecture are smaller than the ones using the NSA architecture, with a discrepancy of 15 Mbps for case 1, 20 Mbps for case 2 and 3 and 40 Mbps for case 4. The difference is justified, as the number of broadcast signals such as the System Information Block (SIB) signals and paging, that contain information regarding the cell, is higher for the SA architecture than for the NSA architecture. This leads to less available resources for NR data transmission and hence the decrease on NR only throughput.

SHARING RATIO	20%	30%	40%	50%	60%	70%	30%	40%	50%	60%	70%
	NSA ARCHITECTURE						SA ARCHITECTURE				
CASE 1	-17%	-18%	-19%	-20%	-22%	-23%	-12%	-15%	-17%	-20%	-22%
CASE 2	-14%	-15%	-17%	-18%	-20%	-21%	-10%	-13%	-16%	-18%	-21%
CASE 3	-17%	-19%	-20%	-22%	-24%	-25%	-13%	-16%	-19%	-22%	-25%
CASE 4	-16%	-18%	-20%	-22%	-23%	-25%	-13%	-16%	-19%	-22%	-26%

Table 27: % loss of the DL DSS LTE+NR throughput in comparison to NR only.

Table 27 presents the DL DSS LTE+NR throughput loss, in percentage, when compared to the DL NR only throughput. We can observe that losses between a minimum of 10% and a maximum of 26% are observed, depending on the case studied and the sharing ratio adopted.

The loss of throughput that occurs when using DSS is anticipated, as the available resources are shared between LTE and NR, which leads to less resources dedicated to

NR transmission, compared to a system that is fully NR dedicated. Notwithstanding, a loss between 10% and 26% is not a substantial percentage loss taking in account the fact that the there is no need for the operator's point of view to buy new bandwidth, as it is shared with the LTE technology. Calculating the average loss for each case, we obtain that for case 1 for NSA we observe 19.8% throughput average loss and for SA 17.2%. For case 2, we get 17.5% for NSA and 15.6% for SA architecture. For case 3, the average loss is of 21.2% for NSA and 19% for SA. Finally, for case 4 we obtain 20.6% for NSA and 19.2% loss for SA.

In addition, it is observed that as we increase the sharing ratio the decrease on the DSS LTE+NR throughput is more noticeable. The reason is that as the sharing ratio increases, leading to a higher number of available resources for NR transmission, the more synchronization signals and overhead signals are transmitted in the slots dedicated for NR transmission.

Following, we perform measurements on the uplink side, for case 5 from table 25, using both NSA and SA architecture.

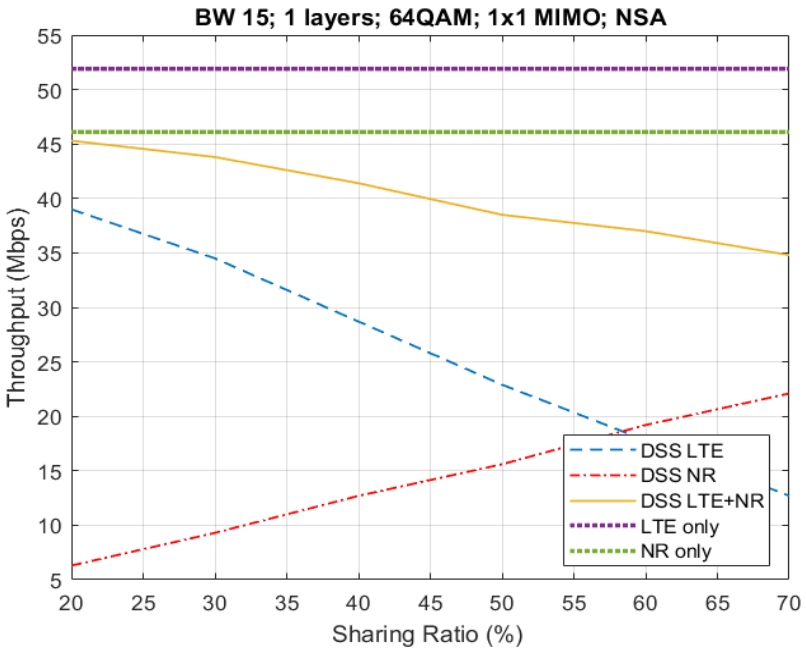

Figure 75: Throughput results for UL NSA architecture for case 5.

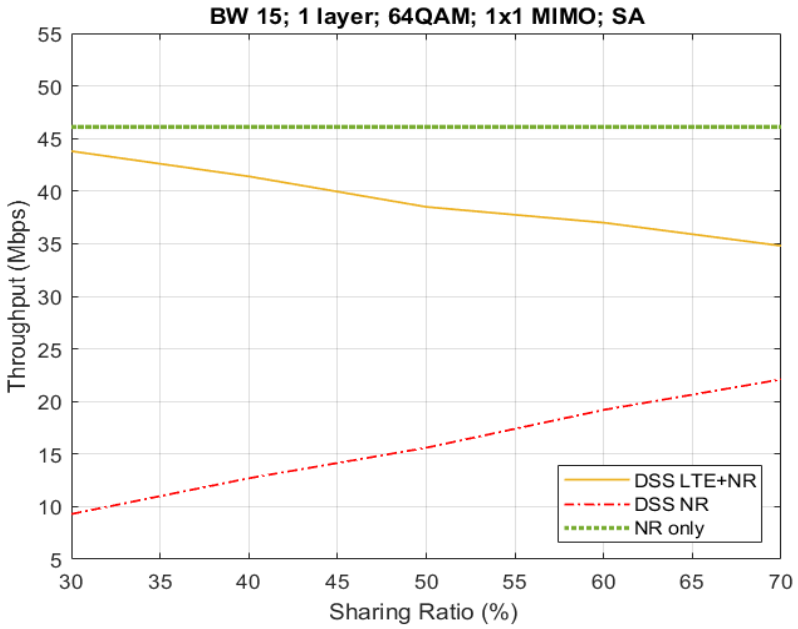

Figure 76: Throughput results for UL SA architecture for case 5.

Figures 75 and 76 present the throughput results for the uplink side, using the NSA and SA architecture, respectively. It can be observed that for the NSA architecture a maximum LTE only throughput of 40 Mbps is obtained, while for NR only the throughput reaches up to 22 Mbps. Comparing the DSS LTE+NR and NR only throughputs from both figures we can conclude that the values are similar. Hence, no difference is visible between the NSA and SA architecture. The reason for the similarity in the values obtained is that from one architecture type to another there is no need for the transmission of any additional channels which would occupy extra resources.

SHARING RATIO	20%	30%	40%	50%	60%	70%	30%	40%	50%	60%	70%
	NSA ARCHITECTURE						SA ARCHITECTURE				
CASE 5	-2%	-5%	-10%	-17%	-20%	-25%	-5%	-10%	-17%	-20%	-25%

Table 28: % loss of the UL DSS LTE+NR throughput in comparison to NR only.

Table 28 depicts the loss on throughput percentage that occurs when using the DSS technology in comparison to a NR only system. As we concluded above, the results for the NSA and SA architecture are similar. Therefore, we can observe a minimum loss of 2% when using a sharing ratio of 20% and a maximum loss of -25% for a sharing ratio of 70%, meaning that LTE occupies 30% of the available resources while NR occupies 70%.

In conclusion, from the results obtained, it is clear that using the DSS technology brings a major advantage of not needing extra dedicated bandwidth for NR systems, which from the operator's point of view leads to an improvement of spectrum efficiency and cost reduction. The main compromise of implementing the DSS technology is the throughput decrease. However, as we observed, a maximum loss of 25% on throughput can occur. The results obtained in this chapter led to the publication of the following paper:

1. G. Barb, M. Otesteanu and M. Roman, "Dynamic Spectrum Sharing for LTE-NR Downlink MIMO Systems," 2020 International Symposium on Electronics and Telecommunications (ISETC), Timisoara, 2020, ISBN: 978-1-7281-9513-1.

7. Concluding Remarks and Contributions

This chapter presents the conclusion remarks for this dissertation, presenting for each chapter the main contributions and future remarks, if the case applies.

In the first chapter an introduction and overview on all the mobile generations was presented, detailing individually the associated standards, main requirements and target values reached, channel structure, network architecture, frequency bands used and other specific information, such as multiple access schemes and duplex modes adopted for each generation. The objectives and motivation for this dissertation were defined, followed by the thesis outline and research contributions that resulted from the research work.

Chapter 2 focused on the next mobile generation, 5G. Detailed information was gathered and presented in an organized way, regarding all the important and essential aspects of 5G communication systems, such as the main use cases, proposed requirements, standardization and roll-out, new network architectures, frequency spectrum, massive MIMO and beamforming and new proposed multiple access schemes.

In chapter 3, a study on channel models proposed to be used for link-level simulations for 5G NR systems was performed. The study included the TDL and CDL channel models and its variations for both NLOS and LOS environments. The channel model characteristics were defined, alongside with the demonstration on how to obtain the channel coefficient's equations. Firstly, a comparison between the TDL NLOS channel models is performed, using different QAM modulations and several MCS index values, so that we understand the behavior of the 5G system in different conditions. The results obtained through the link-level simulations showed that the best performing channel was the TDL_A, followed by the TDL_B and lastly TDL_C. In addition, we obtained the maximum throughput values and needed SNIR to obtain them for each case. The overall results obtained have a great value in the design of new channel models for the next mobile generation systems. Following, we performed a study on the influence of the delay spread in TDL and CDL channels. In order to evaluate the influence of the DS parameter, we performed simulations in different environment scenarios, such as indoor office, rural macro cell, urban micro cell street canyon and urban macro cell, each one with different DS values. We analyzed that for both TDL and CDL channels, the NLOS profiles had an overall better performance, in terms of throughput and BER, than the LOS profiles. Moreover, we obtained values for the maximum throughput and its associated SNIR values. For CDL_A, we observed that the system had an increased performance with the urban micro cell street canyon environment compared to the urban macro cell scenario, that has higher DS values. We concluded that in order to optimize the performance of the 5G system we recommend using short DS values (18 and 32 ns) when adopting the TDL_E channel. If we select the CDL_A channel, then we recommend using a DS of 47 ns. As for future

work, it is of interest to study the effect of DS using other channel models and different environment scenarios.

Chapter 4 discussed digital beamforming techniques and the use of massive MIMO for 5G communication systems. Two techniques were described individually and its performance compared - Grid of beams beamforming and eigen based beamforming – using 64QAM and 256QAM modulations with the highest values of MCS. The simulation results showed that GoB beamforming had a lower BER rate than EBB and it even reached the minimum BER value sooner than EBB, stabilizing at a SNIR of 15 dB while EBB needed 24 dB. The maximum throughput values for each technique were obtained. We observed that GoB reached the maximum values 7 dB of SNIR sooner than EBB, from which we concluded that the use of GoB beamforming led to an overall improved performance of the 5G NR system, in terms of both BER and throughput, compared to the use of EBB.

In chapter 5, we studied the new multi-numerology proposed for 5G communication systems. The characteristics of the different numerologies were presented as well as the frames structures for each case. The performance of a 5G NR communication system was evaluated using different numerologies proposed for 5G, in order to assess how its behavior was affected. Two different environments were studied – indoor office and urban micro cell street canyon. From the results obtained, we concluded that the worst case scenario was defined by a SCS of 30 kHz with a carrier frequency of 6 GHz, while the best case scenario was represented by a SCS of 120 kHz with 28 GHz carrier frequency. The increased performance values obtained in this study confirmed the importance of having a flexible numerology for future communication systems. In addition, we verified that for the indoor office environment, the maximum throughput is reached faster than for the street canyon environment.

Chapter 6 introduced a new technology/feature that we have demonstrated to be extremely valuable for mobile communication systems – dynamic spectrum sharing – between LTE and NR technologies. Firstly, the definition of DSS is presented. Phase 1 DSS and Phase 2 DSS are detailed, for both uplink and downlink, regarding its characteristics, subframe allocation, how to calculate the sharing ratio and dimensioning impact. For Phase 1 DSS, we evaluated the performance of a 5G system using physical and static equipment at Nokia Networks Laboratory. We proposed different allocation schemes according to specific sharing ratios. We performed a comparison of the spectrum usage for LTE and NR when adopting the DSS feature and without. In addition, we measured the throughput obtained for both LTE and NR, using the proposed allocation schemes for each sharing ratio. The results obtained clearly demonstrated that there is a major advantage in using the DSS technology due to the fact that there is a cost reduction for the mobile operator alongside an optimization on the spectrum usage. However, there is a compromise on data rates, but we have shown that for Phase 1 DSS for a sharing ratio of 60%, the decrease for NR throughput is only 23%, while for Phase 2 DSS the maximum decrease is of 25%.

Consequently, the main contributions for each chapter are listed below. For the introductive chapters:

- Presentation and description of the main characteristics of 5G communication systems using an organized, precise and detailed approach.

For chapter 3, regarding sub-section 3.2 - Performance Evaluation Using TDL Channels for 5G MIMO Systems, the comparison of the three TDL profiles for NLOS environments led to the understanding on the aptness of each one of them depending on environment requirements. Moreover:

- Description of the characteristics of all TDL and CDL channel models for both NLOS and LOS environments.
- Configuration of the simulation setup in order to compare the performance of TDL_A, TDL_B and TDL_C channel profiles in a 5G system using different modulation schemes.
- BER and throughput results of the performance of TDL_A, TDL_B and TDL_C profiles that reach maximum throughput values of 165 Mbps, 383 Mbps and 516 Mbps for 16QAM, 64QAM and 256QAM modulation, respectively.
- Comparison of the performance of the TDL_A, TDL_B and TDL_C channels, from which resulted that if we are dealing with poor environment conditions, it is more suitable to use the TDL_A profile. Additionally, it is the channel model that achieves an overall better system performance, regardless of the MCS index and modulation scheme. On the other hand, the TDL_C profile needs extremely good environment conditions in order to reach its maximum throughput when using 256QAM modulation, which was not possible with the setup used.
- Study that in order to minimize BER values it is proposed, from the results obtained, to use the TDL_A profile with a higher modulation scheme as well as a high MCS index value. In order to increase the throughput of the 5G system it is proposed to also adopt the TDL_A profile and select MCS index values that have higher target code rates and spectral efficiency.

Regarding sub-section 3.3 - Influence of Delay Spread in TDL and CDL Channel Models, we concluded on the appropriate DS values for two of the TDL and CDL channel profiles. In addition:

- BER and throughput results for all TDL and CDL channel profiles using a DS value of 18 ns. Among the NLOS and LOS profiles, it is shown that the NLOS profiles have an increased performance.
- Analysis of the influence of the DS in the performance of the 5G system using TDL_E and CDL_A channel models. For TDL_E, from the results obtained, it is recommended to adopt short DS values, specifically 18 and 32 ns, in order to optimize its performance. For CDL_A, it is recommended to adopt a DS of 47 ns.

For chapter 4, the main contribution relies on the fact that we have demonstrated that using beamforming is advantageous for 5G systems and from the comparison between EBB and GoB beamforming techniques we have shown that GoB beamforming is more valorous to the system’s performance. Furthermore:

- Description of the functionality of the grid of beams and eigen based beamforming digital methods.
- Configuration of the simulation setup in order to compare both digital beamforming methods.

- Comparison of BER and throughput results of the 5G system using EBB and GoB beamforming. It is shown that GoB beamforming has a lower BER rate than EBB. In terms of throughput, even though EBB reaches a slightly higher maximum value than GoB beamforming, it needs an additional 7 dB of SNIR to reach it. In conclusion, GoB beamforming is more advantageous than EBB.

For chapter 5, the main contribution consists on the reinforcement on the importance of using a flexible numerology for the future mobile generation systems, as well as:

- Definition and presentation of the flexible OFDM numerologies proposed for 5G and the future mobile generations.
- Configuration of the simulation setup for the study of the OFDM multi-numerology proposed for 5G communication systems.
- Evaluation of the OFDM multi-numerology by obtaining BER and throughput results in two different environment scenarios. It is shown that the best performance is obtained when using a SCS of 120 kHz with a carrier frequency of 28 GHz, followed by the case with a SCS of 60 kHz and a carrier frequency of also 28 GHz. The worst performance is obtained when using a SCS of 30 kHz with a carrier frequency of 6 GHz.
- Study that in order to improve the performance of the system, meaning lower BER values and high throughput values, it is needed to increase the SCS values while using higher values for the carrier frequency.

For chapter 6, we performed physical experiments for the study of a novel technique named DSS, that, as the results displayed, brings massive advantages for the operator's point of view. Particularly the contributions are as follows:

- Presentation of the novel technique dynamic spectrum sharing, its characteristics and roll-out phases, Phase 1 and Phase 2, for uplink and downlink.
- Demonstration of how the sharing ratio for Phase 2 DSS is calculated for downlink and uplink.
- Elaboration of the configuration for the physical experimental setups for Phase 1 DSS and Phase 2 DSS measurements.
- Proposal of different resource allocation schemes for LTE-NR Phase 1 DSS according to the different possible sharing ratios.
- Measuring the system's throughput in order to study the impact of Phase 1 DSS using different sharing ratios. It is demonstrated that for a sharing ratio of 60%, the maximum allowed, NR has a decrease on throughput of 23%. However, the additional 10 MHz dedicated to NR are no longer necessary, since it uses the already existing bandwidth of LTE, demonstrating the advantage of using Phase 1 DSS.
- Study of Phase 2 DSS for downlink and uplink using both NSA and SA NR architectures.
- Measuring the system's throughput in order to evaluate the impact of Phase 2 DSS using different sharing ratios.
- Calculation of the downlink and uplink DSS LTE+NR throughput percentage loss in comparison to NR only, obtaining values between 10% and 26% for downlink and 2% up to 25% for uplink. Notwithstanding, it is remarked that that using DSS brings the massive benefit of not needing extra dedicated

bandwidth for NR systems, which from the operator’s point of view leads to an improvement of spectrum efficiency and cost reduction.

8. References

[1] A. Brand and H. Aghvami, Multiple Access Protocols For Mobile Communications: GPRS, UMTS and Beyond, John Wiley & Sons, Ltd, 2002.

[2] S. Chia, "Mobile Network Evolution Beyond 3G," *IEEE Radio and Wireless Symposium,* pp. 269-272, Long Beach, CA, 2007.

[3] A. Gameiro, "Redes sem Fios (Wireless Networks)," in *University Course Presentation*, University of Aveiro, DETI, 2016.

[4] 4GAmericas, "GSM: Global System for Mobile Communications," [Online]. Available: https://web.archive.org/web/20140208025938/http://www.4gamericas.org/index.cfm?fuseaction=page&sectionid=242. [Accessed 18 04 2020].

[5] G. Gu and G. Peng, "The survey of GSM wireless communication system," *International Conference on Computer and Information Application,* pp. 121-124, Tianjin, 2010.

[6] P. Chitrapu and B. Aghili, "Evolution of GSM into the Next Generation Wireless World," *IEEE Long Island Systems, Applications and Technology Conference,* pp. 1-10, NY, 2007.

[7] A. Kukushkin, "Types of Mobile Network by Multiple-Access Scheme," in *Introduction to Mobile Network Engineering: GSM, 3G-WCDMA, LTE and the Road to 5G*, Wiley, 2018, pp. 3-4.

[8] T. L. Singal, Wireless Communications, Tata McGraw-Hill Education, 2010.

[9] G. K. Viju and K. A. Ibrahim, "Comparative analysis of distributed architecture with existing GSM mobile architecture," *3rd International Conference on Computer Research and Development,* pp. 6-9, Shanghai, 2011.

[10] W. Zhao, R. Tafazolli and B. G. Evans, "System architecture for GSM-satellite integration," *Proceedings of PIMRC '96 - 7th International Symposium on Personal, Indoor, and Mobile Communications,* vol. 3, pp. 953-957, Taipei, Taiwan, 1996.

[11] J. T. J. Penttinen, "3GPP Mobile Communications: GSM," in *The Telecommunications Handbook: Engineering Guidelines for Fixed, Mobile and Satellite Systems*, Wiley, 2013, pp. 281-369.

[12] M. Sauter, "Global System for Mobile Communications (GSM)," in *From GSM to LTE-Advanced: An Introduction to Mobile Networks and Mobile Broadband*, Wiley, 2014, pp. 1-71.

[13] A. Kumar, "How GSM works ?," [Online]. Available: https://www.geeksforgeeks.org/how-gsm-works/. [Accessed 22 05 2020].

[14] A. S. and S. Kumar, "Handover in GSM Networks," in *Fifth International Conference on MEMS NANO, and Smart Systems*, Dubai, United Arab Emirates, 2009.

[15] J. Khan, "Handover management in GSM cellular system," *International Journal of Computer Applications,* vol. 8, no. 12, pp. 14-24, 2010.

[16] P. Knight, "Network planning using GSM and GSM based standards," *IEE Colloquium on GSM and PCN Enhanced Mobile Services ,* pp. 5/1-5/8, London, UK, 1991.

[17] Girish Yenni, "GSM-Basics of Technology Training," NOKIA, 2017.

[18] Nokia Networks, *2G,3G,4G Introduction Presentation,* 2020.

[19] C. Ferrer and M. Oliver, "Overview and capacity of the GPRS (General Packet Radio Service," *Ninth IEEE International Symposium on Personal, Indoor and Mobile Radio Communications,* vol. 1, pp. 106-110, Boston, MA, USA, 1998.

[20] A. Sikora, A. Yunitasari and M. Dold, "GPRS and UMTS services for ultra low energy M2M-communication," *IEEE 7th International Conference on Intelligent Data Acquisition and Advanced Computing Systems (IDAACS),* pp. 494-498, Berlin, 2013.

[21] W. Cheng, L. Chen, Y. Dou and Z. Lei, "Mobile user time-of-day regularity analysis in GPRS network," *IET International Conference on Communication Technology and Application,* pp. 713-717, 2011.

[22] A. Gyasi-Agyei, S. J. Halme and J. H. Sarker, "GPRS-features and packet random access channel performance analysis," in *Proceedings 2000 (ICON 2000). Networking Trends and Challenges in the New Millennium*, Singapore, 2000.

[23] K. W. Richardson, "UMTS Overview," *Electronics & Communication Engineering Journal,* vol. 12, no. 3, pp. 93-100, 2000.

[24] T. L. Lee, C. Faure and D. Grandblaise, "Impact of FDD/TDD co-existence on overall UMTS system performance," *IEEE VTS 53rd Vehicular Technology Conference,* vol. 4, pp. 2655-2659, Rhodes, Greece, 2001.

[25] S. E. Soehartono and Iskandar, "FDD and TDD comparison for consideration of slot spectrum assignment in Indonesia," *7th International Conference on Telecommunication Systems, Services, and Applications (TSSA),* pp. 266-269, Bali, 2012.

[26] A. Chemeris, "Open Source 4G Radio," 2011. [Online]. Available: https://www.slideshare.net/ipse/open-source-4g-radio. [Accessed 12 06 2020].

[27] R. Prasad and T. Ojanpera, "An overview of CDMA evolution toward wideband CDMA," *IEEE Communications Surveys,* vol. 1, no. 1, pp. 2-29, 1998.

[28] A. Toskala, H. Holma and P. Muszynski, "ETSI WCDMA for UMTS," *IEEE 5th International Symposium on Spread Spectrum Techniques and Applications,* vol. 2, pp. 616-620, Sun City, South Africa, 1998.

[29] L. L. Hanzo, L.-L. Yang, E-L, Kuan and K. Yen, "CDMA Overview," in *Single and Multi-Carrier DS-CDMA: Multi-User Detection, Space-Time Spreading, Synchronisation, Networking?and Standards*, Wiley-IEEE Press, 2004, pp. 35-80.

[30] D. Tipper, *UMTS Overview,* Graduate Telecommunications and Networking Program - University of Pittsburgh, 2016.

[31] C. A. Fischer, K. Han and Z. Wang, "Accounting solutions in the UMTS core network," *Bell Labs Technical Journal,* vol. 6, no. 2, pp. 65-73, 2002.

[32] N. Anderson, "Paired and Unpaired Spectrum," in *LTE – The UMTS Long Term Evolution: From Theory to Practice, Second Edition*, John Wiley & Sons, 2011.

[33] A. Abbas, "Mobile Handset Cellular Network," [Online]. Available: https://www.slideshare.net/ProfArshadAbbas/lectures-on-2-g3g35g4g. [Accessed 07 07 2020].

[34] 3GPP, "TS 21.101 version 5.4.0 Release 5," 2003.

[35] 3GPP, "TS 21.101 version 6.0.0 Release 6," 2005.

[36] 3GPP, "TS 21.101 version 7.0.0 Release 7," 2007.

[37] J. Wannstrom, "3GPP - HSPA," [Online]. Available: https://www.3gpp.org/technologies/keywords-acronyms/99-hspa. [Accessed 08 07 2020].

[38] H. Holma, A. Toskala and P. Tapia, "HSPA+ Evolution to Release 12: Performance and Optimization," *Wiley,* pp. 421-431, 2013.

[39] A. B. Maya, "Thesis: Evolulcion Arquitectura de Red Movil 3GPP R99 A R11," *Instituto Politecnico Nacional,* 2013.

[40] "LTE Introduction," in LTE and the Evolution to 4G Wireless: Design and Measurement Challenges," *Wiley,* pp. 1-10, 2013.

[41] S. Yi, S. Chun, Y. Lee, S. Park and S. Jung, "Overview of LTE and LTE-Advanced New Features," in *Radio Protocols for LTE and LTE-Advanced* , Wiley, 2013, pp. 151-158.

[42] "System Architecture Evolution," in LTE and the Evolution to 4G Wireless: Design and Measurement Challenges," *Wiley,* pp. 195-228, 2013.

[43] H. Holma and A. Toskala, "LTE Release 8 and 9 Overview," in *LTE Advanced: 3GPP Solution for IMT-Advanced* , Wiley, 2012, pp. 14-29.

[44] G. Barb and M. Otesteanu, "4G/5G: A Comparative Study and Overview on What to Expect from 5G," in *International Conference on Telecommunications and Signal Processing (TSP)*, Milan, 2020.

[45] H. Wang, L. Kondi, A. Luthra and S. Ci, 4G Wireless Video Communications, John Wiley & Sons, 2009.

[46] J. Mountassir, H. Balta, M. Kovaci and A. Isar, "Study of multiple access schemes in 3GPP LTE OFDMA vs. SC-FDMA," *International Conference on Applied Electronics,* pp. 1-4, Pilsen, 2011.

[47] C. Azurdia-Meza, Thesis: Analysis, Design, and Implementation of Parametric Nyquist ISI-Free Pulses in Wireless Communications Systems, 2013.

[48] L.Hanzo, W.Webb and T.Keller, Single and Multi-carrier Quadrature Amplitude Modulation, John Wiley & Sons, 2001.

[49] N. Cvijetic, "OFDM for Next-Generation Optical Access Networks," *Journal of Lightwave Technology,* vol. 30, no. 4, pp. 384-398, 2012.

[50] G. Barb, "Master Thesis: Linear Equalization Techniques for Hybrid Systems in the Millimeter Wave Band of Communications," DETI, University of Aveiro, 2017.

[51] C. Ciochina and H. Sari, "A review of OFDMA and single-carrier FDMA," *European Wireless Conference (EW),* pp. 706-710, Lucca, 2010.

[52] K. M. Shazzad, Orthogonal Frequency Division Multiple Access (OFDMA), Canada: University of Windsor, 2007.

[53] H. G. Myung, "Introduction to single carrier FDMA," in *15th European Signal Processing Conference*, Poznan, pp. 2144-2148, 2007.

[54] A. Elnashar and M. A. El-saidny, "LTE and LTE-A Overview," *Practical Guide to LTE-A, VoLTE and IoT: Paving the way towards 5G, Wiley,* pp. 1-86, 2018.

[55] S. Kanchi, S. Sandilya, D. Bhosale, A. Pitkar and M. Gondhalekar, "Overview of LTE-A technology," *2013 IEEE Global High Tech Congress on Electronics,* pp. 195-200, Shenzhen, 2013.

[56] P. Gogoi, A. Sarma, R. Borah and B. Saikia, "On the evolution of downlink physical layer in multi-antenna 3GPP LTE / LTE-A: A review," *2015 International Symposium on Advanced Computing and Communication (ISACC),* pp. 290-296, Silchar, 2015.

[57] Nokia Corporation, "5G use cases and requirements," *Nokia White Paper,* p. 6, 2016.

[58] GSMA Intelligence, "The Mobile Economy Report," 2014.

[59] S. S. Das and R. Prasad, ""Introduction to 5G," in Evolution of Air Interface Towards 5G," *River Publishers,* pp. 1-8, 2018.

[60] G. Barb and M. Otesteanu, "On the Influence of Delay Spread in TDL and CDL Channel Models for Downlink 5G MIMO Systems," *IEEE 10th Annual Ubiquitous Computing, Electronics & Mobile Communication Conference (UEMCON),* pp. 958-962, New York City, NY, USA, 2019.

[61] J. Guillermo, "How 5G Relates to SDN and NFV Technologies – Part III: Architecture (Continued)," *Dell Technologies,* 2019.

[62] M. S. Han, J. W. Lee, C. G. Kang and M. J. Rim, "System-level Performance Evaluation with 5G K-SimSys for 5G URLLC System," *16th IEEE Annual Consumer Communications & Networking Conference (CCNC),* pp. 1-5, Las Vegas, NV, USA, 2019.

[63] M. Shafi, A. Molisch, P. Smith, T. Haustein, P. Zhu, P. D. Silva, F. Tufvesson, A. Benjebbour and G. Wunder, "5G: A Tutorial Overview of Standards, Trials, Challenges, Deployment, and Practice," in *IEEE Journal on Selected Areas in Communications, vol. 35, no. 6*, 2017.

[64] C. Gheorghe, D. A. Stoichescu and R. Dragomir, "Latency requirement for 5G mobile communications," *10th International Conference on Electronics, Computers and Artificial Intelligence (ECAI),* pp. 1-4, 2018.

[65] A. Al-Dulaimi, X. Wang and C.-L. I, "Standardization: The Road to 5G," in *5G Networks: Fundamental Requirements, Enabling Technologies, and Operations Management*, Wiley-IEEE Press, 2018, pp. 691-708.

[66] G. Barb and M. Otesteanu, "5G: An Overview on Challenges and Key Solutions," in *2018 International Symposium on Electronics and Telecommunications (ISETC)*, Timisoara, pp. 1-4, 2018.

[67] S. E. Hassani and A. Haidine, "Roadmap towards beyond 4G: Key technologies and challenges for 5G," *International Conference on Wireless Networks and Mobile Communications (WINCOM),* pp. 1-6, Marrakech, 2015.

[68] T. Maksymyuk, M. Klymash and M. Jo, "Deployment strategies and standardization perspectives for 5G mobile networks," in *13th International Conference on Modern Problems of Radio Engineering, Telecommunications and Computer Science (TCSET)*, Lviv, 2016.

[69] Nokia Networks, "An introduction to 3GPP 5G New Radio," *Network Engineering Information,* 2019.

[70] 3GPP, "3GPP Specs," [Online]. Available: https://www.3gpp.org/ftp/specs/archive/. [Accessed 30 07 2020].

[71] A. E. Rhayour and T. Marzi, "5G Architecture: Deployment scenarios and options," *International Symposium on Advanced Electrical and Communication Technologies (ISAECT),* pp. 1-6, Rome, Italy, 2019.

[72] X. Zhao, J. Chen, P. Li, Z. Li, C. Hu and W. Xie, "5G NSA Radio Access Network Sharing for Mobile Operators : Design, realization and field trial," *IEEE 20th International Conference on Communication Technology (ICCT),* pp. 454-461, Nanning, 2020.

[73] D. Koziol and H. Määttänen, "Network Architecture and NR Radio Protocols," in *5G New Radio: A Beam-based Air Interface*, Wiley, 2020, pp. 25-93.

[74] G. Liu, Y. Huang, Z. Chen, L. Liu, Q. Wang and N. Li, "5G Deployment: Standalone vs. Non-Standalone from the Operator Perspective," *IEEE Communications Magazine,* vol. 58, no. 11, pp. 83-89, 2020.

[75] Z. Pi and F. Khan, "An introduction to millimeter-wave mobile broadband," *IEEE Communications Magazine,* vol. 49, no. 6, pp. 101-107, 2011.

[76] W. R. e. al, "Millimeter-wave beamforming as an enabling technology for 5G Cellular communications: theoretical feasibility and prototype results," *IEEE Communications Magazine,* vol. 52, no. 2, pp. 106-113, 2014.

[77] A. Alkhateeb, O. E. Ayach, G. Leus and R. W. Heath, "Channel Estimation and Hybrid Precoding for Millimeter Wave Cellular Systems," *IEEE Journal of Selected Topics in Signal Processing,* vol. 8, no. 5, pp. 831-846, 2014.

[78] T. L. Marzetta, "Massive MIMO: An Introduction," *Bell Labs Technical Journal,* vol. 20, pp. 11-22, 2015.

[79] B. N. Bertenyi, S. Kooropaty, H. Zhou, X. Chen, W. Kim, Y. Dai, X. Xu and Xiaodong, "5G NR Radio Interface," *Journal of ICT Standardization,* vol. 6, pp. 31-58, 2018.

[80] G. Gampala and C. J. Reddy, "Massive MIMO — Beyond 4G and a basis for 5G," *International Applied Computational Electromagnetics Society Symposium (ACES),* pp. 1-2, Denver, CO, 2018.

[81] D. Schoolar, Massive MIMO Comes of Age, Ovum TMT Intelligence, 2017.

[82] G. Barb, M. Otesteanu, F. Alexa and A. Ghiulai, "Digital Beamforming Techniques for Future Communications Systems," *12th IEEE/IET International Symposium on Communication Systems, Networks and Digital Signal Processing,* 2020.

[83] A. F. Molisch, V. V. Ratnam, S. Han, Z. Li, S. L. H. Nguyen, L. Li and K. Haneda, "Hybrid beamforming for massive MIMO: A survey," *IEEE Communications Magazine,* vol. 55, no. 9, pp. 134-141, 2017.

[84] R. Magueta, D. Castanheira, A. Silva, R. Dinis and A. Gameiro, "Hybrid Multi-User Equalizer for Massive MIMO Millimeter-Wave Dynamic Subconnected Architecture," *IEEE Access,* vol. 7, pp. 79017-79029, 2019.

[85] D. Castanheira, G. Barb, A. Silva and A. Gameiro, "A multi-user linear equalizer for uplink broadband millimeter wave massive MIMO," *Digital Signal Processing,* vol. 92, pp. 62-72, 2019.

[86] P. Banelli, S. Buzzi, G. Colavolpe, A. Modenini, F. Rusek and A. Ugolini, "Modulation Formats and Waveforms for 5G Networks: Who Will Be the Heir of OFDM?: An overview of alternative modulation schemes for improved spectral efficiency," *IEEE Signal Processing Magazine,* vol. 31, no. 6, pp. 80-93, Nov. 2014.

[87] F. Luo and C. Zhang, "Signal Processing for 5G: Algorithms and Implementations," *John Wiley & Sons,* 2016.

[88] N. Michailow, M. Matthé, I. S. Gaspar, A. N. Caldevilla, L. L. Mendes, A. Festag and G. Fettweis, "Generalized Frequency Division Multiplexing for 5th Generation Cellular Networks," *IEEE Transactions on Communications,* vol. 62, no. 9, pp. 3045-3061, 2014.

[89] J. Mazo, "Faster-than-Nyquist signaling," *Bell System Technology Journal,* vol. 54, pp. 1450-1462, 1975.

[90] L. Lv, L. Yang, H. Jiang, T. H. Luan and J. Chen, "When NOMA Meets Multiuser Cognitive Radio: Opportunistic Cooperation and User Scheduling," *IEEE Transactions on Vehicular Technology,* vol. 67, no. 7, pp. 6679-6684, 2018.

[91] F. Zhou, Y. Wu, Y. Liang, Z. Li, Y. Wang and K. Wong, "State of the Art, Taxonomy, and Open Issues on Cognitive Radio Networks with NOMA," *IEEE Wireless Communications,* vol. 25, no. 2, pp. 100-108, 2018.

[92] Y. Li, B. Ai, X. Cheng, S. Lin and Z. Zhong, "A TDL Based Non-WSSUS Vehicle-to-Vehicle Channel Model," *International Journal of Antennas and Propagation,* 2013.

[93] S. Chiu, "Propsim 5G channel models and channel emulations," *Keysight Technologies,* January 2018.

[94] 3GPP, "Study on channel model for frequency spectrum above 6 GHz," *ETSI TR 138 900 V14.2.0,* 2017.

[95] D. Reed, "On Channel Model Tap Reduction for 5G NR mmW Testing," *IEEE Asia-Pacific Conference on Antennas and Propagation (APCAP),* pp. 464-468, Auckland, 2018.

[96] B. M. e. al, "3D channel model in 3GPP," *IEEE Communications Magazine,* vol. 53, no. 3, pp. 16-23, March 2015.

[97] A. F., Taranetz and M. Rupp, "3GPP 3D MIMO channel model: a holistic implementation guideline for open source simulation tools," *EURASIP Journal on Wireless Communications and Networking,* vol. 1, Dec 2016.

[98] G. Barb, M. Otesteanu, G. Budura and C. Balint, "Performance Evaluation of TDL Channels for Downlink 5G MIMO Systems," *International Symposium on Signals, Circuits and Systems (ISSCS),* Iasi, Romania, 2019.

[99] A. Grami, "Introduction to Digital Communications - Chapter 6," *Academic Press,* pp. 193-225, 2016.

[100] M. Showkat, J. A. Sheikh and A. I. Khan, "A New Beamforming Technique in 5G Environment for Reliable Transmission," *4th International Conference on Computing Communication and Automation (ICCCA),* pp. 1-5, Greater Noida, India, 2018.

[101] S. Saur, H. Halbauer, A. Rueegg and F. Schaich, "Grid-of-Beams (GoB) Based Downlink Multi-User MIMO," *IEEE 802.16 Broadband Wireless Access Working Group,* 2008.

[102] T. Pairon, C. Oestges, M. Drouguet and C. Craeye, "Efficient Evaluation of Energy Focusing Based on Eigen-Beamforming," *13th European Conference on Antennas and Propagation (EuCAP),* pp. 1-5, Krakow, Poland, 2019.

[103] J. V. e. al., "Numerology and frame structure for 5G radio access," *IEEE 27th Annual International Symposium on Personal, Indoor, and Mobile Radio Communications (PIMRC),* pp. 1-5, 2016.

[104] T. Bag, S. Garg, Z. Shaik and A. Mitschele-Thiel, "Multi-Numerology Based Resource Allocation for Reducing Average Scheduling Latencies for 5G NR Wireless Networks," *European Conference on Networks and Communications (EuCNC),* pp. 597-602, Valencia, Spain, 2019.

[105] A. A. Zaidi, R. Baldemair, V. Moles-Cases, N. He, K. Werner and A. Cedergren, "OFDM Numerology Design for 5G New Radio to Support IoT, eMBB, and MBSFN," *IEEE Communications Standards Magazine,* vol. 2, no. 2, pp. 78-83, June 2018.

[106] N. Patriciello, S. Lagen, L. Giupponi and B. Bojovic, "5G New Radio Numerologies and their Impact on the End-To-End Latency," *IEEE 23rd International Workshop on Computer Aided Modeling and Design of Communication Links and Networks (CAMAD),* pp. 1-6, Barcelona, 2018.

[107] G. Barb, M. Otesteanu, F. Alexa and F. Danuti, "OFDM Multi-Numerology for Future 5G New Radio Communication Systems," *International Conference on Software, Telecommunications and Computer Networks (SoftCOM),* Split, Hvar, Croatia, 2020.

[108] M. Matinmikko-Blue, S. Yrjölä, V. Seppänen, P. Ahokangas, H. Hämmäinen and M. Latva-aho, "Analysis of Spectrum Valuation Approaches: The Viewpoint of Local 5G Networks in Shared Spectrum Bands," *IEEE International Symposium on Dynamic Spectrum Access Networks (DySPAN),* pp. 1-9, Seoul, 2018.

[109] L. W. e. al, "4G 5G Spectrum Sharing: Efficient 5G Deployment to Serve Enhanced Mobile Broadband and Internet of Things Applications," *IEEE Vehicular Technology Magazine,* vol. 13, no. 4, pp. 28-39, 2018.

[110] A. Roessler, "Impact of spectrum sharing on 4G and 5G standards a review of how coexistance and spectrum sharing is shaping 3GPP standards," *IEEE International Symposium on Electromagnetic Compatibility & Signal/Power Integrity (EMCSI),* pp. 704-707, Washington, DC, 2017.

[111] Nokia Networks, "LTE-NR DSS phase I," *Network Engineering,* 2020.

[112] G. Barb, M. Otesteanu and M. Roman, "Dynamic Spectrum Sharing for LTE-NR Downlink MIMO Systems," *International Symposium on Electronics and Telecommunications (ISETC),* Timisoara, 2020.

[113] Nokia Networks, "LTE-NR DSS with CRS Rate Matching," *Network Engineering,* 2020.

[114] A. Al-Dulaimi, X. Wang and C.-L. I, "Standardization: The Road to 5G," in *5G Networks: Fundamental Requirements, Enabling Technologies, and Operations Management*, IEEE, 2018, pp. 691-708.

[115] 3GPP. [Online]. Available: https://www.3gpp.org/ftp/Specs/archive/. [Accessed 30 07 2020].

[116] G. Gu and G. Peng, "The survey of GSM wireless communication system," *International Conference on Computer and Information Application,* pp. 121-124, Tianjin, 2010.